Nuclear Inst. and Methods in Physics Research, A 957 (2020) 163402

Contents lists available at ScienceDirect

Nuclear Inst. and Methods in Physics Research, A

journal homepage: www.elsevier.com/locate/nima

The instrument suite of the European Spallation Source

K.H. Andersen [1,*,a], D.N Argyriou [1], A.J. Jackson [1], J. Houston [1], P.F. Henry [1,3,b], P.P. Deen [1,8], R. Toft-Petersen [1,13], P. Beran [1,23], M. Strobl [1,9], T. Arnold [1,3], H. Wacklin-Knecht [1], N. Tsapatsaris [1], E. Oksanen [1], R. Woracek [1], W. Schweika [1,4], D. Mannix [1,12,35], A. Hiess [1], S. Kennedy [1], O. Kirstein [1], S. Petersson Årsköld [1], J. Taylor [2], M.E. Hagen [1], G. Laszlo [1], K. Kanaki [1], F. Piscitelli [1], A. Khaplanov [1], I. Stefanescu [1], Th. Kittelmann [1], D. Pfeiffer [1], R. Hall-Wilton [1], C.I. Lopez [1], G. Aprigliano [1], L. Whitelegg [1,13], F.Y. Moreira [1,7], M. Olsson [1], H.N. Bordallo [1,11], D. Martín-Rodríguez [1], H. Schneider [1], M. Sharp [1], M. Hartl [1], G. Nagy [1,24], S. Ansell [1,25,c], S. Pullen [1,26], A. Vickery [1,11,d], A. Fedrigo [1,11,27], F. Mezei [1], M. Arai [1], R.K. Heenan [3], W. Halcrow [3], D. Turner [3], D. Raspino [3], A. Orszulik [3], J. Cooper [3], N. Webb [3], P. Galsworthy [3], J. Nightingale [3], S. Langridge [3], J. Elmer [3], H. Frielinghaus [5], R. Hanslik [6], A. Gussen [6], S. Jaksch [5], R. Engels [4], T. Kozielewski [4], S. Butterweck [6], M. Feygenson [4], P. Harbott [4], A. Poqué [6], A. Schwaab [6], K. Lieutenant [4], N. Violini [4], J. Voigt [4], T. Brückel [4], M. Koenen [6], H. Kämmerling [6], E. Babcock [5], Z. Salhi [5], A. Wischnewski [4], A. Heynen [6], S. Désert [7], J. Jestin [7], F. Porcher [7], X. Fabrèges [7], G. Fabrèges [7], B. Annighöfer [7], S. Klimko [7], Th. Dupont [7], Th. Robillard [7], A. Goukassov [7], S. Longeville [7], Ch. Alba-Simionesco [7], Ph. Bourges [7], J. Guyon Le Bouffy [7], P. Lavie [7], S. Rodrigues [7], E. Calzada [8], M. Lerche [8,e], B. Schillinger [8], Ph. Schmakat [8], M. Schulz [8], M. Seifert [8], W. Lohstroh [8], W. Petry [8], J. Neuhaus [8], L. Loaiza [8], A. Tartaglione [8], A. Glavic [9], S. Schütz [9], J. Stahn [9], E. Lehmann [9], M. Morgano [9], J. Schefer [9], U. Filges [9], Ch. Klauser [9], Ch. Niedermayer [9], J. Fenske [10], G. Nowak [10], M. Rouijaa [10], D.J. Siemers [10], R. Kiehn [10], M. Müller [10], H. Carlsen [11], L. Udby [11], K. Lefmann [11], J.O. Birk [11,12,9,14], S. Holm-Dahlin [11,12], M. Bertelsen [2,11], U. Bengaard Hansen [11], M.A. Olsen [11], M. Christensen [12], K. Iversen [12], N.B. Christensen [13], H.M. Rønnow [15], P.G. Freeman [15,37], B.C. Hauback [16], R. Kolevatov [16], I. Llamas-Jansa [16], A. Orecchini [17,18], F. Sacchetti [17,18], C. Petrillo [17,18], A. Paciaroni [17,18], P. Tozzi [18], M. Zanatta [17,19], P. Luna [20], I. Herranz [20], O.G. del Moral [20], M. Huerta [20], M. Magán [20], M. Mosconi [20], E. Abad [20], J. Aguilar [20], S. Stepanyan [20], G. Bakedano [20], R. Vivanco [20,21], I. Bustinduy [20], F. Sordo [20,21], J.L. Martínez [20,22], R.E. Lechner [36,1], F.J. Villacorta [20], J. Šaroun [23], P. Lukáš [23], M. Markó [24], M. Zanetti [28,3], S. Bellissima [29], L. del Rosso [29], F. Masi [30,3], C. Bovo [3], M. Chowdhury [3], A. De Bonis [3], L. Di Fresco [31,3], C. Scatigno [31,3], S.F. Parker [3], F. Fernandez-Alonso [38,39,40], D. Colognesi [29], R. Senesi [31,32], C. Andreani [31,41], G. Gorini [30,33], G. Scionti [34], A. Schreyer [1]

[1] European Spallation Source ERIC, P.O. Box 176, 22100 Lund, Sweden
[2] Data Management and Software Centre, European Spallation Source ERIC, Ole Maaløes Vej 2200 Copenhagen N, Denmark
[3] ISIS Facility, Rutherford Appleton Laboratory, Chilton, Didcot, Oxfordshire OX11 0QX, United Kingdom
[4] Jülich Centre for Neutron Science JCNS, Forschungszentrum Jülich GmbH, 52428 Jülich, Germany

* Corresponding author.
E-mail address: andersenkh@ornl.gov (K.H. Andersen).
[a] Current address: Oak Ridge National Laboratory, 1 Bethel Valley Road, Oak Ridge, TN 37830, USA.
[b] Current address: ISIS Facility, Rutherford Appleton Laboratory, Chilton, Didcot, Oxfordshire OX11 0QX, UK.
[c] Current address: MAX IV Laboratory, Lund University, P.O. Box 118, 221 00 Lund, Sweden.
[d] Current address: JJ X-ray A/S, DTU Science Park, Dr. Neergaards Vej 5D, 2970 Hørsholm, Denmark.
[e] Current address: Lawrence Berkeley National Laboratory, One Cyclotron Road, Berkeley, CA 94720, USA.

https://doi.org/10.1016/j.nima.2020.163402
Received 20 December 2019; Accepted 4 January 2020
Available online 10 January 2020

[5] Jülich Centre for Neutron Science JCNS at Heinz Maier-Leibnitz Zentrum (MLZ), Forschungszentrum Jülich GmbH, Lichtenbergstrasse, 85748 Garching, Germany
[6] Central Institute of Engineering, Electronics and Analytics ZEA-1: Engineering and Technology, Forschungszentrum Jülich GmbH, Wilhelm-Johnen-Strasse, 52428 Jülich, Germany
[7] Université de Paris-Saclay, CNRS, CEA, Laboratoire Léon Brillouin, 91191 Gif-sur-Yvette, France
[8] Heinz Maier-Leibnitz Zentrum, Technische Universität München, Lichtenbergstr. 1, 85748 Garching, Germany
[9] Paul Scherrer Institut, 5232 Villigen PSI, Switzerland
[10] Helmholtz-Zentrum Geesthacht, Geesthacht, Germany
[11] Niels Bohr Institute, University of Copenhagen, Universitetsparken 5, 2100, Copenhagen Ø, Denmark
[12] Department of Chemistry, Aarhus University, Langelandsgade 140, 8000 Aarhus, Denmark
[13] Department of Physics, Technical University of Denmark, 2800 Kgs Lyngby, Denmark
[14] Danish Technological Institute, Gregersensvej, 2630 Taastrup, Denmark
[15] Laboratory for Quantum Magnetism, Institute of Physics, École Polytechnique Fédérale de Lausanne, 1015 Lausanne, Switzerland
[16] Institute for Energy Technology, P.O. Box 40, 2027 Kjeller, Norway
[17] Dipartimento di Fisica e Geologia, Università degli Studi di Perugia, 06123 Perugia, Italy
[18] CNR-IOM c/o Dipartimento di Fisica e Geologia, Università degli Studi di Perugia, 06125 Perugia, Italy
[19] Dipartimento di Fisica, Università di Trento, via Sommarive 14 Povo, 38123 Trento, Italy
[20] Consorcio ESS-Bilbao. Parque Tecnológico Bizkaia. Poligono Ugaldeguren III, Pol. A, 7B, 48170 Zamudio, Spain
[21] Instituto de Fusión Nuclear-UPM. C José Gutiérrez Abascal, 2-28006 Madrid, Spain
[22] Instituto de Ciencia de Materiales de Madrid, Consejo Superior de Investigaciones Científicas, 28049 Madrid, Spain
[23] Nuclear Physics Institute ASCR, Czech Republic
[24] Neutron Spectroscopy Department, Wigner Research Centre for Physics, Konkoly Th. M. 29-33, 1122 Budapest, Hungary
[25] MAX IV Laboratory, Lund University, P.O. Box 118, 221 00 Lund, Sweden
[26] Australian Nuiclear Science and Technology Organisation, New Illawarra Road, Lucas Height, New South Wales 2234, Australia
[27] Consiglio Nazionale delle Ricerche, Istituto dei Sistemi Complessi, Sesto Fiorentino, FI, Italy
[28] Consiglio Nazionale delle Ricerche, Dipartimento di Scienze Fisiche e Tecnologie della Materia, Roma, Italy
[29] Istituto di Fisica Applicata "Nello Carrara", CNR-IFAC, Sesto Fiorentino, FI, Italy
[30] Università degli Studi di Milano-Bicocca, Dipartimento di Fisica, Milano, Italy
[31] Università degli Studi di Roma "Tor Vergata", Dipartimento di Fisica e Centro NAST, Roma, Italy
[32] Istituto per i Processi Chimico Fisici, Sezione di Messina, CNR, Messina, Italy
[33] Istituto per la Scienza e Tecnologia dei Plasmi, CNR, Milano, Italy
[34] Università della Calabria, Dipartimento di Fisica, Arcavacata di Rende (CS), Italy
[35] Institut Néel CNRS/UGA UPR2940, 25 rue des Martyrs BP 166, 38042 Grenoble Cedex 9, France
[36] Helmholtz Zentrum Berlin für Materialien und Energie, Hahn-Meitner-Platz 1, 14109 Berlin, Germany
[37] Jeremiah Horrocks Institute for Mathematics, Physics and Astronomy, University of Central Lancashire, Preston, PR1 2HE, United Kingdom
[38] Department of Physics and Astronomy, University College London, Gower Street, London, WC1E 6BT, United Kingdom
[39] Materials Physics Center, CSIC-UPV/EHU, Paseo Manuel Lardizabal 5, 20018 Donostia -San Sebastian, Spain
[40] IKERBASQUE, Basque Foundation for Science, Maria Diaz de Haro 3, 48013 Bilbao, Spain
[41] Consiglio Nazionale delle Ricerche, Istituto di Stuttura della Materia, Roma, Italy

ARTICLE INFO

Keywords:
Slow neutron scattering
Pulsed neutron instrumentation
Accelerator-based neutron facilities
ESS instrument suite

ABSTRACT

An overview is provided of the 15 neutron beam instruments making up the initial instrument suite of the European Spallation Source (ESS), and being made available to the neutron user community. The ESS neutron source consists of a high-power accelerator and target station, providing a unique long-pulse time structure of slow neutrons. The design considerations behind the time structure, moderator geometry and instrument layout are presented.

The 15-instrument suite consists of two small-angle instruments, two reflectometers, an imaging beamline, two single-crystal diffractometers; one for macromolecular crystallography and one for magnetism, two powder diffractometers, and an engineering diffractometer, as well as an array of five inelastic instruments comprising two chopper spectrometers, an inverse-geometry single-crystal excitations spectrometer, an instrument for vibrational spectroscopy and a high-resolution backscattering spectrometer. The conceptual design, performance and scientific drivers of each of these instruments are described.

All of the instruments are designed to provide breakthrough new scientific capability, not currently available at existing facilities, building on the inherent strengths of the ESS long-pulse neutron source of high flux, flexible resolution and large bandwidth. Each of them is predicted to provide world-leading performance at an accelerator power of 2 MW. This technical capability translates into a very broad range of scientific capabilities. The composition of the instrument suite has been chosen to maximise the breadth and depth of the scientific impact of the early years of the ESS, and provide a solid base for completion and further expansion of the facility.

1. Introduction

The European Spallation Source (ESS) is currently under construction in Lund, Sweden. When complete, it will provide a suite of 22 neutron beam instruments to the scientific user community, arranged around a spallation neutron target and moderator assembly, fed by a 5 MW proton accelerator. The facility, including all the instruments, is designed to provide world-leading performance, with new and unique instrumental capabilities providing the means to make progress and achieve breakthroughs across a broad spectrum of physical and biological sciences. The scientific and technical vision is described in the ESS Technical Design Report (TDR) [1].

Unlike conventional pulsed spallation sources, where the proton pulse impacting the target is of the order of 1 μs in length, the ESS is designed to deliver significantly longer proton pulses. The ESS accelerator delivers a 2 GeV proton pulse of 2.86 ms in length, with a repetition rate of 14 Hz, impacting on a tungsten target in which fast neutrons are produced by spallation. These are then slowed down in a moderator-reflector assembly which will produce the world's highest brightness of cold and thermal neutrons, using liquid parahydrogen and water, respectively. The moderator geometry was the topic of a careful optimisation [2,3] in which source properties, guide design and instrument performance were considered together so as to maximise instrument performance while allowing an unprecedented level of flexibility and upgradeability. The moderator system makes use of the new concept

of low-dimensional moderators with a moderator height of 3 cm and a "butterfly" layout of the hydrogen and water moderators, allowing all instrument positions to choose freely between cold and thermal neutron spectra.

The particular time structure of the ESS neutron source provides a number of advantages for the instruments [4,5]:

- The low repetition rate lends itself naturally to measuring over a large bandwidth of neutron energies, which is particularly useful for studying hierarchical systems with structure (or vibrations) over many length (or time-) scales. This characteristic is enhanced by the moderator design, in which the adjacent placement of the cold and thermal moderators allows instruments to use both spectral ranges simultaneously, becoming effectively "bispectral".
- The pulse length of 2.86 ms provides adequate wavelength resolution with very high flux for low-resolution applications, such as small-angle scattering, reflectometry, imaging and single-crystal diffraction. For instruments requiring high resolution, it provides an unparallelled level of flexibility, with the pulse length for each instrument selected using a "pulse-shaping" chopper placed close to the monolith shielding of the target station, with a variable opening time allowing an optimal and tuneable trade-off between resolution and beam intensity for each experiment.

In this Introduction to the instrument suite at the ESS, we will outline how the main design parameters of the facility were optimised: the neutron source time structure, the design of the moderators, the layout of the instrument halls and the choice of the initial suite of instruments.

1.1. Optimising the source time structure

At a long-pulse source such as the ESS, the time width of the slow-neutron pulses is primarily determined by the duration τ of the proton pulse incident on the target, which greatly exceeds the moderation time in the moderator-reflector assembly. The accelerator time structure is essentially defined by τ, together with the repetition period T of the proton pulses. One of the early challenges of the ESS design was to decide on the optimal combination of τ and T for the facility as a whole, balancing cost and capability of the accelerator while maximising the performance of the neutron beam instruments.

For reference the accelerator repetition rates of currently-operating pulsed spallation sources cover a range of frequencies from 10 Hz (ISIS Target Station 2) to 20 Hz (Lujan Center), 25 Hz (J-PARC Material and Life Science Experimental Facility), 50 Hz (ISIS Target Station 1) and 60 Hz (Spallation Neutron Source, Oak Ridge). At these facilities, the time width of the neutron pulses is primarily determined by the moderator characteristics rather than the duration of the proton pulse, and is typically of the order of 10–100 μs, varying with neutron energy and moderator design.

At an early stage in the ESS project, the technical baseline was set for a 20 Hz repetition rate with a proton pulse length of 2 ms, resulting in a duty cycle of $\tau/T = 1/25$ and a peak power of 125 MW when operating at a time-average accelerator power of 5 MW. These parameters were influenced by the experience of the superconducting linac at the SNS as to the optimal compromise between performance, reliability and cost, resulting in the peak accelerator power at the ESS being capped at 125 MW. However, analysis of a straw-man suite of 22 instruments indicated a number of potential issues in instrument layout and performance, which could be resolved by small but impactful changes to the repetition rate and proton pulse length, while maintaining the peak power and duty cycle [6].

1.1.1. Simplicity

When the wavelength resolution required by the instrument is better than that provided by the source pulse length, a pulse-shaping chopper is used to reduce the effective pulse length. This introduces the advantage of allowing the wavelength resolution to be adjusted on the fly to choose the optimal trade-off between resolution and flux for each experiment. The implementation of pulse-shaping choppers varies somewhat for different instrument types.

Chopper spectrometers extract a pulsed monochromatic beam of neutrons by phasing a chopper with a short opening time placed close to the sample, with respect to the source pulse. In this case, the optimum repetition rate is often higher than that given by the neutron source itself. This is addressed at the ESS by making use of repetition-rate multiplication (RRM), in which a sequence of different wavelengths is selected from each source pulse [7,8], allowing the time frame to be usefully filled between subsequent proton pulses, and greatly increasing the dynamic range of the measurement. In this case, the pulse-shaping chopper can be placed some distance from the source and run at an integer multiple of the source frequency, such that subsequent chopper openings extract different incident energies.

The majority of instruments at pulsed sources make use of a continuous wavelength band. They are termed "white-beam" instruments, though in practice their bandwidth usually needs to be restricted in order to avoid frame overlap. When a pulse-shaping chopper is needed on a white-beam instrument, it is always placed as close to the source as possible, in order to minimise the reduction in bandwidth, resulting from the finite distance L_1 between the source and the chopper. At ESS L_1 is set by the dimensions of the target shielding monolith and the shutter system around it to around 6.3 m. When the ratio between L_1 and the length L_2 between the pulse-shaping chopper and the instrument's detectors is equal to the duty cycle τ/T, the wavelength band transmitted through the pulse-shaping chopper fully fills the available time frame, avoiding both frame overlap and wasting counting time on unnecessary waiting time between subsequent neutron pulses. This is known as the "natural" length of the instrument and is illustrated in Fig. 1(a).

The bandwidth of a white-beam instrument with a pulse-shaping chopper can be expressed rather simply as $\Delta\lambda \approx 4T/L_2$, where the bandwidth $\Delta\lambda$ is in Å, L_2 is in m and T is in ms. Instruments which are set to the natural length thus have a fixed bandwidth, unless they choose to skip pulses, which is usually not optimal. Some white-beam instruments therefore choose a length which is less than the natural length, in order to achieve a larger bandwidth. When such instruments use a pulse-shaping chopper to adjust their wavelength resolution, they employ a technique known as wavelength-frame multiplication (WFM), in which the reduction in bandwidth imposed by the placement of the pulse-shaping chopper is compensated by extracting a sequence of pulses [9]. In WFM, the pulse-shaping chopper is run at an integer multiple of the source frequency, extracting a sequence of pulses each covering a wavelength band which, when combined, overlap to leave no gaps in wavelength coverage, resulting in a full bandwidth equivalent to running with no pulse-shaping chopper or with one placed very close to the source. The time-distance diagram of 3-fold WFM is shown in Fig. 1(b).

About half of the instruments in the straw-man suite (SANS, reflectometry, spin-echo, monochromator-based) were not very sensitive to the time structure and therefore did not greatly influence the process of optimising the time structure. The other instruments generally employed pulse-shaping choppers with opening times which could be varied from very short to the full length of the proton pulse. Their optimum length was given by their wavelength-resolution requirement when operating in their lowest-resolution mode of 5%–10%, which is achieved by accepting the full source pulse. For a proton pulse length of $\tau = 2$ ms, corresponding to a 20 Hz repetition rate, this resulted in instrument lengths of typically 100 m, increasing linearly with pulse length. At a repetition rate of 14 Hz, corresponding to a proton pulse length of $\tau = 1/(25 \times 14\ \text{Hz}) = 2.86$ ms, the optimum length of these instruments was approximately 160 m. This coincides with the natural length of an instrument with a pulse-shaping chopper.

Running the neutron source at 14 Hz and 2.86 ms, thus allows many of the instruments to run without WFM, reducing the need for complicated multiplexing chopper systems, greatly simplifying their data reduction procedure, and avoiding systematic errors associated with merging overlapping data sets.

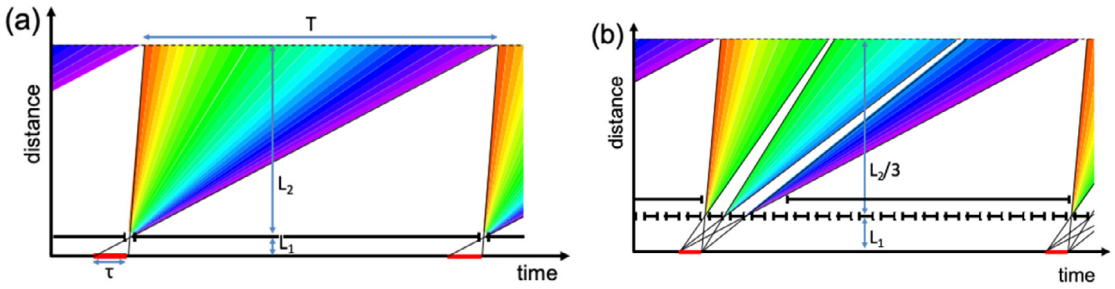

Fig. 1. Pulsing schemes for white-beam instruments at a long-pulse source. (a) Illustrating the "natural" length of an instrument with a pulse-shaping chopper: fully filling the time frame with the bandwidth transmitted by the pulse-shaping chopper. (b) using three-fold wavelength-frame multiplication to achieve the same objective on an instrument one-third of the length. Note that an additional chopper has been added to the WFM scheme, in order to avoid contamination of the signal from the unwanted additional openings of the fast pulse-shaping chopper. This is known as a "bandwidth" or "frame-overlap" chopper.

1.1.2. Flexibility, operability and upgradeability

By choosing a source repetition rate of 14 Hz, the optimum length of many of the instruments thus comes out to be 160 m. This means that a single dedicated instrument hall can be built for those instruments instead of several smaller halls, improving many of the operational aspects: sample environment and sample preparation labs can be situated more conveniently with shorter distances to transport samples and equipment between the instruments and fewer labs required to service the instruments. It also reduces the cost of the buildings.

Having a common length for many types of instruments will also allow ESS to plan better, reserving space for expansion of the instrument hall for future instruments. In addition, it gives more scope for instrument upgrades, as the instrument length optimised for the original instrument is more likely to be optimal for the upgraded version. This builds in flexibility for the future.

The 160 m instruments will have longer guides than any existing instruments. A considerable effort has therefore gone into ensuring that the performance of such very long neutron guides firstly is well understood and optimised [10–14] and secondly that the building infrastructure is able to ensure a high stability of the guide supports. For the majority of their length, these long neutron guides will therefore be supported by piles which rest on the bedrock below the floor. The piles are decoupled from the floor on which the guide shielding will rest, which is less sensitive to movements.

1.1.3. Favouring cold-neutron performance through increased bandwidth

In the analysis of the variation in performance of the straw-man instrument suite with the time structure, the overall effect averaged over the suite was largely neutral. This global averaging, however, concealed some significant deviations from the mean when moving from 20 Hz and 2 ms to 14 Hz and 2.86 ms.

(a) SANS, reflectometry and spin-echo instruments benefitted from the increased wavelength range offered by the longer repetition period. Their performance did not suffer significantly from the degraded wavelength resolution arising from the correspondingly increased pulse length. 7 of the 22 instruments fell into this category.
(b) Some instruments made only limited use of the source time structure. These included fundamental physics and crystal-monochromator instruments, for which mainly the time-average flux is important. 2 of the 22 instruments fell into this category.
(c) Instruments such as chopper spectrometers which employ RRM had a weak preference for shorter repetition periods. They use RRM to compensate for the fact that their preferred repetition frequency is much higher than the source frequency. A higher source frequency would reduce their need for RRM and makes their data-collection strategy more similar to existing instruments, simplifying their data analysis. 3 of the 22 instruments fell into this category.
(d) Very high resolution instrument such as backscattering and high-resolution diffraction also had a preference for shorter repetition periods. These instruments cut out only a small fraction of the pulse length to achieve the desired resolution and did not benefit greatly from the increased wavelength range offered by the increase in repetition period. 3 of the 22 instruments fell into this category.
(e) Instruments which employ WFM had a weak preference for a longer repetition periods, as it removes the need for WFM as described in the previous section. 7 of the 22 instruments fell into this category.

The biggest winners were the intrinsically low-resolution instruments in category (a) above. This is consistent with a strategy of favouring the performance of the cold-neutron instruments, addressing questions in soft condensed matter and the life sciences. Favouring the natural strengths of a long-pulse source in this is way will serve to maximise its scientific impact.

1.1.4. Increasing the plateau region of the neutron pulse

Many of the instruments at the ESS will employ a pulse-shaping chopper to define the source time structure. When the pulse at the source is significantly longer than the opening time of the pulse-shaping chopper, a regular trapezoidal resolution function is obtained by phasing the chopper to open during the plateau region of the source pulse. When the source pulse is comparable to the opening of the pulse-shaping chopper, a less favourable resolution is obtained, as well as a loss of integrated flux, as illustrated in Fig. 2.

As can be appreciated from these figures, using a chopper to extract a 2.00 ms wide pulse would result in an even more favourable comparison for the 2.86 ms moderator pulse. For instruments where the shape of the resolution function is of high importance, their design should be adapted to use only the flat top of the source pulse.

1.2. Moderator design

A key design feature of the ESS moderator system is the flexibility allowed by co-locating thermal (water) and cold (parahydrogen) moderators, so that both are viewable at the entrance window of the guides serving the instruments. This allows all instruments to freely choose the spectrum they need by aligning their guide system to point at the desired source and, if required, employ a bispectral switch system [13,15,16] to stitch the cold and thermal spectra together, thus increasing the available bandwidth. This became a design requirement on the moderator and beam extraction system from an early stage in the project: to allow each beamport to freely choose its neutron spectrum: cold, thermal or bispectral, thus maximising the flexibility availability to instrument designers and hence instrument performance.

The TDR design of the ESS moderators employed volume parahydrogen moderators, as pioneered and implemented at J-PARC [17] with slab-shaped water wings acting as the sources of thermal neutrons. This

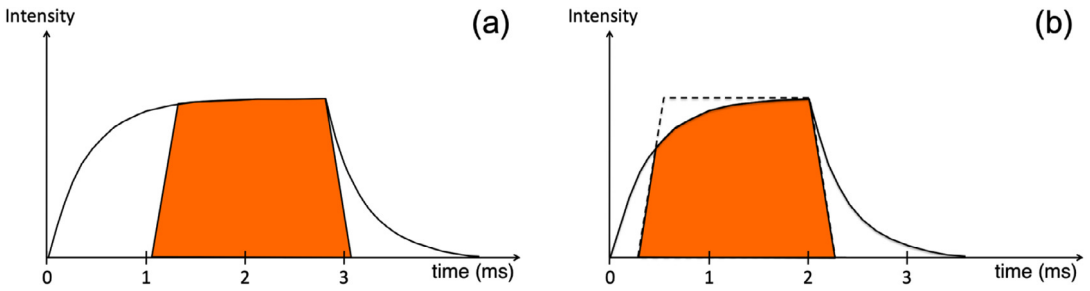

Fig. 2. Pulse-shaping chopper with a 1.5 ms opening, using a 2.86 ms (a) and a 2.00 ms source pulse (b).

was calculated to deliver a time-average neutron brightness equivalent to that of the ILL. Shortly after publication of the TDR [1], it was realised that significant increases in both cold and thermal neutron brightness could be achieved by reducing the height of the moderators. Some of the brightness increase is offset by the reduced illumination of the neutron guide system when viewing a smaller source. This trade-off was the subject of a comprehensive optimisation study [2], resulting in the choice of a height of 3 cm for both the cold and thermal moderators. Compared to the TDR moderator system, the instrument suite gained an average flux increase of about a factor of 2. The ESS moderator performance is illustrated in Fig. 3, in which a single neutron pulse at a wavelength of 5 Å is shown in comparison to the leading neutron sources of today.

While the vertical dimensions of the moderators were being optimised for maximising the flux on the instruments, a variety of possible horizontal layouts of the cold and thermal moderators were also considered. These were evaluated based on three criteria: (1) side-by-side co-location of cold and thermal moderators to allow spectral flexibility for as many beamports as possible, (2) large projected width of both moderators seen from the guide entrance, to maximise the guide illumination, (3) high spectral brightness for as many beamports as possible. The best solution to these constraints was the "Butterfly" geometry, shown in Fig. 4.

By having a single moderator assembly above the spallation target serve all of the currently-planned instruments, we leave scope for a future, as yet unspecified moderator below the target. This provides an upgrade path for future capabilities which might include enhanced performance for very cold neutrons or a large-area cold moderator for a dedicated particle-physics experiment.

1.3. Facility layout

The primary upgrade path of the ESS was identified from an early stage as the addition of more instruments in the main experimental halls, rather than the construction of a second target station. This is a departure from the approach taken at the current short-pulse spallation sources, several of which already have or are considering a future second target station. Tied to the ESS upgrade path is the upgradeability of the first target station. This is limited by the number and size of the openings in the target monolith through which neutron beams can be extracted. Current short-pulse spallation sources incorporate between 20 and 23 such beamports. The ESS target monolith is designed to allow the extraction of neutron beams through 42 beamports, at an angular spacing of 6°, about half the angular separation at other facilities. This large number of beamports ensures adequate scope for increasing the number of instruments at the ESS before needing to build a second target station. Adding instruments at a single target station is far more cost-effective: it adds value to existing infrastructure, such as the experimental halls and the target station, and does not require an expensive upgrade to the accelerator in order to provide proton beam to more than one target station.

The beamports at ESS serve instrument halls which are arranged in sectors, labelled with their compass directions, as shown in Fig. 5. The 42 beamports are labelled by their sector (N, S, E, W) and a number between 1 and 11 where 1 is used for the beamport at 30° to the proton beam axis. By convention, the beamports perpendicular to the proton beam axis are labelled S11 and W11.

The West sector is designed for instruments with an average length of 165 m. That length is determined by the closest distance which a pulse-shaping chopper can be placed to the source, of $L_1 = 6.3$ m, and the source duty cycle of $\tau/\mathrm{T} = 1/25$. The instrument length which allows the full bandwidth transmitted by the pulse-shaping chopper to be used, while just avoiding frame overlap, is given by $L_1(1+T/\tau) = 165$ m, as illustrated in Fig. 1(a).

The South sector is foreseen for instruments between 50 m and 80 m in length, while instruments in the East and North sectors will be shorter still (down to about 20 m). The instrument halls are designed to allow instruments to populate all the beamports in the West and South sectors, while the shorter length of the instruments in the North and East sectors will cause some instruments to prevent the use of adjacent beamports due to the lateral size of their instrument components such as their cave shielding. In the North sector, where the shortest instruments are, we expect to be able to use every other beamport, resulting in an effective beamline separation of 12°, as achieved at current short-pulse spallation sources. The East sector will be intermediate. The net result is that we expect about 32–35 of the beamports to be useable at any one time.

The instrument halls are dimensioned to accommodate the 22 instruments foreseen within the current scope of the ESS. A significant upgrade to that number might require extensions to the halls or the construction of new halls. To facilitate such construction, a number of areas adjacent to the North, South and West sectors have been designated as upgrade areas which are kept clear for future expansion.

The target monolith is surrounded by a shielding structure, known as the bunker, which provides a common shielded space in which instrument components such as choppers are installed, and separated from the experimental halls by a 3.5 m thick shielding wall. The open bunker volume extends to a distance of 11.5 m from the target centre-line for the North and East sectors, and 24.5 m for the South and West sectors due to the greater instrument length in those sectors. This both saves on the cost of shielding for individual instruments, and provides additional integrated shielding around the target monolith, so as to satisfy the very low background requirements of the instruments. Access inside the bunker will take place only during accelerator shutdowns. Maintenance and installation of the in-monolith optics of individual instruments is performed by horizontal extraction of the monolith beam plugs into the bunker area.

Due to the small angular separation of the beamlines, there are no beam shutters integrated into the monolith. Instead, at the monolith wall at 5.5 m from the target centre-line, a 50 cm long light shutter system (LSS) is installed at each beamline, which allows the insertion of a gamma blocker into the beam axis, intended only to be used when the proton beam is off, so as to allow safe access into the bunker area for maintenance. Each instrument has one or more beam shutters located downstream from this position, to allow normal operation of the beamline and/or maintenance access to components upstream of the instrument cave.

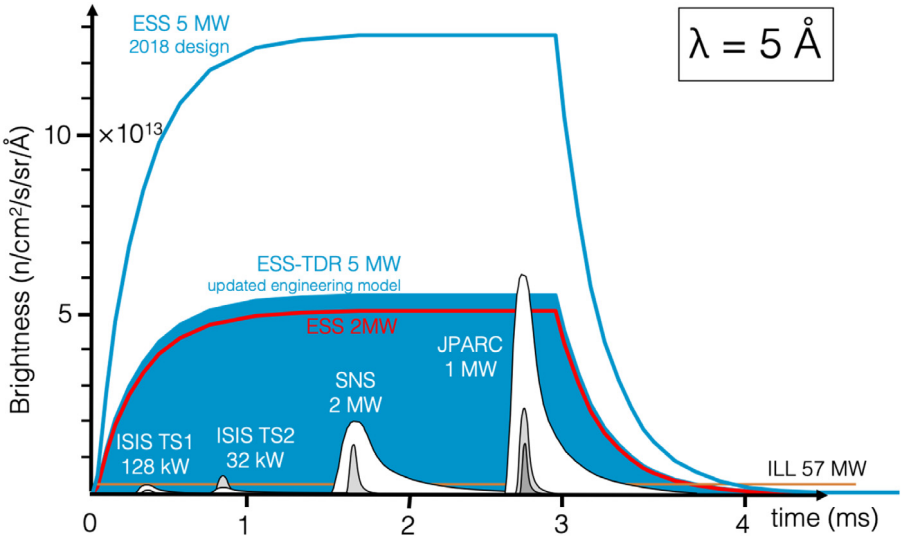

Fig. 3. Time-dependent brightness of the ESS cold moderator at a wavelength of 5 Å. For comparison, the source brightness available at the neutron sources ISIS in the UK, SNS in the US, J-PARC in Japan, and ILL in France are shown for the moderators used for this wavelength. For ISIS, SNS and JPARC, the pulse shapes of more than one moderator are shown, to illustrate the trade-off between resolution and intensity available there. For ESS, three pulse heights are shown: That corresponding to the TDR moderator design (full blue), the current design at 5 MW of accelerator power (blue line), and at 2 MW (red line), corresponding to the accelerator power in 2025, at the end of the ESS construction project.

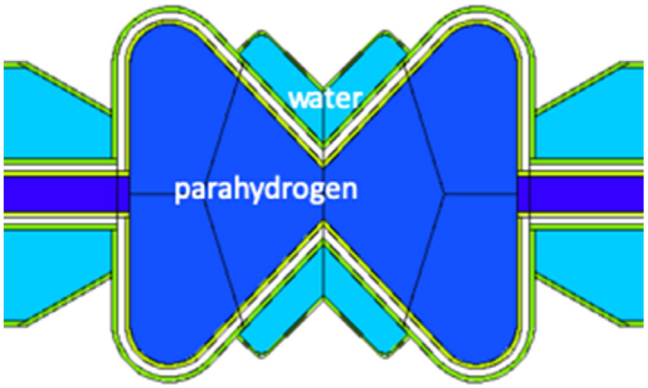

Fig. 4. Butterfly moderator design. The dark blue colour indicates parahydrogen. The main hydrogen volume is about 24 cm wide. The light blue volumes are water. The proton beam is incident from the right. Each beamport is oriented to point at the nearest water-hydrogen junction. Cold or thermal spectra can be extracted by tilting the guide system within the beamport to point at the adjacent hydrogen or water region, respectively. More detail on the moderator optimisation and beam extraction can be found in [2,3]. (For interpretation of the references to colour in this figure legend, the reader is referred to the web version of this article.)

1.4. Instrument selection

As mentioned earlier, a reference suite of 22 instruments was assembled for the TDR in 2013, based on a set of science drivers, identified at the time, which was used for outlining the technical and scientific scope of the ESS project, as well as for planning and budget purposes.

All instruments were designed to make optimal use of the unique design of the ESS neutron source, in order to maximise their scientific output. The high source brightness can be used in a number of transformative areas:

- Measuring very small amounts of sample, or to probe volumes/areas of larger, non-uniform samples
- Measuring very quickly, giving access to kinetics on the tens of ms time scale
- Making parametric studies, covering large volumes of parameter space such as temperature, flow conditions, magnetic field, pressure, etc.
- Studying weak effects, i.e. small cross-section events requiring high counting statistics
- Polarised-neutron studies, allowing the separation of coherent, incoherent and magnetic scattering, again at the expense of beam intensity

An instrument selection process was set up, consisting of annual competitive proposal rounds. Instrument concepts were developed around their science case, resulting in instrument proposals being submitted over three proposal rounds in 2013, 2014 and 2015. In each proposal round, the submitted proposals were peer-reviewed and ranked in order of scientific interest that would best serve the future scientific community of the ESS. A strategy for early scientific success was formulated which prioritised instruments falling within the following categories:

- World-class instruments that address the needs of the bulk of the user community and thus bring in our community and ensure early high-impact science.
- Instruments that build on the unique strengths of the ESS source, providing transformative new capabilities.
- Instruments catering to science communities with limited neutron usage today, but with clear potential to bring large scientific impact.

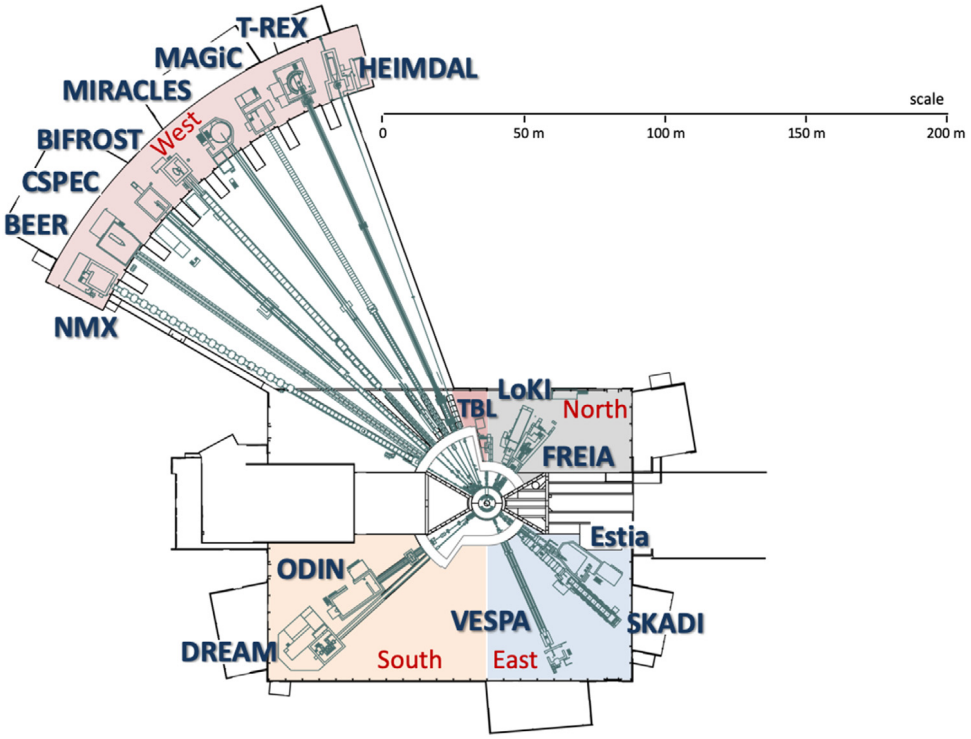

Fig. 5. Layout of the Instrument Suite, arranged in the four experimental halls labelled with their compass directions. The proton beam is incident from the right.

Over the course of this process, 39 individual instrument concepts were studied. Of these, some competing concepts were merged into collaborative proposals, and a few did not result in complete concepts. A total of 26 instrument proposals were submitted over the three proposal rounds, resulting in the suite of 15 instruments listed in Table 1, which is shown together with the remaining instruments from the TDR reference suite. A complete listing of the instrument concepts studies can be found in [18]

The 15-instrument suite includes many workhorse, general-purpose instruments addressing wide and varied user communities, while also including a number of more specialised instruments, consistent with the early success strategy. The science enabled by the instruments will be supported by a number of essential activities related to sample environment, user laboratories, instrument technologies, control and analysis software, and so on, the description of which generally falls outside the remit of this paper. One instrument technology which deserves a specific mention, however, is in the area of neutron detectors. The instrument projects are supported by significant developments in detectors in order to deal with the very high count rates expected at ESS, and also to provide alternative technologies based on thin films of ^{10}B to compensate for the reduced availability and increased cost of ^{3}He gas over the last decade. Many of the instrument concepts outlined here would not be feasible without these developments.

The present paper provides a systematic overview of the initial instrument suite of the ESS. It is intended as a reference for the instrument suite, and can be considered as a partial update to the TDR. It covers both the scientific scope and technical performance of each of the 15 user instruments, as well as a test beamline for characterising the moderator performance.

The instruments all pass through a series of project phases, and at the time of writing, all of them have passed from preliminary to detailed engineering design. Their scope and performance have thus been fixed and form the basis of the descriptions in this paper.

For all instruments, their design has been optimised and their performance thoroughly evaluated using both analytical calculations and Monte-Carlo ray-tracing simulations by means of the established software packages McStas [19] and VITESS [20].

Many instruments have well-identified upgrade paths to expand their day-one scope, often involving an increase in detector coverage. This occasionally motivates aspects of the design of the instrument, in which case it is covered in the instrument descriptions, though in all cases, the emphasis is on the day-one scope. Instrument performance is given at an accelerator power of 2 MW, the power level foreseen within the ESS construction budget.

The instruments are arranged by instrument class: Section 2 covers instruments measuring large-scale structures, including small-angle neutron scattering, reflectometry and macromolecular crystallography. Section 3 covers the instruments for imaging and engineering diffraction, as well as the test beamline, while Section 4 describes the diffraction instruments, covering both powder and single-crystal instruments. The spectroscopy instruments are covered in Section 5, including both direct-geometry (monochromatic) instruments and indirect-geometry instruments. The paper concludes with a summary and outlook section.

2. Instruments for large-scale structures

The functionality of a material or macromolecule is very often related to the nuclear and magnetic structure and interactions on the nanometre to micrometre length scale. The types of system studied by instruments in this class include macromolecules, molecular assemblies, nanoparticles, complex fluids, polymers, composites, alloys and geological materials.

ESS has five instruments that fall into the category of large-scale structures. These instruments focus on providing new scientific capability through enabling exploration of wider parameter spaces in more detail, measurements on smaller samples and gauge volumes, and shorter time-scale kinetics measurements. Two small-angle neutron scattering (SANS) instruments, LoKI and SKADI, provide nanometre to micrometre nuclear and magnetic structure. Two neutron reflectometers, Estia and FREIA, provide the nuclear and magnetic structure of thin films up to a few hundred nanometres in thickness with a resolution of a few Ångström. The neutron macromolecular crystallography instrument, NMX, provides atomic resolution structure of

Table 1
ESS Instrument Suite. Highlighted and named instruments (e.g. ODIN) are those which are currently in construction. The others are the remaining instruments from the TDR reference suite, which serve as placeholders for instruments 16–22. The main scientific communities addressed by the instruments are indicated with the symbols shown.

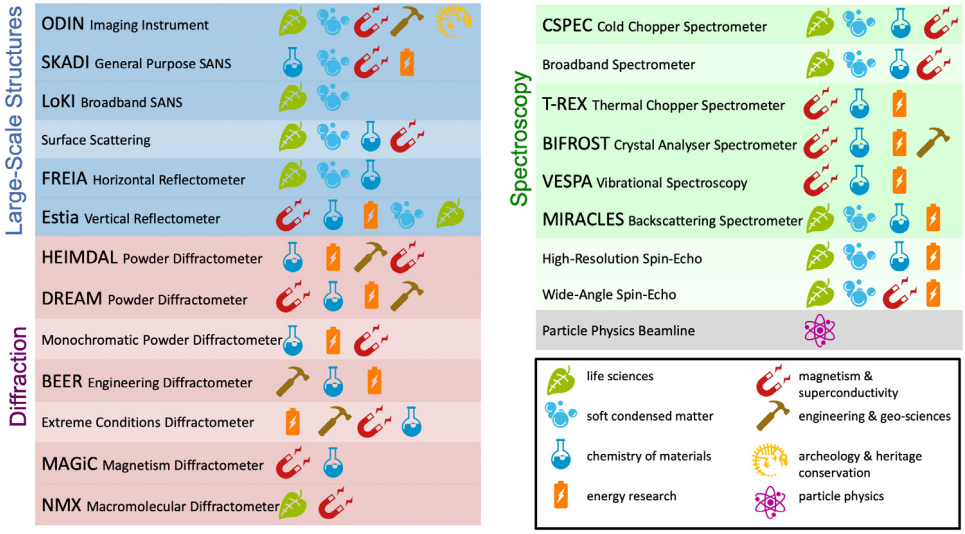

macromolecules, primarily proteins, making use of the sensitivity of neutron scattering to hydrogen.

LoKI and SKADI are a complementary pair of SANS instruments that together cover the resolution-bandwidth space available at ESS, both viewing the cold part of the moderator.

The two SANS instruments together deliver Q-range coverage from 2 $Å^{-1}$ to 1 × 10^{-4} $Å^{-1}$, spanning the size range from nanometres to micrometres. A broad range of sample environment can be used on both instruments interchangeably, and SKADI enables studies of magnetic materials with the availability of a polarised beam and support for the use of a polarised-^{3}He analyser.

The two reflectometers work together to support the full range of science done with the technique. The instruments enable access to horizontal, free-liquid surfaces (FREIA), buried and free interfaces in the horizontal and vertical planes, and the study of magnetic materials (Estia). Both instruments have high beam flux and unique designs that enable fast measurements. The Selene guide concept of Estia enables access to measurements on samples as small as 1 mm^2.

The SANS and reflectometry instruments all make full use of the flexibility afforded by the ESS time structure to deliver access to a wide Q-range in a single measurement (Fig. 6). The instruments also have operational modes that enable the Q-range and resolution to be tailored to the experiment in question.

The NMX Macromolecular Diffractometer is a time-of-flight (TOF) quasi-Laue diffractometer optimised for small samples and large unit cells dedicated to the crystallographic structure determination of biological macromolecules. The main scientific driver is to locate the hydrogen atoms relevant for the function of the macromolecule.

2.1. LoKI — *Broad-band small-angle neutron scattering*

2.1.1. *LoKI science case*

LoKI is one of two small-angle neutron scattering (SANS) instruments at ESS, designed with the needs of the soft matter, materials, and bio-science communities in mind. The trend in all these fields is towards complexity and heterogeneity. These factors manifest themselves both spatially and temporally, and therefore the high flux (up to 2 × 10^8 n s^{-1} cm^{-2} at sample position at 2 MW accelerator power), small beam sizes and wide simultaneous Q-range (10^{-3} to 2 $Å^{-1}$) available at LoKI, will make it optimal for performing structural and time-resolved studies.

The small beam sizes/high flux available at LoKI are expected to make scanning, flow-through and microfluidic experiments routine.

Table 2
LoKI Quick Facts. L_1 and L_2 refer to the length of the collimation section (end-of-guide to sample) and sample-detector distance, respectively.

LoKI Quick Facts	
Instrument Class	SANS
Moderator	Cold
Primary Flightpath	23.5 m, L_1 = 3, 5, 8 m
Secondary Flightpath	L_2 = 1.5 m, 3 m, 5–10 m
Wavelength Range	2–22 Å
Standard Mode (14 Hz)	
Bandwidth	7.5 Å [L_2 = 10 m] 10 Å [L_2 = 5 m]
Flux at Sample at 2 MW	4 × 10^8 n s^{-1} cm^{-2} [L_1 = 3 m] 5.6 × 10^7 n s^{-1} cm^{-2} [L_1 = 8 m]
Q-Range	0.01–2 $Å^{-1}$ [L_1 = 3 m, L_2 = 1.5, 5 m] 0.005–2 $Å^{-1}$ [L_1 = 8 m, L_2 = 1.5, 10 m]
Pulse Skipping Mode (7 Hz)	
Bandwidth	15 Å [L_2 = 10 m] 20 Å [L_2 = 5 m]
Flux at Sample at 2 MW	2 × 10^8 n s^{-1} cm^{-2} [L_1 = 3 m] 2.8 × 10^7 n s^{-1} cm^{-2} [L_1 = 8 m]
Q-Range	0.005–2 $Å^{-1}$ [L_1 = 3 m, L_2 = 1.5, 5 m] 0.002–2 $Å^{-1}$ [L_1 = 8 m, L_2 = 1.5, 10 m]

The wide simultaneous Q-range will benefit dynamic structures, such as systems under shear. A high flux and good signal-to-noise ratio will allow for high throughput, and greatly improve the study of weakly scattering biological samples. Large area detector arrays have been developed, which allow the entire Q-range to be accessed without any movement of the main instrument optics or the sample.

Moreover, LoKI is uniquely suited to studying dynamic systems, which change their structure over short periods of time, enabling "single-shot" kinetic measurements in sub-second time scales, similar to modern day X-ray facilities. Such changes may be induced by internal and external influences, such as flow, stress/strain, temperature, chemical composition, pressure, humidity, magnetic and electric fields. LoKI also aims to answer the ever-growing demand by the user community to perform *in situ* and/or simultaneous characterisation of the system under investigation with SANS. Thus, LoKI has been designed with a flexible sample area with the potential to support the use of multiple simultaneous techniques, integrated with neutron data collection so that correlation of analysis between methods can be routinely employed.

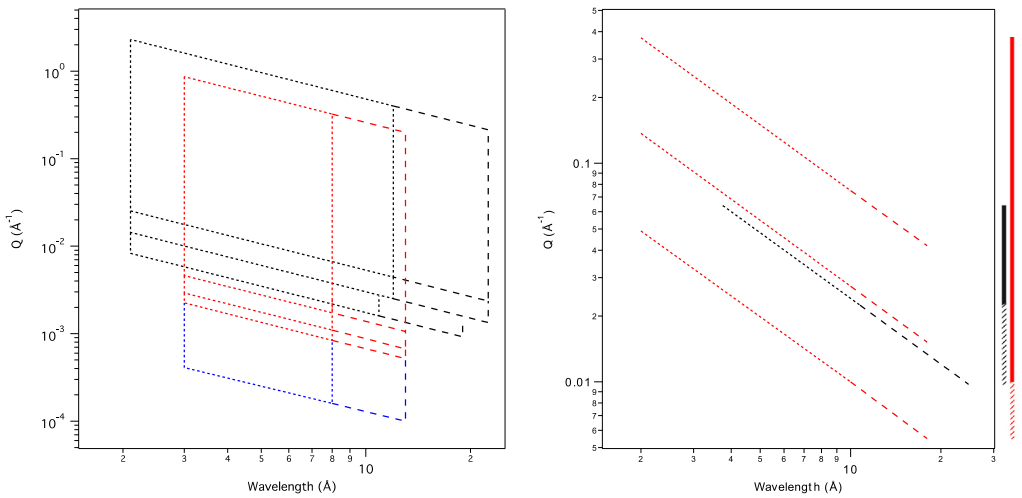

Fig. 6. (a) Q-space available at each instrument with different collimation settings (black = LoKI, red = SKADI, blue = SKADI VSANS) in a single measurement at 14 Hz (short dashes) and 7 Hz (short dashes and long dashes) using a 10 × 10 mm^2 sample aperture and typical wavelength ranges. (b) Q ranges available to the reflectometry instruments (black = Estia, red = FREIA) at 14 Hz (short dashes) and with pulse-skipping (short and long dashes, 4.7 Hz for Estia, 7 Hz for FREIA), using typical wavelength ranges and incident angles (0.45°, 1.25° and 3.42° for FREIA and 1.1° for Estia) and without moving the sample. Bars to the right shows the simultaneous Q-range available. (For interpretation of the references to colour in this figure legend, the reader is referred to the web version of this article.)

As the key scientific drivers for LoKI are to allow fast measurements across the scientific scope of SANS research, it is expected to cover a wide-range of scientific interests, including:

- Complex fluids under flow using rheology and microfluidics;
- Formation of gels *in situ*;
- Weakly scattering biological systems;
- Non-equilibrium systems involving fast exchange kinetics;
- *In operando* fuel cells and batteries;
- Materials which transform their structures in response to external stimuli, e.g. light, temperature, pressure and magnetic and electric fields.

2.1.2. LoKI instrument layout

LoKI is located in the north sector on beamport N7 and views the cold part of the moderator. An overview of LoKI can be seen in Fig. 7 and the main instrument parameters can be found in Table 2. The instrument makes use of a pair of benders located in the monolith and the bunker wall. The benders have a radius of curvature of 61.25 m, with 5 channels and m = 3 supermirror coatings on all surfaces. The bender pair provides for twice out of line-of-sight curvature to minimise the intrinsic background, and offsets the beamline down vertically by approximately 0.5 m. The guide size is 30 mm × 25 mm (H × V) throughout the instrument.

The in-bunker section of the instrument consists of a bandwidth chopper pair at 6.5 m from the source, a straight m = 2 guide section, and an instrument shutter. The bandwidth chopper pair selects the wavelength range and the two discs are configured to cut the beam from the same direction and provide a variable opening *via* changing the relative phasing of the pair.

After the second bender, which is placed in the bunker wall, is another chopper pair, placed at 15.1 m from the source, to suppress frame overlap. Similarly to the bandwidth choppers, the frame overlap chopper discs cut the beam from the same direction and allow for a variable opening. The frame overlap chopper pair is followed by the collimation section which consists of two moveable blocks, each made of steel and polyethylene, and each containing an open beam tube with boronated walls and an m = 2 guide section.

The combination of positions of the two blocks gives LoKI possible collimation lengths of 8 m, 5 m, and 3 m, with 4-jaw slits used to define the beam size and position. After the collimation is a flight tube of adjustable length leading to the sample position, at 23.5 m from the source, where a choice of 4-jaw slit or pre-defined apertures are available to match the beam size to sample requirements.

Using the full ESS pulse of 2.86 ms and two pairs of choppers will provide a wavelength band of up to 10 Å at 14 Hz and up to 20 Å at 7 Hz. Space for additional wavelength frame multiplication (WFM) choppers is reserved in the bunker to allow upgrade to a measurement configuration with improved wavelength resolution.

The LoKI sample area has been designed to support installation of any ESS standard sample environment and has a mounting and interchange system that allows easy transfer of equipment between LoKI and SKADI.

The detector array system on LoKI is composed of multiple banks of stacked ^{10}B-coated straw-tubes [21] from Proportional Technologies Inc. The front banks are centred at ~1.5 m from the sample, and the middle banks are centred at ~3 m from the sample, tilted slightly to maximise coverage. Finally, the rear bank is moveable between 5 m and 10 m from the sample. This design and technology provides large coverage with good efficiency.

2.1.3. LoKI expected performance

Simulations using McStas indicate that LoKI will have a maximum flux on sample of 2 × 10^8 n s^{-1} cm^{-2} using the 3 m collimation length at 2 MW accelerator power. The flux on sample is dependent on the collimation choice and Fig. 8 shows the flux on sample as a function of beam divergence which is relevant for both minimum Q and $\Delta Q/Q$ resolution

2.2. SKADI — Small-angle neutron scattering with high resolution

2.2.1. SKADI science case

The Small-K Advanced DIffractometer, SKADI, is one of two SANS beamlines at ESS. It is a versatile SANS instrument designed with high resolution and very low Q SANS measurements in mind (see Table 3).

The scientific areas targeted by SKADI include investigations of smart materials, biological and medical research, magnetic materials and materials for energy storage, as well as experiments on nanomaterials and nanocomposites. These experiments have a high potential impact on science and society. In order to maximise the applicability of the results of these studies, SKADI is designed to accommodate *in-situ* measurements with custom-made sample environments to provide real-world conditions. These scientific areas need to close the structure determination gap between traditional SANS and imaging methods in order to examine bulk structure out towards several micrometres.

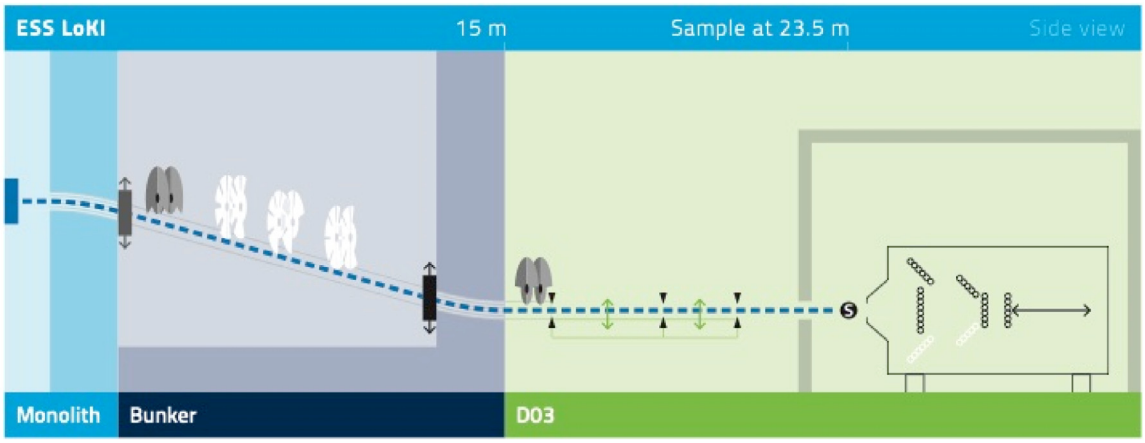

Fig. 7. LoKI instrument layout. Components shown in white are foreseen upgrades.

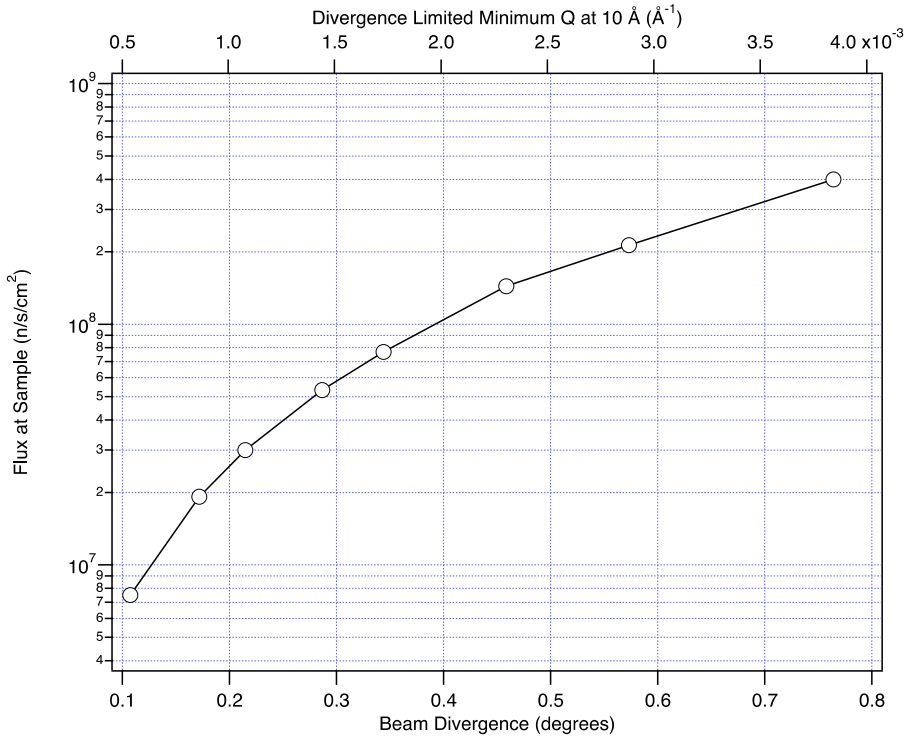

Fig. 8. LoKI flux as a function of beam divergence and divergence-limited minimum Q. The beam divergence given is the full width of the divergence distribution. The minimum Q is determined by the longest wavelength of 10 Å in the standard 14 Hz mode, as well as, in practice, the beam stop size and detector resolution.

Mechanical processing and in-situ macroscopic treatments (heat, pressure, shear forces) are another area of scientific focus for SKADI. Understanding the microstructural effects of processing steps on alloys, nanocomposites, and additive manufactured components is important for optimising their properties and lifetime. These types of studies often require large equipment to be installed on the beamline and SKADI has a flexible sample area design that can accommodate large, floor-mounted, sample environment.

The study of magnetic materials is enabled through the use of solid-state polarisers upstream of the collimation and support for a ^{3}He analyser after the sample. The high Q-resolution available on SKADI, combined with access to very low Q, will support studies of skyrmions and vortex lattices in superconductors.

2.2.2. SKADI instrument layout

SKADI is a classical pinhole SANS instrument with a maximum collimation length of 20 m, combined with a maximum sample-to-detector distance of 20 m [22]. The instrument is located on beamport E3 and the 3 cm × 3 cm neutron guide all along the instrument is designed for optimum brilliance transfer from the cold moderator.

The sample position is moved out of line of sight of the moderator using a deflector-type guide geometry, which offsets the beam by 20 cm within the bunker. This is designed to minimise the transport of high-energy radiation along the beamline, and combined with shielding around the detector tank is designed to ensure a low intrinsic background. A heavy shutter directly inside the bunker wall allows maintenance access to all out-of-bunker components during operation of the neutron source, including access to the sample area to change samples and equipment. The instrument layout is shown schematically in Fig. 9.

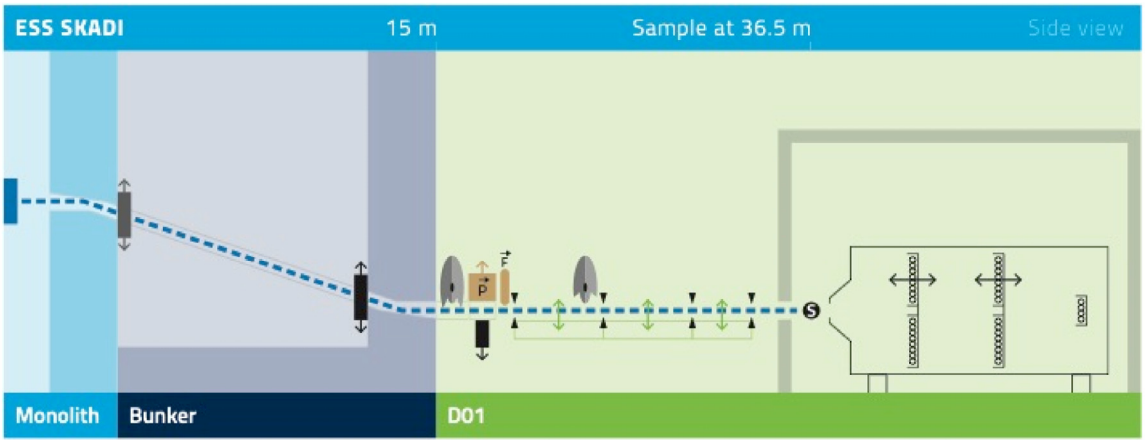

Fig. 9. SKADI instrument layout.

Table 3
SKADI Quick Facts. L_1 and L_2 refer to the length of the collimation section (end-of-guide to sample) and sample-detector distance, respectively.

SKADI Quick Facts	
Instrument Class	SANS
Moderator	Cold
Primary Flightpath	36.5 m, $L_1 = 4$, 8, 14, 20 m
Secondary Flightpath	$L_2 = 0.8$–4 m, 4–18.5 m, 20 m
Wavelength Range	3–21 Å
Polarised Incident Beam	Optional
Q-Range for VSANS option	Down to 10^{-4} Å^{-1}
Standard Mode (14 Hz)	
Bandwidth	5 Å [$L_2 = 20$ m]
Flux at Sample at 2 MW	9×10^8 n s^{-1} cm^{-2} [$L_1 = 4$ m]
	1×10^8 n s^{-1} cm^{-2} [$L_1 = 20$ m]
Q-Range	0.004–1 Å^{-1} [$L_1 = 4$ m, $L_2 = 1.6$, 20 m]
	0.001–1 Å^{-1} [$L_1 = 20$ m, $L_2 = 1.6$, 20 m]
Pulse Skipping Mode (7 Hz)	
Bandwidth	10 Å [$L_2 = 20$ m]
Flux at Sample at 2 MW	4.4×10^8 n s^{-1} cm^{-2} [$L_1 = 4$ m]
	5×10^7 n s^{-1} cm^{-2} [$L_1 = 20$ m]
Q-Range	0.001–1 Å^{-1} [$L_1 = 4$ m, $L_2 = 1.6$, 20 m]
	0.0005–1 Å^{-1} [$L_1 = 20$ m, $L_2 = 1.6$, 20 m]

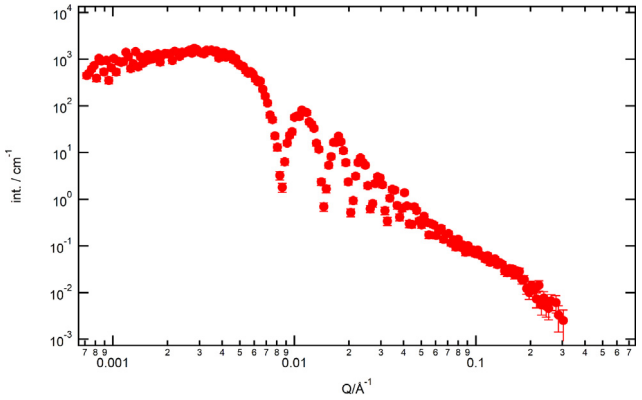

Fig. 10. McStas-simulated 1 s experiment on SKADI of suspended 500 Å spheres in solution at 20 m collimation distance. The illuminated sample volume was 3 × 3 × 1 mm^2 . Input parameters for the sample were the standard arguments for the McStas SANS_benchmark2 component for sample number 6, resulting in a volume concentration of 0.001 and a scattering-length density difference of 6×10^{-6} Å^{-2} . Key features such as the ability to perform in very short times and good resolution for large particles are demonstrated.

Immediately outside the bunker wall is the polariser unit consisting of a set of two polarising supermirror assemblies, optimised for the wavelength ranges between 3 and 8 Å and above 8 Å, respectively. After the polariser, there is an adiabatic spin-flipper to invert the beam polarisation direction.

Following the polariser unit is the collimation section, where four collimation settings of 20, 14, 8 and 4 m are available. A very-small-angle neutron scattering (VSANS) setup, employing converging slit collimators ending 2 m from the sample, will allow access to wavevector transfer values down to Q ≈ 10^{-4} Å^{-1}, equating to probing structures up to several micrometres in size.

The wavelength band is selected using two single disc choppers. The standard wavelength band used by SKADI will be 3 to 8 Å, but any 5 Å wide wavelength band up to 21 Å can be used.

SKADI features a new detector concept, SoNDe (Solid-State Neutron Detector) [23,24], employing scintillators directly coupled to photomultiplier tubes, and capable of fully exploiting the increased flux and brilliance of the ESS source. The detectors are arranged into 3 banks, with the forward two being moveable. These multiple banks of detectors at different distances, combined with the instrument bandwidth, will allow experiments to be performed in a single measurement over a wide Q-range. The moveable detectors allow the Q-range to be tuned and optimised for the experiment in question.

2.2.3. SKADI expected performance

The performance of SKADI was assessed based on neutronic simulations using the McStas package. A sample aperture size of 1 × 1 cm^2 is foreseen as the standard operation mode. Using the 8 m collimation setting this leads to a flux on the order of 10^8 n s^{-1} cm^{-2} at the sample position at 2 MW accelerator power. Combined with the large space available for sample environment and the wide available Q-range this will allow for fast dynamic measurements of samples undergoing irreversible transitions, such as the straining of a sample beyond the elastic limit or chemical synthesis in the sample environment. Another possibility to exploit the high flux and high resolution of SKADI is given for samples with low contrast and very small differences between sample conditions, such as ligand exchange on coated nanoparticles. All these possibilities can be combined with polarised scattering, opening up another area of possible samples and setups for SKADI. The fast exposure and ability to resolve large particles is shown in Fig. 10.

2.3. Estia — Focusing reflectometer for small samples

2.3.1. Estia science case

Estia is a reflectometer with a vertical-sample geometry (horizontal scattering plane) and an option for polarisation analysis. The instrument uses a truly focusing neutron guide, based on the Selene concept [25], that allows the accurate control of the beam footprint at the

Table 4
Estia Quick Facts.

Estia Quick Facts	
Instrument Class	Reflectometry
Moderator	Cold
Primary Flightpath	35 m
Secondary Flightpath	4 m
Wavelength Range	3.75–28 Å
Polarised Incident Beam	Optional
Polarisation Analysis	Optional
Sample Orientation	Vertical
Total Q-Range	0.001 to 3.15 $Å^{-1}$/−0.001 to −0.3 $Å^{-1}$
Standard Mode (14 Hz)	
Bandwidth	7 Å
Flux at Sample at 2 MW[a]	6×10^8 n s^{-1} cm^{-2}
Relative Q-Range	$Q_{max} = 2.85 \times Q_{min}$
Q-Resolution $\Delta Q/Q$	7.8%–3.0% over Q-range
2-Pulse Skipping Mode (4.7 Hz)	
Bandwidth	21 Å
Flux at Sample at 2 MW[a]	2×10^8 n s^{-1} cm^{-2}
Relative Q-Range	$Q_{max} = 6.6 \times Q_{min}$
Q-Resolution $\Delta Q/Q$	7.8%–1.3% over Q-range

[a]Full-divergence beam averaged over 5(H) × 10(V) mm^2.

sample position, which will make experiments on samples down to just 1 mm^2 feasible. For regular sample sizes (~1 cm^2) the high intensity of the focused beam will reduce measurement times to just a few seconds, giving users the opportunity to explore large physical parameter spaces with routine application of full polarisation analysis. The large detector angle coverage of Estia allows large wave-vector transfer reflectometry even with the longest wavelengths and the access of low-order Bragg-peaks. Dedicated low temperature, magnetic field and solid–liquid sample environment complete the instrument capabilities.

With these features, Estia will be perfectly suitable for any kind of study of surface and thin film properties in many areas of materials science, physics, chemistry and biology. Especially *in operando* studies and systems where large surface areas cannot be prepared easily will profit from the focusing beam. Example systems include exchange bias, multiferroics, battery materials, spontelectrics, cell membranes, magnetic nanoparticles, topological magnets, artificial spin-ices, self-assembly at solid–liquid interfaces, drug delivery and surface reactions.

2.3.2. Estia instrument layout

An overview of the Estia instrument can be seen in Fig. 11 and the main instruments parameters are listed in Table 4. Two vertically separated neutron beams are extracted from the cold moderator using a set of feeder optics. The feeder is composed of planar elliptical mirrors on the top, bottom and right side (looking down-stream) that refocus the beam on a spot 11 m away within the neutron bunker, with a horizontal block separating the two beampaths. The mirrors are segmented along the beam into one half that is placed within the monolith insert and the other situated inside a vacuum vessel within the bunker. The light shutter area does not contain any neutron optics and the divergence gaps due to this 0.5 m open region are filled by reducing the ellipses' short axis for the second mirrors. In front of the feeder focus is the 14 Hz bandwidth selection chopper. A set of L-shaped neutron absorbers within the same vacuum vessel form the so called virtual source, which cuts down the beam to the size of the sample surface.

The shape of the virtual source slit is projected to the sample location by a set of two elliptical neutron reflectors in the horizontal and vertical planes, the so-called Selene guide, which corrects leading-order aberration effects. As this projection requires extreme precision from the neutron guide, the elliptical reflectors for the two directions of one Selene guide section are placed within a single C-shaped carrier frame with interferometric metrology and remote adjustable kinematic mounts for the reflectors. The whole system is then placed on a heavy-duty kinematic mount with temperature stabilisation and inside a large vacuum vessel. This system is designed to allow for an upgrade to an additional Selene guide set for the second beam that was extracted by the feeder that also passes through the virtual source.

The projection produced by the Selene guide places the sample position at 35 m from the moderator. The reflected beam is recorded by a 2D position sensitive detector 4 m from the sample. A detector arm with air pads that can be rotated to a scattering angle of up to 140° supports the detector, flight tube and polarisation analyser. The sample positioning is performed using a rotation stage and a precision hexapod system. A liquid He flow cryostat can be attached to the hexapod with a fast connection kinematic mount inside a cryomagnet with open bore.

Neutron polarisation and frame overlap suppression are performed before and after the intermediate focus between the Selene guide mirrors using spiral-shaped transmission mirrors. The spin states are selected with radio frequency spin-flippers and the analysis uses two subsequent spiral mirrors on the detector arm. The reflection of the first analyser mirror can be collected on a different area of the detector to support measuring of two spin-states simultaneously.

The whole neutron flight-path, starting from the outer feeder vessel up to a sapphire window in front of the sample is evacuated and does not contain permanent neutron windows, in order to minimise beam losses due to scattering and absorption. The flight tube on the detector arm is filled with He gas to reduce background and intensity loss from air scattering. Due to the high rate and resolution requirements, Estia will use an ESS-designed detector based on ^{10}B layers under small angle (multi-blade design) that will deliver an unprecedented count-rate capability and 0.5 mm resolution in the reflection direction.

2.3.3. Estia expected performance

Neutronics calculations show that the neutron optics in Estia should be able to focus the beam down to sizes of 0.1 mm × 1 mm without any optical components close to the sample, thus allowing selected areas of the sample to be measured within large sample environment. Neutron flux at the sample position will be of the order of 10^9 n s^{-1} cm^{-2}, allowing measurements on 1 mm^2 samples within a few hours, as the one shown in Fig. 12. By reducing the chopper to 1/3 source frequency, the wavelength band can be extended, allowing a large Q-range of 0.01–0.14 $Å^{-1}$ to be measured without moving the sample. For 1 cm^2 samples this allows time-resolved experiments with sub-second time resolution.

2.4. FREIA — Fast reflectometer for extended interfacial analysis

2.4.1. FREIA science case

FREIA is a novel horizontal-sample geometry reflectometer with a broad simultaneous Q-range for structural and time-resolved studies. The instrument design has been optimised for the long-pulse source of the ESS and caters principally for soft condensed matter and life sciences, where both the structure and kinetics are of interest during the formation of thin films or in their response to environmental changes. While the sensitivity of neutrons to different isotopes and magnetic properties offers significant benefits in studies of multicomponent systems, there are significant gains to be made at ESS by taking advantage of the flux increase to allow studies of:

- Self-assembly of surfactants, polymers and proteins at interfaces
- Rearrangement processes in thin films, such as inter-diffusion or annealing processes
- Encapsulation and release of components
- Switchable materials and response to external stimuli
- Surface reactions

The key scientific drivers for the FREIA concept are to allow fast measurements across the scientific scope of reflectometry research

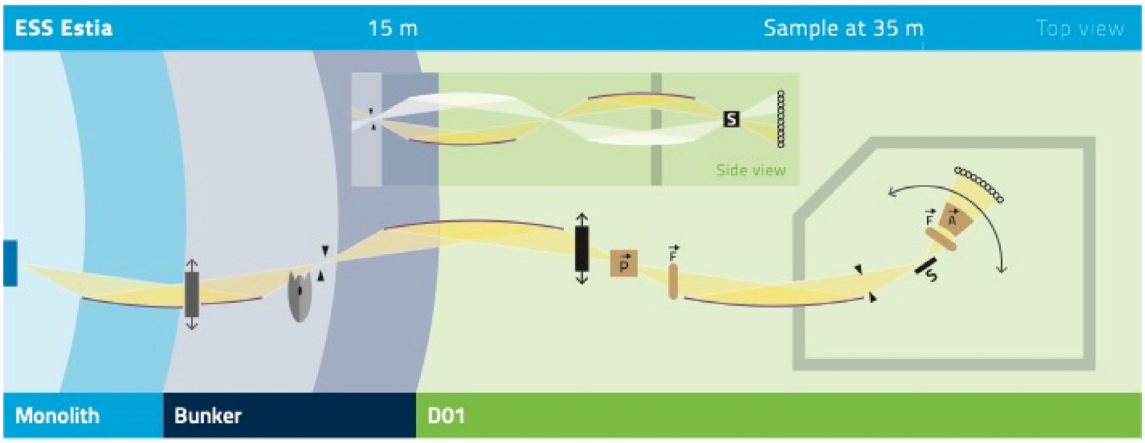

Fig. 11. Estia instrument layout. Components shown in white are foreseen upgrades.

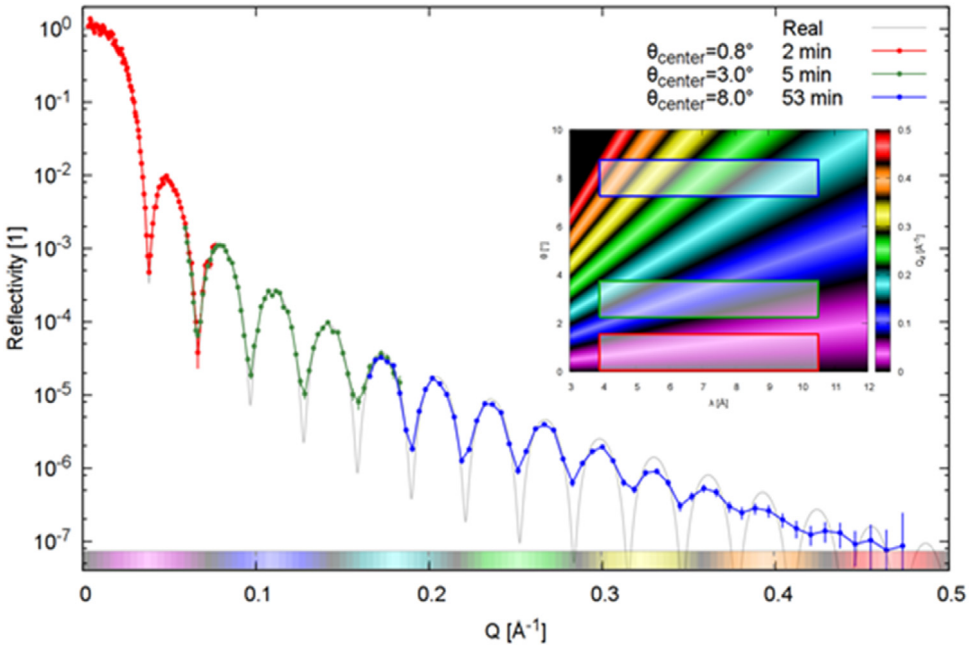

Fig. 12. Simulated experiment on a 1 mm^2 sample of a 20 nm nickel layer on silicon measured with Estia using the full divergence of 1.5°.

including free liquid interfaces. To achieve this, a novel guide and collimation system have been developed, which allow the entire Q-range to be accessed without any movement of the main instrument optics or the sample. The horizontal sample geometry combined with variable resolution will cater for a broad range of interfaces and samples, including smaller samples than currently used at existing sources.

2.4.2. *FREIA instrument layout*

An overview of the FREIA instrument is shown in Fig. 13. FREIA views the cold moderator and is located in the North hall on port N5. The instrument has a downward-oriented elliptical guide focusing a neutron beam with a broad vertical divergence and wavelength range onto a horizontal sample surface. From this high-divergence beam, a range of incident angles can be selected to cover the Q-range of interest without moving the sample.

The collimation system will have three possible modes. The first option is a standard pair of slits that will allow complete freedom to select an angular resolution or incident angle within a range of approximately 0.2°–3.7° for 1% $\leq \Delta\theta/\theta \leq$ 10% (depending on the desired beam footprint on the sample). Typical sample sizes are expected to be 30 mm (across the beam) by 40 mm (along the beam direction), although this can be reduced to 20 mm or extended to circa 80 mm. The second option allows fast measurements over the full Q-range to be carried out because the collimation system will be able to rapidly switch between up to three well-collimated incident angles. Since this means angle changes are achieved without moving the sample, this arrangement avoids the measurement dead time related to angle changes and settling times for free liquid surfaces. The speed of this switching will initially allow full Q-range measurements to be made in a few seconds, but a foreseen fast-shutter upgrade will increase this to a sub-second timescale. Finally, the collimation system will also allow for an m = 6 supermirror to be inserted to deflect the beam upwards and thereby allow reflections from underneath the interface to be measured (appropriate for liquid–liquid samples or where complex sample environments are required above the sample).

Also under consideration during ongoing design work is a "Full-divergence" mode. This may be appropriate for certain suitable samples and allows the full 3.5° divergent beam to impinge on the sample, in a manner similar to the standard mode of operation of Estia. This is likely to give a significant boost in flux, but is also likely to result in a significantly higher background since the FREIA optics are not optimised for this operation mode.

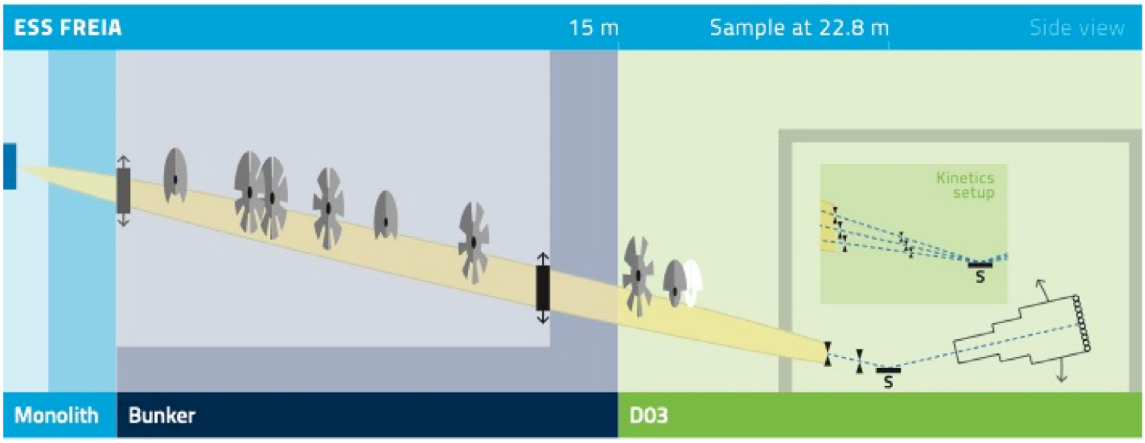

Fig. 13. FREIA instrument layout. Components shown in white are foreseen upgrades.

Table 5
FREIA Quick Facts. All values quoted for the high-resolution and high-flux modes assume the incident angles stated, an angular resolution of 2.5% $\Delta\theta/\theta$ and a beam footprint of 8 × 3 cm^2 . In all cases, the flux quoted is for an area perpendicular to the beam, sized for the same 8 × 3 cm^2 footprint. The flux number for the full-divergence mode is preliminary.

FREIA Quick Facts	
Instrument Class	Reflectometry
Moderator	Cold
Primary Flightpath	22.8 m
Secondary Flightpath	3.0 m
Polarised Incident Beam	Available as a foreseen upgrade
Sample Orientation	Horizontal
Representative Incident Beam Angles	0.45°, 0.9°, 3.4° (full range 0.2°–3.7° depending on angular resolution)
Standard Mode (14 Hz)	
Wavelength Range	2-10 Å
Flux at Sample at 2 MW	1 × 10^5, 5 × 10^5, 7 × 10^6 n s^{-1} cm^{-2} [high res (WFM) mode] 1 × 10^6, 4 × 10^6, 6 × 10^7 n s^{-1} cm^{-2} [high flux mode] 1 × 10^8 n s^{-1} cm^{-2} [full divergence mode]
Q-Range	0–1 Å^{-1} (solid samples) 0.0045–0.38 Å^{-1} (free liquids)
Q-resolution	3%–3.5% [high res (WFM) mode] 5%–23% (across free-liquid Q-range) [high flux mode] 2%–6% [full divergence (WFM) mode]
Pulse Skipping Mode (7 Hz)	
Wavelength Range	2–18 Å
Flux at Sample	5 × 10^5, 2 × 10^6, 3 × 10^7 n s^{-1} cm^{-2} [high flux mode]
Q-Range	0–1 Å^{-1} (solid samples) 0.002–0.38 Å^{-1} (free liquids)
Q-resolution	3%–23% (across free-liquid Q-range) [high flux mode]

The natural resolution of the instrument is medium to low ($\Delta Q/Q$ = 5%–23% (full width) depending on wavelength and incident angle), and it will also be possible to skip pulses to extend the bandwidth and average resolution in this mode. A foreseen chopper upgrade will improve the pulse-skipping bandwidth. In the high-resolution mode ($\Delta Q/Q$ < 5%), FREIA will use a Wavelength-Frame-Multiplication (WFM) chopper system, but this mode cannot be used in combination with pulse-skipping.

FREIA will use the same "multi-blade" ESS detector design [26–29] as used on Estia. The sample-detector distance is 3 m and the detector will cover 4.75° (V) and 3.8° (H) with 0.5 mm resolution (V) and 2.5 mm resolution (H) to allow for off-specular measurements. A foreseen upgrade will extend this angular coverage to 5.7° (H & V).

Table 6
NMX Quick Facts.

NMX Quick Facts	
Instrument Class	Large-Scale Structures
Moderator	Cold
Primary Flightpath	157 m
Secondary Flightpath	0.2–1.0 m
Wavelength Range	1.8–10 Å
Bandwidth	1.74 Å
Flux at Sample at 2 MW	1 × 10^9 n s^{-1} cm^{-2} (1.8–3.5 Å)
Wavelength Resolution $\Delta\lambda/\lambda$	2%–4% (over wavelength range)
Beam Divergence	Adjustable up to ±0.2°
Beam Size	0.2–5 mm

2.4.3. FREIA expected performance

The increase in flux and the ability to switch angles without moving the sample on FREIA will mean that full reflectivity curves can be measured significantly faster than on current instrumentation (see Fig. 14). For the case of the low-resolution mode this will mean complete measurements on the order of seconds, and for the high-resolution mode around 10–15 min rather than the 30 min to 2 h that have historically been required, depending on the scattering contrast. We expect this to mean significant improvements to the time-resolution achievable in kinetic studies and to the throughput of samples in a typical experiment. Alternatively, the increase in flux can be used to reduce the sample size. The standard footprint length of 40 mm is already smaller than generally used elsewhere and smaller samples are also feasible.

2.5. NMX — Macromolecular diffractometer

2.5.1. NMX science case

Macromolecular crystallography is a work-horse method in structural biology, but the vast majority of structures are determined using X-rays as the incident radiation. Yet the functionally critical hydrogen atoms are almost always invisible in X-ray structures.

The NMX Macromolecular Diffractometer is a time-of-flight (TOF) quasi-Laue diffractometer optimised for small samples and large unit cells dedicated to the crystallographic structure determination of biological macromolecules. The main scientific driver is to locate the hydrogen atoms relevant for the function of the macromolecule.

The ESS long pulse source is well suited for a quasi-Laue macromolecular diffractometer that can spread the background in the TOF dimension, while the Bragg peaks are observed at a defined TOF. Therefore, a macromolecular diffractometer at the ESS could be used either to study systems with smaller crystals or larger unit cell volumes. Growing well-ordered protein crystals of cubic millimetre volume is extremely

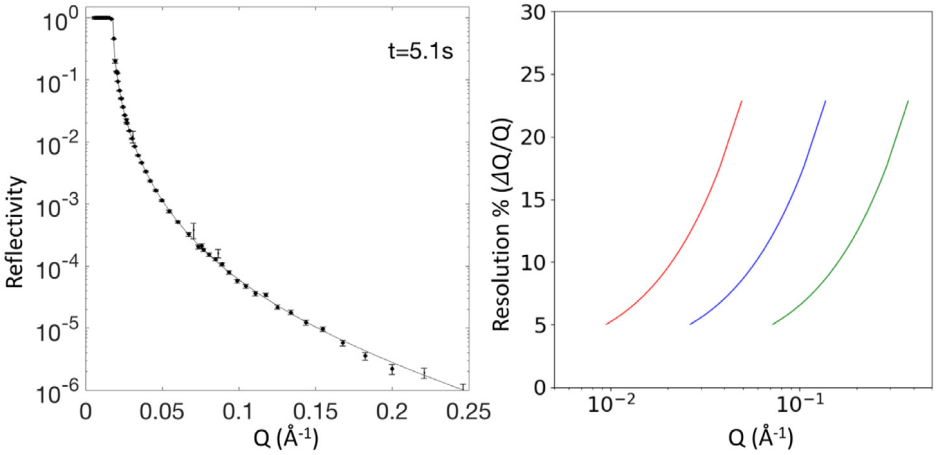

Fig. 14. (Left) Simulated reflectivity from a 40 × 40 mm^2 air-D_2 O interface with the WFM system off and angular resolution $\Delta\theta/\theta$ = 4%, taken from the FREIA instrument proposal. (Right) The simulated resolution on FREIA in this high-flux mode for the three angles of incidence listed in Table 5.

difficult, so the instrument is optimised for sub-millimetre crystal sizes. As the background from incoherent scattering increases dramatically if all ^{1}H cannot be replaced by ^{2}H, the instrument proposed here has a significant inherent advantage with systems where per-deuteration cannot be achieved. Many challenging and interesting proteins fall into this category, as they cannot be expressed in prokaryotic systems with high enough yield.

One of the limiting factors with current instruments is that the fixed detector geometry only allows a maximal unit cell edge of ~150 Å to be resolved without a compromise in the diffraction resolution (d_{min}). The NMX instrument allows larger unit cells to be resolved by increasing the crystal-to-detector distance, which incurs an increase in the data collection time, but reflections to the same d_{min} can still be observed by swinging the detector in scattering angle 2θ. Many of the scientifically most interesting systems, such as proton pumping membrane proteins, crystallise in large unit cells, so being able to resolve a large unit cell edge is a unique advantage. The combination of a neutron flux comparable to leading high flux reactor instruments, such as LADI-III, together with the advantages of time-of-flight – the ability to resolve large unit cells and the ability to better separate signal from background – leads to world-leading performance particularly with the experimentally most challenging systems. This will transform neutron macromolecular crystallography into a technique that can answer a significantly larger number of hydrogen-related questions in biomolecular science than before.

2.5.2. NMX instrument layout

The instrument is located at beamport W1 in the west sector and will view the cold part of the moderator assembly. The neutron flight path length from the moderator to the sample is 157.6 m, which leads to a wavelength resolution $\Delta\lambda/\lambda$ of 4.0% at 1.8 Å. The nominal bandwidth with no frame-overlap (assuming a pulse length of 2.86 ms) is 1.72 Å. The main instrument parameters can be found in Table 6 and the instrument layout is shown schematically in Fig. 15.

The beam delivery system transports the neutron beam from the moderator to the sample. The monolith insert contains a guide starting 2089 mm from the centre of the moderator cold source, which is parallel in the horizontal direction but tapers vertically from 28 mm to 45 mm. The guide is 30 mm wide and the coating on all sides is m = 2. The in-monolith guide section is 3.5 m long, followed by a 0.5 m straight 30 × 45 mm^2 guide section with m = 1 coating inside the light shutter system immediately outside the monolith. A curved guide with a curvature radius of 1200 m starts immediately after the gamma shutter and deflects the beam out of line-of-sight from the moderator at 17 m. The curving is achieved with straight guide elements that are 500 mm long. 36 pieces are required for the 18 m distance between the gamma shutter and the bunker wall insert. The m-value is m = 2.3 on the outward side of the curve, while m = 1 is sufficient on the three other sides. The guide cross-section is 30 × 45 mm^2 throughout the curve. After the curved guide ends, before the 3.5 m thick bunker wall, an insert allows neutron optical elements to be placed inside the wall. The insert will contain an m = 2 guide quasi-parabolically tapering horizontally from 30 × 45 mm^2 to 45 × 45 mm^2 cross-section. Outside the bunker follows a straight guide with 45 × 45 mm^2 cross-section and m = 1. The final 10 m of the guide will consist of a focusing element. The focal distance is 9 m, which places the focal point past the sample position, so that the sample is illuminated by a convergent rather than fully divergent beam. The half parabola starts at 144 m from the moderator and consists of ten 500 mm pieces, followed by twenty 250 mm pieces. The cross-section at the start of the focusing is 45 × 45 mm^2 and 30 × 30 mm^2 at the end.

The chopper system consists of two chopper units for wavelength selection. All choppers are operating at 14 Hz frequency and with a 70 cm disc diameter. The first chopper unit has a single disc with a 78° opening and is located outside the common shielding bunker at 28.67 m from the moderator directly after the first shutter. The choice of this position is largely driven by the maintainability and serviceability considerations of placing the chopper unit outside the common shielding bunker and outside line-of-sight to the moderator. The second chopper unit is located at 51 m from the moderator. It consists of two co-rotating discs with 140° openings. The first disc defines the opening time of the unit and the second disc defines the closing time, so that the relative phase between the two discs defines the total open time. This allows the nominal bandwidth to be chosen by simply re-phasing the two discs. The setting that allows full transmission of the nominal bandwidth also leads to a significant penumbra in the neighbouring frame, which is not expected to be problematic for most experiments. This penumbra can, however, be easily eliminated by narrowing the nominal bandwidth.

The collimation system consists of slits and collimation tubes that define the beam at the sample position in terms of the size and divergence. The collimation length of 3.65 m allows a 5 × 5 mm^2 sample area to be illuminated with the full ±0.1° divergence. For smaller samples slightly higher divergences can be used if needed.

The sample is positioned in the beam with a six-axis robotic goniometer.

The detector system consists of three detector panels mounted on a six-axis robotic arm each. Each arm is placed on a high-precision rail, effectively adding another axis. This setup allows to position the panels at 0.2–1 m distance from the sample anywhere in the top hemisphere up to 165° scattering angle at the panel edge. The detector panels themselves are based on a gas-electron multiplier (GEM) with a Gd converter [30] in order to achieve ~200 μm spatial resolution.

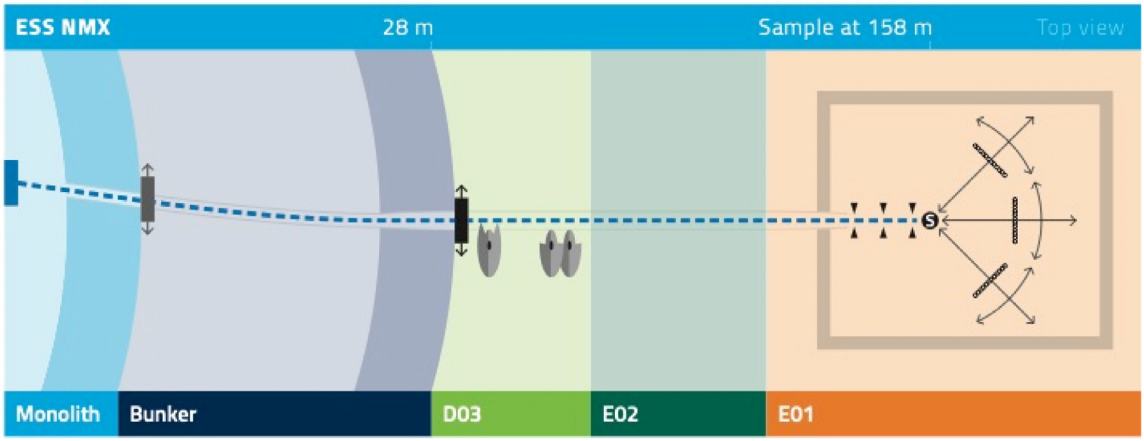

Fig. 15. NMX instrument layout.

2.5.3. NMX expected performance

Scientific performance is a very complex and intrinsically subjective quantity to measure and depends on many other factors than the purely technical performance of the instrument and its components. The assessment below tries to address those aspects of the technical performance that affect the data collection time. The principal technical challenges are the limited crystal size and the high background.

The data collection time depends strongly on the crystal size and other crystal properties such as symmetry, mosaicity, hydrogen content and the background from the surrounding mother liquor. The other relevant variables are the beam brilliance and the solid angle subtended by the detectors.

The neutronic performance was evaluated by ray-tracing Monte Carlo simulations using the McStas package. The beam profile at the sample position is essentially a top-hat function with a negligible halo which will be achieved by using a pinhole that is moved sufficiently close before the sample (typically a few mm). The time-averaged flux from the ray-tracing Monte Carlo simulations is 1.5×10^9 n s^{-1} cm^{-2} with $\pm 0.2°$ divergence. This flux is significantly higher than, for example, the measured flux of 5×10^7 n s^{-1} cm^{-2} at LADI-III (ILL) at its new H143 position for a 3–4 Å wavelength range [31].

The time-averaged flux comparison does not take into account the signal-to-background gain from using the time-of-flight Laue method. In the absence of any background from the crystal or its surrounding mother liquor the counting time required to reach a given signal-to-noise ratio for a single Laue spot is essentially defined by the spectral flux at the wavelength where the reflection is excited and the detector noise. If, however, we take into account the background, the counting time needed for a given signal-to-noise ratio in the absence of wavelength resolution (conventional Laue) becomes a function of the spectral flux (and detector efficiency) at all the wavelengths within the wavelength range where background is generated and the integral of that background across the wavelength range used. In the case of using the TOF information as well, the counting time is defined by the background only at the wavelength where the reflection is excited. If we assume the background to be fairly uniform across the wavelength range, the gain factor over a continuous source Laue instrument of similar time averaged flux (such as LADI-III) depends very strongly on the level background from the sample. With the concept proposed here, the time width of a reflection is ~4 ms, which is 6% of the 71.4 ms timeframe. This means that the effective background is lowered by a factor of ~20 by using the TOF method. In macromolecular crystallography the background from the crystal and its surroundings is typically very much larger than the actual Bragg peak heights, especially for the weakest reflections that define the required counting time. Therefore, the impact of lowering the effective background is most pronounced for large unit cells where the average intensity of reflections falls rapidly with resolution. The implication is that the counting time required for the same crystal can be reduced by a factor of 20 or – more importantly – a crystal 20 times smaller can be used. This represents a conservative estimate of the performance gain, as e.g. no improvements in detector efficiency or reductions in gamma-ray background have been considered.

The ability to move the detectors allows data collection from moderately large unit cell systems despite the relatively modest TOF resolution. This relies on the high spatial resolution of the detectors [30], which allows the reflections to be separated in a combination of detector coordinates and TOF (Fig. 16).

3. Instruments for imaging and engineering diffraction

The high flux and unique time structure of the ESS opens unprecedented possibilities also for samples and processes that are to be studied by dedicated Imaging and Engineering Diffraction instruments. This instrument class consists of ODIN (Optical and Diffraction Imaging with Neutrons) and BEER (Beamline for European materials Engineering Research). Both are multi-purpose instruments that will be capable of addressing many different scientific questions within their scope (engineering materials and processes, cultural heritage, energy devices, etc.) due to their high degree of flexibility, pulse-shaping options and adaptability. In particular, the sophisticated pulse-shaping options allow a flexible trade-off between high flux and high wavelength resolution whenever needed, allowing unprecedented in-situ studies for which specialised sample environment can be accommodated in the spacious experimental caves.

Engineering diffractometers are specialised diffraction instruments that are characterised by the ability to define gauge volumes within larger samples, often of complex shape, while detectors and wavelength resolutions are optimised for high precision d-spacing measurements from which lattice strain and residual stress can be deduced [32]. A special feature of BEER will be to offer very fast strain measurements using a newly developed variant of the pulse-shaping method in which several high-resolution pulses are extracted from the same source pulse. On top of this, standard pulse shaping at BEER will offer the possibility for very fast phase transition studies – in particular during real-time processing – where the wavelength resolution can be relaxed in order to gain intensity. Moreover, an extended detector coverage will allow to efficiently measure texture and to follow texture evolution during in-situ studies.

Neutron Imaging has (mainly within the last decade) evolved from a basic attenuation-based contrast technique into several more advanced imaging techniques by exploiting the wave-particle duality of neutrons and their magnetic moment [33,34]. It can now be considered as one of the most versatile neutron-based characterisation methods, which

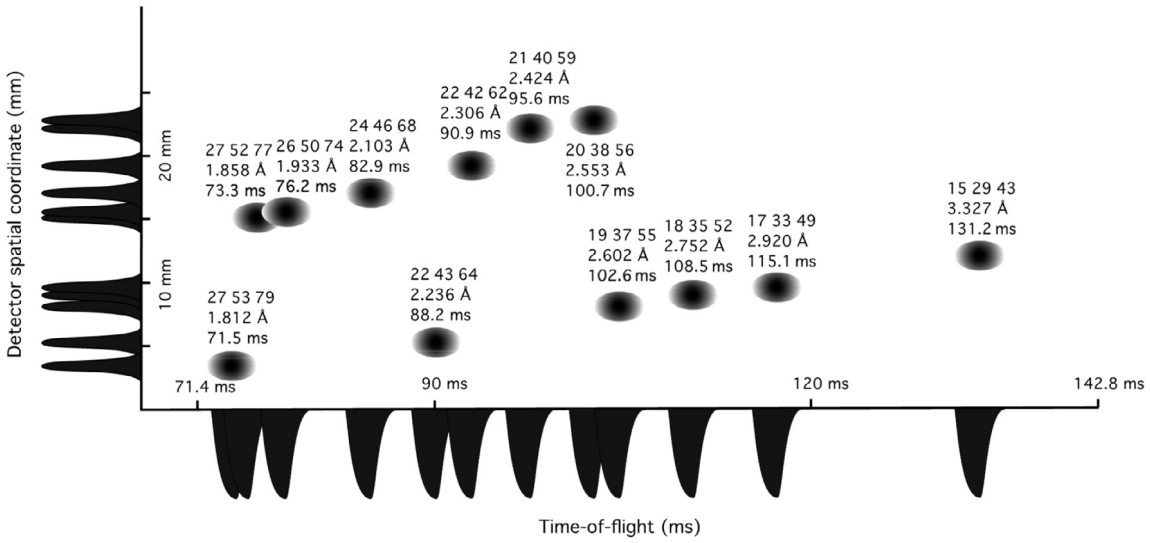

Fig. 16. The separation of some simulated example high-resolution reflections from bovine heart cytochrome c oxidase at 1 m detector distance in the spatial and time-of-flight dimensions on NMX.

is also reflected in its broad user base at existing facilities. Several of the utilised imaging techniques have different requirements regarding wavelength resolution and accommodating them efficiently within the same instrument has been a challenge. The long ESS pulse in combination with the WFM pulse-shaping choppers at ODIN will provide the most efficient way to satisfy these requirements within one instrument while offering the flexibility to adapt to future developments.

It is mainly in the user community, where significant overlap between BEER and ODIN can be expected. As a real-space technique, imaging is especially useful for probing spatial variations e.g. within "real world" engineering samples, cultural heritage artefacts, or assembled components and devices, while engineering diffraction can then probe specific locations in greater detail. An ongoing trend and development is to not only exploit diffraction contrast in transmission imaging itself but also to complement imaging with diffraction detectors, as spatial information in real space can be combined with complementary information from reciprocal space [35]. While especially the latter methods are still under development, one can expect some major improvements by the time the ESS instruments become operational. One upgrade option at ODIN foresees to complement the instrument with diffraction detectors, while imaging will be one of the day-one configurations available at BEER. Tomography-driven diffraction experiments, i.e. locating regions within a sample of complex geometry by 3D-imaging that should be investigated in more detail by engineering diffraction, will be another common application where synergies between instruments in this class can be expected.

The strategy to centralise software and data management (including analysis) for all instruments at the ESS Data Management and Software Centre will enable an even more efficient toolbox for investigating samples using more than one instrument.

Both BEER and ODIN will provide ample space in the sample area to allow not only for large and complex samples but also for bulky sample environments. The high flux of the ESS will enable in-situ and in-operando studies that will set the instruments apart from most instruments at current facilities. It is planned that sample environments will be shared across instruments, where in particular ODIN and BEER will have several common requirements on their capabilities, such as (thermo-)mechanical loading and processing, simulation of industrial processes and thermal treatments to name a few. The differing requirements due to the different experimental geometries will be accounted for by adaptable designs.

The test beamline is also briefly described in this section. Though it is not foreseen to be made available for scientific experiments within the user programme, it will play an important role firstly in characterising the neutron source and later in supporting the user programme on the other instruments in a variety of ways, including method developments, component characterisation and crystal alignment.

Table 7
BEER Quick Facts.

BEER Quick Facts	
Instrument Class	Engineering Diffraction
Moderator	Bispectral
Primary Flightpath	158 m
Secondary Flightpath	2 m
Wavelength Range	0.8–6 Å
Bandwidth	1.7 Å
d-spacing Range	0.6–7 Å
Pulse-Shaping Mode	
Resolution Δd/d	Adjustable 0.22–0.3(0.53[a])%
Flux at Sample at 2 MW	Adjustable 1.8–4.4(13[a]) × 10^7 n s^{-1} cm^{-2}
Modulation Mode	
Resolution Δd/d	Adjustable 0.13%–0.45%
Flux at Sample at 2 MW	Adjustable 2.3–13 × 10^7 n s^{-1} cm^{-2}

[a]Available as a foreseen upgrade.

3.1. BEER — Advanced engineering diffractometer

3.1.1. BEER science case

BEER — the Beamline for European materials Engineering Research is a time of flight diffractometer dedicated to the support of the latest progress in development, fabrication, optimisation, and degradation monitoring of modern engineering materials by neutron scattering analysis. The main tasks of BEER are the following (see Table 7):

- enabling fast in-situ and in-operando characterisation of materials and their micro-structure during processing conditions close to real ones
- providing state-of-the-art and fast analysis of residual stresses, microstructure/crystallographic texture characterisation and phase analysis.

The newly developed pulse modulation technique extracts several short pulses out of the long ESS pulse [36] using a dedicated chopper system. It leads to the multiplexing of Bragg reflections and thus to substantial intensity gains for high-symmetry materials while preserving the resolution.

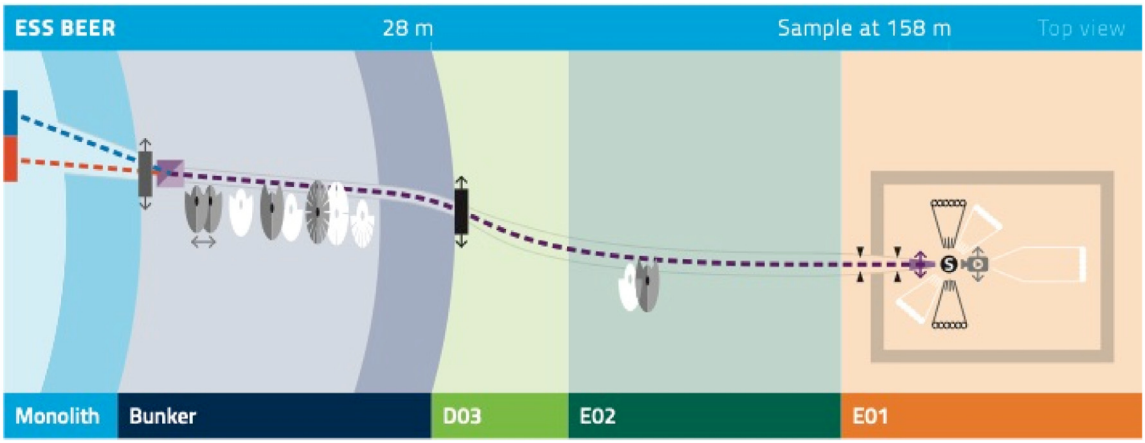

Fig. 17. BEER instrument layout. Components shown in white are foreseen upgrades.

With the ability to switch between the modulation technique and the standard pulse-shaping technique, BEER is a versatile engineering diffractometer providing an easily tuneable trade-off between resolution and flux across wide wavelength and resolution ranges. Together with a large detector coverage, BEER enables sub-second in-situ measurements for many applications, fast residual strain scans even in samples with complex geometry, phase analysis of complex composite systems where high resolution can be employed if needed, as well as the study of texture evolutions during processing. While it can be expected that the majority of users at BEER will come from the engineering materials community, it should be noted that at existing facilities, the spatial scanning possibilities have also attracted users with the objective to study e.g. cultural heritage objects or energy devices.

3.1.2. BEER instrument layout

An overview of the BEER instrument can be seen in Fig. 17. Neutrons from the cold and thermal moderator are extracted and merged into the neutron guide using a bi-spectral switch (150 double-coated Si blades), installed just after the monolith light shutter at a distance of 6 m from the source. The following straight guide section with a length of about 4 m contains a chopper cascade with initially 4 chopper discs. The first two choppers, both running at 168 Hz, are used when the pulse-shaping mode is active. The two choppers are operated in optical blind mode providing constant relative wavelength resolution which is tuned by changing the distance between the choppers via a translation stage. The pulse modulation mode uses a modulation chopper containing a disc with several equally distributed openings running with frequencies between 42 and 280 Hz, allowing fine-tuning of the resolution and the Bragg multiplication for the experimental needs. Two additional frame definition choppers, the first placed between the second pulse-shaping chopper and the modulation chopper and the last at 79.55 m define the wavelength band and block undesired frame overlaps between successive sources pulses. The neutron guides following the chopper cascade in the bunker section have a bending radius of R = −2 km, thus closing the direct line-of-sight within the bunker section which ends at 28 m from the source [37]. Outside the bunker, the instrument shutter is installed followed by an expansion of the neutron guide to an optimised cross-section of 40 × 80 mm^2 (H × V) The long curved transport guide section (R = 20 km) delivers the neutrons from 39 m to 144.5 m, only interrupted by the second frame definition chopper. The last section of the optical system focuses the neutron beam vertically onto the sample. Further beam conditioning is possible by three adjustable slits; two located at 152 m and 155 m for beam divergence definition, and a third slit at a variable distance before the sample to define the beam size. The last two metres of the focusing section allow for exchanging the focusing guide by an element with absorbing walls and thus further tuning the divergence of the neutron beam.

Precise positioning of samples and sample environments can be carried out with a robotic system with many degrees of freedom including rotation, e.g. for texture measurements, or a hexapod for samples up to 2 t in weight. It is possible to integrate a wide range of sample environments at BEER, both ESS-provided and user-made ones. Initially, a deformation rig will allow tensile and compression testing with a maximum force capacity of 60 kN and simultaneous heat treatment with temperatures up to 1200 °C. A dilatometer is expected to provide fast, controlled heating and cooling of the sample under load.

Two 1 × 1 m^2 large detectors collect the neutrons scattered from the sample. The detectors are placed at ± 90° and are based on $^{10}B_4C$ converters [38]. This technique combines an inherent high time and position resolution with a high count-rate capability [39]. Each detector is equipped with a set of exchangeable radial collimators which together with the input slit define the gauge volume. The initial set of radial collimators can define horizontal gauge sizes of 1 or 4 mm. Together with the adjustable slit system in front of the sample, they can define a gauge volume from about 1 to 64 mm^2. Further sets of radial collimators are foreseen, extending the range of gauge widths to between 0.5 and 5 mm.

The design of BEER foresees further upgrades of the initial instrument (items shown as white in Fig. 17). Additional choppers for pulse-shaping and additional pulse-modulation modes will extend the available intensity/resolution ranges while two more frame definition choppers will allow for alternating or extending the wavelength band. Extending the detector coverage in the horizontal and vertical plane will allow for simultaneous measurements of additional strain components and in-situ monitoring of texture evolutions. By implementing an additional SANS detector within the large instrument cave, a unique combination of simultaneous diffraction and SANS measurement will become possible and e.g. enable to link the development of precipitates to crystallographic microstructure.

Imaging will be possible from day 1, by borrowing a TOF imaging detector from ODIN, or by using a standard camera-based system. While the latter will be useful for sample positioning and collecting images based on attenuation contrast, the TOF imaging detector will enable e.g. Bragg-edge imaging that can provide complementary information on the phase, strain and texture variations across the sample.

In close proximity to the experimental cave of BEER, a preparation and testing laboratory is available. Pre-aligned sample environments can be easily moved in and out of the cave on a transportation platform. This infrastructure also allows for long-term experiments, by conditioning/testing samples in the preparation laboratory while periodically measuring them using neutrons.

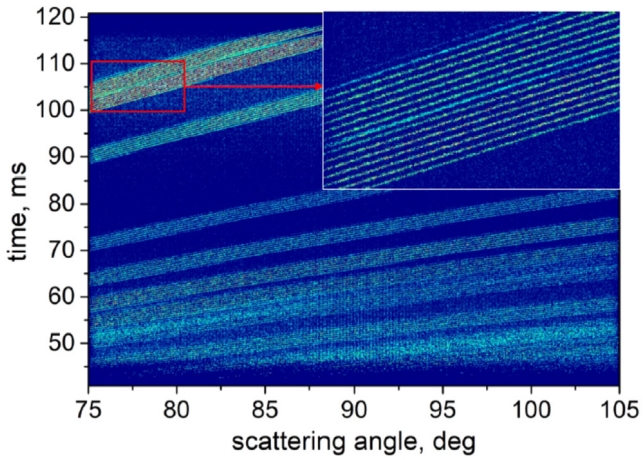

Fig. 18. Simulated pattern of duplex steel as simulated on the 90° detector of BEER in the modulation mode.

3.1.3. BEER expected performance

Based on neutronics calculations for a source power of 2 MW it is expected that the BEER instrument will be comparable in terms of flux with leading existing engineering instruments such as TAKUMI [40] or VULCAN [41,42] when using the pulse-shaping technique, but BEER outperforms them when using the pulse modulation mode. Furthermore, BEER offers a much larger versatility: The resolution Δd/d can be tuned between 0.15 and 0.5% (high- and medium-resolution mode) in the initial state of the instrument. It can be relaxed to 0.8% for the high-flux setting after implementing the upgrades. The simulated average flux on the sample position is of the order of 10^7 to 10^8 n s^{-1} cm^{-2} depending on the resolution.

The modulation technique on BEER allows an increase of the flux on the sample without sacrificing resolution. The simulated diffraction pattern of duplex steel, shown in Fig. 18, demonstrates the principle of the modulation technique: several sub-pulses – well separated in wavelength – arrive at the same time at the detector, producing multiplexed angularly separated Bragg reflections which can be summed up. This technique can be used for highly symmetric materials (like most of the engineering materials are) where the Bragg reflections do not overlap within the spectral bandwidth.

In summary, BEER will push the boundaries of what is possible at present while being a very versatile instrument.

3.2. ODIN — Multi-purpose imaging beamline

3.2.1. ODIN science case

ODIN (Optical and Diffraction Imaging with Neutrons) is a multi-purpose Neutron Imaging instrument. Neutron Imaging, originally based purely on attenuation, has evolved dramatically. Now energy- and polarisation-dependent imaging techniques as well as interferometry-based approaches can be applied across a broad spectrum of scientific disciplines and applications see [35,43–45] and references therein. ODIN will offer a wide variety of methods with unmatched capabilities taking advantage of the full flexibility offered by the unprecedented source time-structure and brightness of ESS. ODIN will open up new research and will not only push the limits of current applications but will add many more by significantly shifting the boundaries of what can be done today (see Table 8).

Simultaneous structural resolution on the macroscopic scale of direct imaging and of microscopic features from small-angle scattering as well as in the atomic range of crystalline lattices can, for example, be combined with the resolution of magnetic interactions with polarised neutrons. Advanced neutron imaging techniques will help to deepen our understanding of phase transitions in high Tc superconductors and magnetic materials, ion propagation in alternative energy devices, structural anomalies in complex industrial materials, and in the study of biological and polymer membranes among many others. The list is vast and broad as well as the impact in industrial and basic research.

Table 8
ODIN Quick Facts.

ODIN Quick Facts	
Instrument Class	Imaging
Moderator	Bispectral
Primary Flightpath	50 m (to pin-hole)
Secondary Flightpath	2–14 m (pin-hole to sample)
Wavelength Range	1–10 Å
Field of View	20 × 20 cm^2
L/D Ratio	Tuneable 300–10,000
Incident Beam Polarisation	Optional
Polarisation Analysis	Optional
Bandwidth at 14 Hz	4.5 Å
White-Beam Mode	
Flux at Sample at 2 MW	1.2×10^9 n s^{-1} cm^{-2} at 10 m, $L/D = 300$
Spatial Resolution	<10 μm
TOF Mode without Pulse-Shaping	
Flux at Sample at 2 MW	9×10^8 n s^{-1} cm^{-2} at 10 m, $L/D = 300$
Spatial Resolution	<10 μm
Wavelength Resolution	$\Delta\lambda/\lambda$ = 10% at λ = 2 Å
TOF Mode with Pulse-Shaping	
Flux at Sample at 2 MW	1×10^8 n s^{-1} cm^{-2} at 10 m, L/D = 300, $\Delta\lambda/\lambda$=1%
Spatial Resolution	~50 μm
Wavelength Resolution	Adjustable <0.5%–1% (constant for all λ)

ODIN will employ the latest detector technology to offer the state-of-the-art spatial resolution on day one, with straightforward benefits: it will enable deeper access to structural and failure analysis in non-destructive testing, materials science, cultural heritage etc. The neutron metallurgical studies of the Titanic rivets and the metal structures of the World Trade Center Twin Towers are famous examples. But also studies of, for example, fuel cells or water uptake studies in plant-root systems will benefit from ODIN with their need to resolve structures in the 5–50 μm range while being able to choose a desired wavelength band for optimal contrast conditions.

Using wavelength-resolved imaging with tuneable medium to high wavelength resolution ($\Delta\lambda/\lambda$ of 1% down to <0.5%), ODIN will provide significantly increased chemical and structural sensitivity compared to traditional instruments with no or only fixed wavelength resolutions. This will contribute to a better understanding of structural phase transition and failure analysis in engineering materials, provide new insights into geological samples (igneous rocks or meteorites for example), and it will not only help with provenance and manufacturing studies of invaluable artefacts but also with the advancement of novel manufacturing techniques. In energy research, this modality enables increased sensitivity, which will help to better understand the processes in rechargeable batteries and hydrogen storage materials for example.

Relatively new techniques such as phase contrast, dark-field contrast and polarised neutron imaging will greatly benefit from the high brilliance and in particular from the long pulse structure of the ESS, which will be optimally exploited by a versatile chopper system. This enables novel quantitative approaches, making such conventionally time-consuming investigations significantly more efficient. These techniques can not only help to visualise inhomogeneities in magnetic fields and structures, magnetic phase transitions, and individual magnetic domains, providing invaluable insights into the structure and behaviour of magnetic materials and superconductors, but also enable spatially resolved SANS studies in engineering materials and soft condensed matter, with the possibility to characterise cracks, pores, sedimentation of colloids or directionality of fibres beyond the spatial resolution limit.

Pioneering neutron imaging techniques, such as Spin-Echo Modulation, Small-Angle Neutron Scattering and Far Field Neutron Interferometry, further underline the need for a new neutron imaging instrument with the uncompromising nature and versatility that ODIN will provide.

3.2.2. ODIN instrument layout

The basic concept of ODIN is based on the considerations in [43,46]. The layout is shown schematically in Fig. 19. ODIN is a medium-length instrument located at beamport S2 and, thanks to the bi-spectral extraction, it will view both the cold and the thermal moderators. The complete chopper system, with the exception of one chopper, is located inside the bunker, as is a heavy shutter. The cave will contain the pin-hole selector system, sample area, detector systems, and the beam stop; it will also provide ample space for sample environments and other equipment needed for specific imaging modalities.

The neutron optics system has been optimised for the transport of divergence of $\pm 0.7^\circ$ both horizontally and vertically in order to have a homogeneously illuminated area of 15×15 cm^2 at the 60 m sample position and up to 20×20 cm^2 at 64 m. Given the choice to use the Wavelength Frame Multiplication (WFM) concept to tune the wavelength resolution, an eye-of-the-needle approach in the horizontal direction is used, for a fast and uniform horizontal chopping of the beam. That is accomplished by a feeder guide that focuses the beam to 1.5 cm in the horizontal direction at the WFM chopper position (centre between the two WFM choppers) followed by a ballistic guide with the first focus between the WFM choppers and the second focus at 50 m, the cave entrance. Given the small size of the new moderator concept, matching the intended maximum size of the pinhole at the entrance of the cave, a ballistic approach has been employed in the vertical direction. The m-coating along the guide was optimised for efficient transport of neutron with wavelengths $\geq$1 Å through extensive McStas simulations.

The chopper system is based on the concept outlined in [47] and in part realised at the ESS test beamline [47,48] installed at HZB in Berlin. It has been specified for ODIN in detail in [49,50]. The main operation modes are outlined in the ODIN instrument proposal [51]. The choppers can all be parked open for a White Beam operational mode without TOF. With just the bandwidth choppers running, TOF imaging is enabled with the wavelength resolution defined by the proton pulse width ($\Delta\lambda/\lambda = 10\%$ at 2 Å). With the pulse-shaping WFM chopper system as well as the rest of the chopper cascade running, the wavelength resolution is adjustable down to $\Delta\lambda/\lambda < 0.5\%$.

The cave structure will be an assembly of borated lining, steel and 2.3 g/cm^3 concrete for shielding purposes. The inside dimensions are 7 m width, 5 m height, and 2.4 and 13.6 m length (along the beam) for the optical and experimental caves, respectively, to provide ample space for versatile sample environment and experimental set-ups. A control hutch and a sample preparation area space will be adjacent to the cave entrance.

The experimental cave of ODIN will be accessible through a sliding door and if necessary also from the whole roof. A pin-hole selector is placed at 50 m from the moderator, and the main measurement positions are foreseen at 52 m, 60 m, and up to 64 m. The first one will be used for high flux measurements (for instance for dynamic processes with high temporal resolutions) with smaller field-of-view requirements, the second one will serve the majority of applications, and the last one is dedicated to the study of larger samples.

The choice of detector is dictated by the specific experiment. For this reason, a portfolio of detectors [52] and an optical bench in the cave will be available in order to offer all the options needed to position sample and detector(s) with high flexibility in the flight path.

The design of ODIN also foresees further upgrades of the initial instrument layout, including neutron grating interferometry, spin echo modulated dark field imaging, polarised neutron imaging and X-ray tomography, where a 90° set-up shall allow taking data from the same sample simultaneously, thus making 4D data comparisons possible. A major upgrade is envisaged and will include the capacity of ODIN for implementing diffraction-supported neutron imaging

3.2.3. ODIN expected performance

The performance of an imaging instrument depends on flux, beam size, divergence and homogeneity of the neutron beam at the sample position. The available wavelength resolution is an additional important performance criterion for TOF based imaging. A flux comparison is shown in Fig. 20 where the ODIN flux was simulated for an ESS power of 2 MW and is compared for different wavelength resolutions with imaging facilities at steady state sources (left) and a short pulse source (right)

Neutron Flux: With its long pulse and high neutron flux, the anticipated flux at the 60 m sample position will be about 1.2×10^9 n s^{-1} cm^{-2} (at 2 MW and at the minimum achievable L/D of 300). This is at least three times higher than currently at steady-state sources. Simulations predict that ODIN will outperform the short-pulse-source instruments even when conditioning the beam for high wavelength resolution.

Beam characteristics: The neutron beam profile at the 60 m sample position is, as a simulation shows, homogeneous over a field of view of about 15×15 cm^2. A pin-hole selector will enable variable collimation up to L/D = 10,000, which is unprecedented.

Wavelength resolution: The anticipated best wavelength resolution of about 0.5% is ambitious but achievable due to the sophisticated chopper system. Currently, steady-state sources offer wavelength resolutions down to about 1% while beam-lines at SNS and J-PARC anticipate around 0.3%. In contrast to the latter, ODIN can trade resolution for flux and hence most efficiently tailor to the needs of specific experiments.

3.2.4. ODIN summary

With its high flux, high beam quality and flexible wavelength resolution ODIN has the potential of setting the state of the art in neutron imaging. This will require steady monitoring and development of all experimental components needed for existing and upcoming advanced techniques, which are currently foreseen as upgrades (e.g. grating interferometry). This, however, appears to be a straightforward task given the collaborative nature of the neutron imaging community of which the ODIN team is an active part.

3.3. Test beamline

The primary purpose of the test beamline is to characterise the target-reflector-moderator system, verifying the performance of the neutron source at the start of operations, and then throughout the operation of the facility. In its basic configuration, it is a pin-hole imaging station for viewing the moderator assembly, with a double-disc chopper at the pin-hole position to provide tuneable wavelength resolution and wavelength band selection. A position sensitive detector (PSD) will be placed at 17 m from the moderators with an adjustable pin-hole at the half-way position, enabling to spatially image the neutrons of different wavelengths emerging from the moderator (see Fig. 21).

Especially, during the early years of ESS, the test beamline will serve to establish the moderator performance as a function of the various operating parameters of the accelerator and target systems, including the proton beam power, stability, pulse length, and beam rastering, as well as the moderator temperature and ortho-para ratio of the hydrogen.

As the facility matures, the test beamline will be adapted to fulfil additional objectives. There are a variety of ways in which it can support the user programme directly, such as aligning and characterising single crystals or performing exploratory imaging or diffraction studies of samples to be measured on one of the user instruments. It will also serve as a local characterisation station to support technical developments in areas such as neutron optics, polarisation, shielding and detectors. Moreover, the test-beamline will provide a platform for the evaluation of novel methods and improvement of existing measurement techniques. Several potential upgrade paths will be possible due to the modular design.

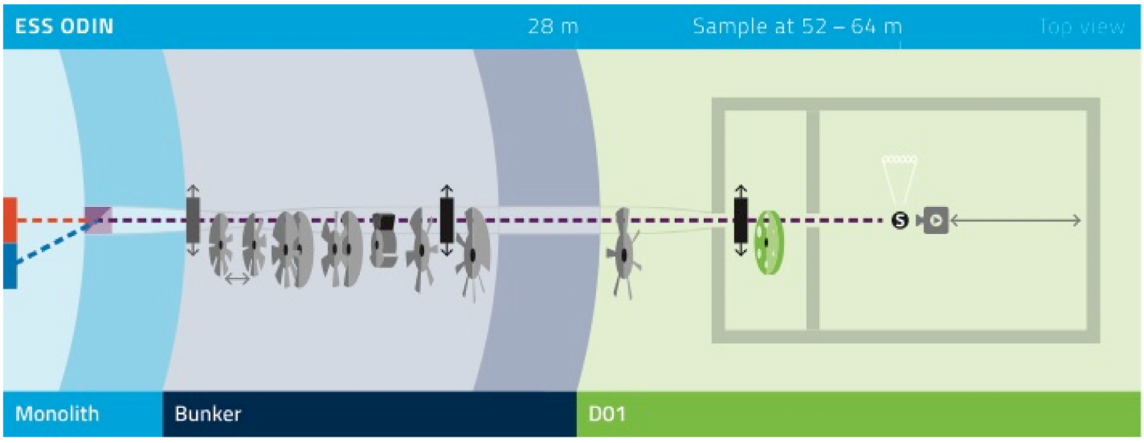

Fig. 19. ODIN instrument layout. Components shown in white are foreseen upgrades.

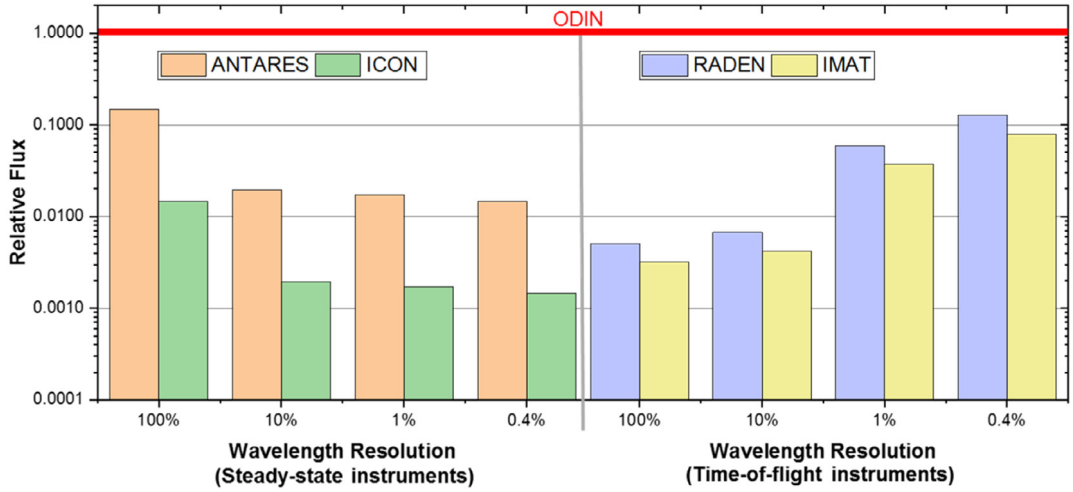

Fig. 20. Flux comparison between ODIN and other imaging facilities for an L/D of 300. The flux on ODIN is defined to be 1.0. The data for this figure are taken from [53–56] and from private communications with the respective instrument teams. While a detailed comparison of these vastly different instruments is beyond the scope of this paper, such calculations can serve as a starting point in comparing the expected performances of ODIN at different experimental conditions with existing facilities.

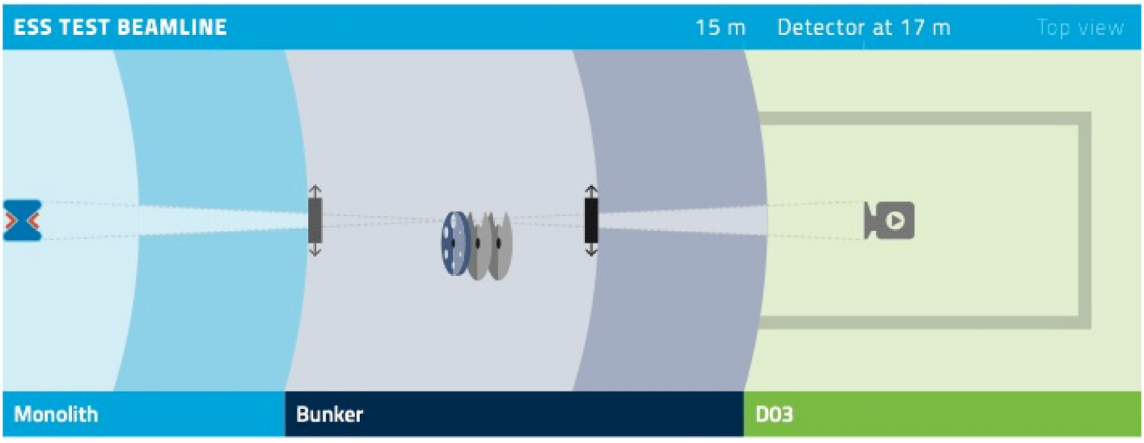

Fig. 21. Test beamline instrument layout.

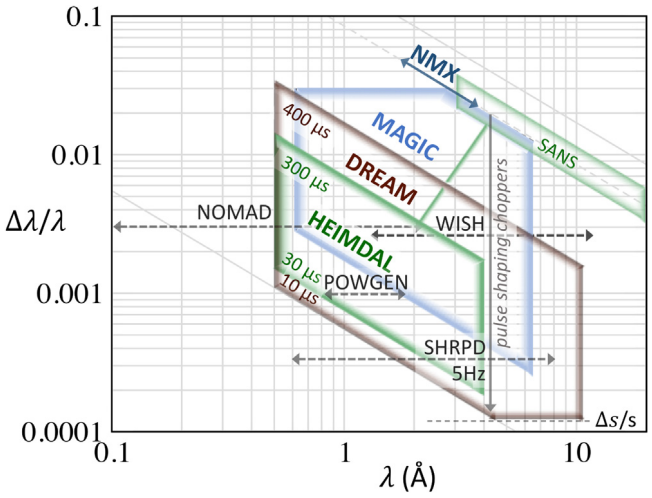

Fig. 22. Comparison of diffractometers at ESS and short pulse spallation sources with respect to wavelength and resolution near backscattering. Pulse shaping at ESS provides a large flexibility to adjust resolution within the shown large areas in a trade-off for intensity, while for other instruments these characteristics appear as horizontal lines. ESS diffractometers are limited to a shortest wavelength of 0.5 Å. Bandwidths are 1.8 Å for HEIMDAL and MAGiC, and 3.6 Å for DREAM. With pulse-shaping the resolution in $\Delta\lambda/\lambda$ improves with wavelength λ, limited at the highest resolutions by path-length uncertainties $\Delta s/s$.

4. Diffraction instruments

The initial diffraction suite at the ESS comprises the two powder diffractometers DREAM and HEIMDAL, and the single-crystal diffractometer MAGiC. In addition, there are diffractometers for macromolecular crystallography and engineering, NMX and BEER, described in the sections on Large-Scale Structures and Engineering, respectively.

Powder diffractometers, in particular, seem naturally suited for short-pulse spallation sources, as they optimally exploit the brilliance from sharp neutron pulses as generated by dedicated, typically poisoned, moderators. In addition, short pulses at short wavelength are required for high Q resolution. So why should we build powder diffractometers at the long-pulse source ESS? The key for competitiveness is the superior peak brightness rather than the huge time-average flux. Pulse-shaping choppers allow tailoring of the time/wavelength resolution appropriately to the need, competitively for wavelengths larger than approximately 0.5 Å. Using different chopper speeds creates a particular value: an enormous *flexibility* in resolution. The results for the ESS diffractometers are shown in Fig. 22. For the sake of comparison, the graph includes also the characteristics of a few powder diffractometers at short-pulse spallation sources: NOMAD and POWGEN at SNS, WISH at ISIS, and SuperHRPD at J-PARC. Note that the natural pulses of short-pulse spallation sources yield single horizontal lines on the graph, while the ESS diffraction instruments use chopper-generated pulses with wavelength-independent opening times, leading to the shown inclined resolution functions. These can be tuned easily with chopper speed from low to extremely high resolution.

The accessible regions of DREAM and HEIMDAL can reach and even significantly improve the resolution of SuperHRPD, and we recall, with superior brightness. Pulse shaping with fixed Δt (or Δd) resolution allows benefitting favourably from the merits of very different powder diffractometers; *e.g.*, the wavelength-band of DREAM comprises suitable resolutions for probing different length-scales covering PDF, crystallography at atomic length scale and also, for large unit cells, subtle symmetry breaking and peak splitting, as if making combined use of NOMAD, POWGEN and SuperHRPD.

The two powder diffractometers are quite complementary with a different sample-detector geometry, vertical (HEIMDAL) versus horizontal (DREAM) cylindrical geometry. Furthermore, with 150 m length the focus of the instrument HEIMDAL lies on an intense short thermal wavelength band of 1.8 Å, while the 75 m long instrument DREAM further includes cold neutrons for a wider band width of 3.6 Å, particularly for studying more complex and larger unit cell structures. Both are upgradeable to access multiple length scales, especially HEIMDAL by including a second cold beam for SANS and imaging options.

A new feature of the ESS is the availability of both thermal and cold moderators for each beamline. Instruments can make use of both, substantially broadening their applicability and science case; MAGiC can switch between thermal and cold sources, while DREAM views simultaneously both moderators via a bi-spectral switch, transparent for thermal and reflecting for cold neutrons.

A common feature of these three diffractometers is a new detector type based on ^{10}B coated cathode elements in an inclined geometry, known as Jalousie-detectors. The many detection layers (typically 10 layers) enable high efficiency (>50% at 1 Å) and high count-rate capability, particularly important for single crystal diffraction. The spatial resolution determined by its multi-wire grid structure on DREAM is approximately 5 mm. HEIMDAL, MAGiC (and also BEER) on the other hand, will use single-sided ^{10}B coated elements, which allows to improve the resolution favourably in the 2θ direction further to typically 2 mm. Since these detectors provide vertical resolution in addition, all instruments, including powder diffractometers, are capable of single crystal diffraction, as well as being sensitive to texture.

The single crystal diffractometer MAGiC will be unique, by having polarised neutrons for both thermal and cold neutron applications within a dedicated science case in magnetism. In the cold neutron range, the natural time resolution is typically sufficient and gives the benefit of the full intense pulse with a high degree of polarisation. Its ability for pulse shaping, however, not only allows for tuning the resolution as required for shorter wavelengths, it can also adapt to even high-resolution powder diffraction, which underscores the flexibility of instruments within the ESS diffraction suite.

Table 9
DREAM Quick Facts.

DREAM Quick Facts	
Instrument Class	Diffraction
Moderator	Bispectral
Primary Flightpath	76.5 m
Secondary Flightpath	1.1 m (end-cap and mantle detectors) 2.5 m (high-resolution and low-angle detectors)
Wavelength Range	0.5–4.1 Å
Flux at Sample at 2 MW	1.4×10^7 n s^{-1} cm^{-2} (Δd = 3×10^{-4} Å) 1.0×10^9 n s^{-1} cm^{-2} (Δd = 2.5×10^{-2} Å)
Q-Range	0.2 (0.01[a])–25 Å^{-1}
Detector Coverage	1.82 (5.12[a]) sr
d-spacing Resolution Δd	Adjustable 3×10^{-4}–2.5×10^{-2} Å

[a]Available as a foreseen upgrade.

4.1. DREAM — Diffraction resolved by energy and angle measurements

4.1.1. DREAM science case

The concept of DREAM utilises favourably the long pulse and unpreceded peak brightness of the ESS by using pulse-shaping choppers and by viewing both thermal and cold moderators, which results in a particularly flexible choice between high resolution (Δd ~ 0.0003 Å in the backscattering detector) and high intensity. Therefore, the science case for DREAM is broad and includes all typical cases for powder diffraction, while particular emphasis is anticipated for studies of magnetic materials, samples with large unit cells, hydrogen storage components, batteries and metal–organic frameworks (see Table 9).

Apart from the science case typically covered by a general-purpose powder diffractometer, the DREAM instrument will offer new capabilities that will further broaden its science case. Total-scattering measurements for pair-distribution function (PDF) analysis will enable studies

of local crystal structure in crystalline, nanostructured and amorphous materials.

In-situ studies of battery and super-capacitor materials under operating conditions will be possible due to high neutron flux and broad detector coverage. A low-angle detector bank will provide an access to a limited SANS region (Q ≥ 0.01 Å) and enable morphology studies, particularly helpful for nano-scaled materials when combined with diffraction and PDF data.

Moreover, challenges of very weak signals in powders will be possible to solve by using single crystal diffraction from sub-mm samples. We will build on and develop further a new ^{10}B-detector technology that will be capable of high position-sensitive resolution and also suitable for the expected high count rates

4.1.2. DREAM instrument layout

The instrument will be located at the beamport S3 and as a bi-spectral instrument will view both the cold and thermal moderators (see Fig. 23). The first optical elements will be located in the beamport insert. The complete chopper system and a heavy shutter will be located inside the bunker.

A stack of Si wafers will reflect neutrons from the cold source into the thermal beam and instrument axis. As a result, the neutron bandwidth will include neutrons from the peak fluxes of both, cold and thermal, moderators, providing wide Q-range up to 25 Å^{--1} in a single frame, which is well suited for diffraction and PDF studies.

A great flexibility in trading between resolution and flux will be achieved by the chopper system, which uses Wavelength Frame Multiplication (WFM) to fill the available bandwidth. This is achieved by the combination of three functions: A Pulse-Shaping Chopper (PSC) system, consisting of two counter rotating discs and operating in multiples of 14 Hz, up to 308 Hz for the high-resolution option. A 14 Hz overlap chopper (OC) is used to eliminate higher harmonics from the PSC. Further down-stream, a band control chopper (BC) is installed for a clean definition of the wavelength band and further to suppress for 6 ms the decaying "after-glow" background of the source. The phase of PSC, BC and OC can be shifted simultaneously to change the wavelength range. A prompt pulse suppression chopper (T0 Chopper) will be installed inside the bunker after the BC chopper (see Fig. 23).

The neutron guide consists of a first semi-elliptical part starting from a focal point in the PSC, followed by a straight section and a final semi-ellipse focusing onto the sample. This 70 m long guide system is optimised for the transport of neutrons with a short wavelength of $\lambda >$ 0.5 Å and a divergence of ±0.25° [57].

A vacuum vessel at the sample position is designed for quick sample environment changes. A cryo-furnace sample changer (T = 4–800 K) will be available to users on the first day of operations. Alternatively, the vessel can be removed for bulky sample environments such as a superconducting magnet or a levitator.

The DREAM detector system is based on developments for the POWTEX instrument [58] and uses several absorbing layers of ^{10}B-coated cathodes in a multi-wire gas detection chamber. The fine 2D position sensitivity is also well-suited for neutron time-of-flight Laue single-crystal diffraction measurements. The detectors will be cylindrically arranged around the beam axis for the best adaption to the Debye–Scherrer cones. The dedicated high-resolution backscattering detector will cover the scattering angles from 168° to 178°. Similarly, in the planned upgrade, a forward low-angle detector bank will extend the Q-range to a minimum of 0.01 Å^{-1}.

4.1.3. DREAM expected performance

Our simulations show an excellent performance of DREAM [59] due to its flexibility in a wide range from high resolution to high intensity settings. This can be used for studying for example small samples of ~1 mm^3 size, or for the detection of fast structural changes with a time resolution in the ms-range for samples as large as 0.5 cm^3.

In order to exploit the full potential of DREAM we are following a new approach to the data analysis, which is based on 2D Rietveld refinements [60] of the angular- and wavelength-dispersive diffraction data (Fig. 24).

The instrument is planned to be available for the day one of user operation at the ESS.

Table 10
HEIMDAL Quick Facts.

HEIMDAL Quick Facts	
Instrument Class	Diffraction
Moderator	Thermal (Bispectral and Cold[a])
Primary Flightpath	157 m
Secondary Flightpath	Diffraction: 0.8 m (SANS: 10 m, Imaging: 4 m[a])
Wavelength Range	0.5–4 Å
Bandwidth	1.7 Å
Flux at Sample at 2 MW	10^6–10^8–10^9 n s^{-1} cm^{-2} (High-resolution – Medium-res. – High-flux)
Q-Range	0.5–25 Å^{-1}
d-spacing Resolution Δd/d	Adjustable 0.04%–1%
SANS and Imaging modes[a]	
Moderator	Cold
Wavelength Range	3–20 Å
Q-Range (SANS)	10^{-3}–4 Å^{-1}
Wavelength Resolution	1.5% at $\lambda = 4$ Å
$\Delta\lambda/\lambda$ (SANS)	0.6% at $\lambda = 11$ Å
Field of View (Imaging)	50 × 50 mm^2
Spatial Resolution (Imaging)	50 μm

[a]Available as a foreseen upgrade.

4.2. HEIMDAL — Multi-length-scale hybrid diffractometer

4.2.1. HEIMDAL science case

HEIMDAL [61] is intended as a multi-length-scale instrument providing structural insight from 0.05 nm to 50 mm in real space. The day-1 instrument of HEIMDAL will be focusing on thermal neutron powder diffraction (TNPD). After upgrade, the instrument will cover additional length scales by combining TNPD with small angle neutron scattering (SANS) and neutron imaging (NI). There is a small gap in the coverage at the μm scale between SANS and NI. The techniques have large variations in their requirements: TNPD uses short wavelengths (λ ~ 0.5–4 Å), focused beam, and high resolution ($\Delta\lambda/\lambda < 0.5\%$) to obtain large Q-range coverage (Q_{max} ~ 25 Å^{-1}) and sharp diffraction peaks. The large Q-space coverage will allow total scattering experiments to be analysed by pair distribution function (PDF) analysis (see Table 10).

The upgraded instrument including SANS, needs long wavelengths and a well-collimated beam to reach small Q (Q_{min} ~ 10^{-3} Å^{-1}). To realise the instrument it is necessary to carefully consider the two different requirements in the design of the instrument. A solution using two beam guides has been designed; TNPD is performed with neutrons extracted from the thermal moderator, while the cold beam for SANS is coming from the cold moderator. The day-1 instrument will be equipped with the thermal guide, while the cold guide will only be partly installed to allow installation of the foreseen SANS and imaging upgrades.

HEIMDAL will excel when performing *in situ* and *operando* studies, where the high ESS flux and the flexible resolution of the instrument will allow the investigation of systems with unprecedented speed. The samples of interest include magnetic materials, energy materials, hierarchical, and porous structures. Energy materials include, *e.g.* batteries, fuel cells, and thermoelectrics. HEIMDAL will also be suitable for making diffraction tomography, where the sample is rastered across a small beam providing diffraction patterns in different voxels. The upgraded version of the instrument combining TNPD and SANS will make HEIMDAL ideal for studying functional materials over broad length scales, and the intense source of ESS enables time-resolved measurements. The user community will include scientists from crystallography, chemistry, physics, material science, polymer, and bio-sciences. The instrument is

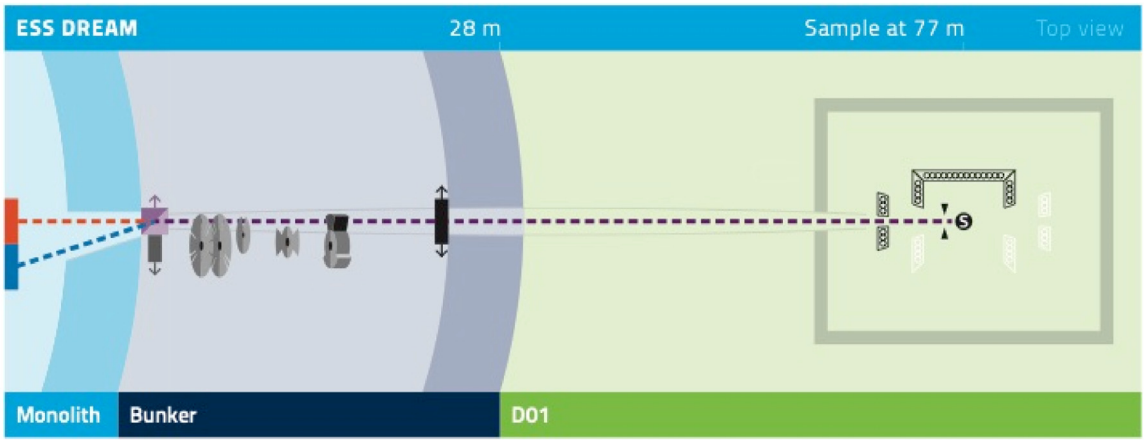

Fig. 23. DREAM instrument layout. Components shown in white are foreseen upgrades.

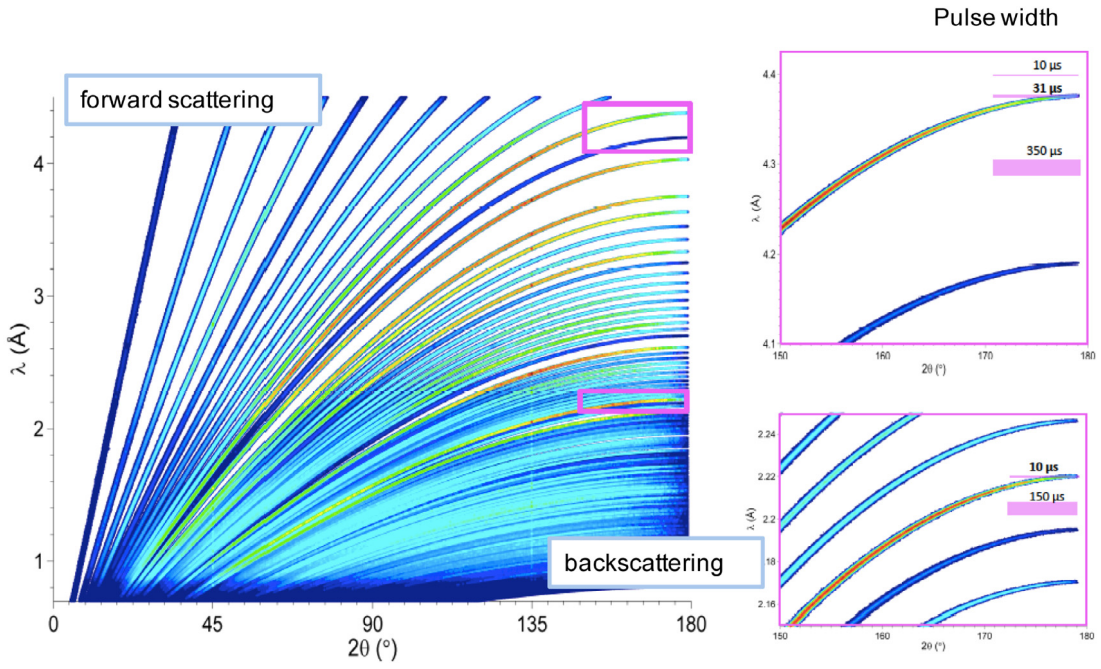

Fig. 24. Simulation of a 2D diffraction pattern on DREAM (wavelength vs diffraction angle) of $Na_2Ca_3Al_2F_{14}$. The inset shows a clear separation of the diffraction lines. The coloured bars show the width of the diffraction lines in the backscattering detectors at various pulse widths.

potentially also interesting for industrial users as it is a single point of entry to investigate samples on a huge range of length scales.

4.2.2. HEIMDAL instrument layout

An overview of the HEIMDAL instrument is shown in Fig. 25. Separate neutron beams are extracted from the thermal and cold moderators. The pulse length of the thermal beam is chosen by a pair of pulse-shaping choppers at 6.5 m, while the cold beam passes underneath the pulse-shaping choppers. The chopper systems of the two beams are designed individually to allow selection of pulse lengths suited for the very different techniques. A T0 chopper in the straight thermal guide suppresses the prompt pulse and a heavy shutter can block both beams to allow for safe access to the instrument cave. Cold and thermal neutrons from the two guides hit the sample at an angle of 4.5° with respect to each other. This gives space for individual collimation of the two beams. A "jaws" slit system in the thermal guide tailors the beam divergence to match the wavelength resolution of the pulse-shaping chopper. The cold guide is equipped with a double pinhole system to ensure a highly collimated beam for SANS. The second pinhole in the cold guide can be removed to provide a large area beam for imaging. The wavelength resolution of the cold beam is sufficient to perform Bragg-edge imaging.

In the experimental cave the sample is surrounded by detectors. The sample area will be assessible from the roof and by a side door. The detectors are raised from the cave floor independent of the false floor in the experimental cave. The radial collimator and the sample table are similarly mounted independently of the false floor in the cave. The sample table can be raised out of the beam position to ease installation of sample environment, which can be craned in/out through the roof. In the day-1 instrument only the TNPD detectors are installed and later, when fully upgraded the SANS and imaging detectors are also installed.

TNPD: The cylindrical diffraction detectors will be placed from 10° to 170° (left) and −60° to −170° (right) to collect the diffracted thermal neutrons. The day-1 instrument will only have coverage from 60° to 170°. The detectors are placed at a distance of 800 mm from the sample and will have an active height of 640 mm, which allows for a coverage of ±22° in the vertical plane. The detectors will have a pixel resolution of 2×7 mm^2 (H × V) and in the backscattering banks, the pixel height is likely to be reduced to 3.5 mm with the use of 128-bit readout electronics. The full detector system allows a Q-coverage from 0.5 to

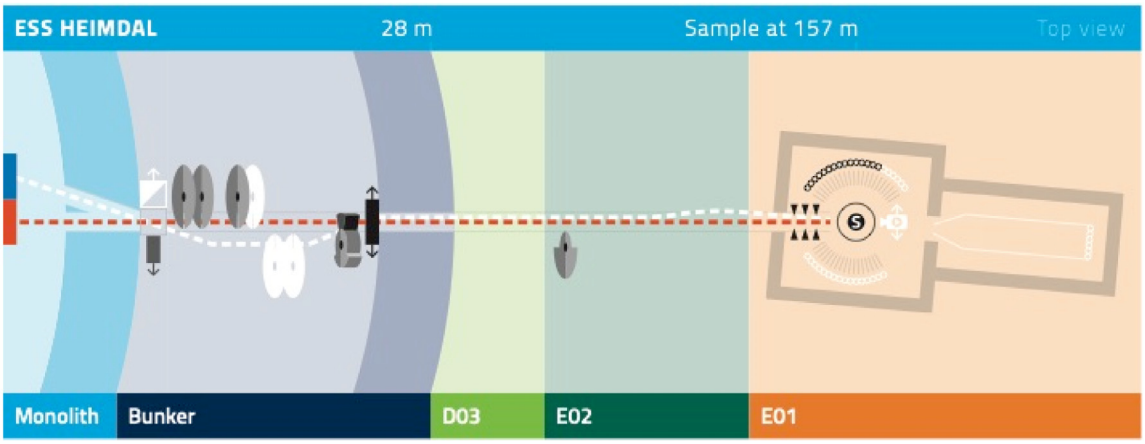

Fig. 25. HEIMDAL instrument layout. Components shown in white are foreseen upgrades.

25 Å^{-1}. Before reaching the detectors, the neutrons will pass a 1° radial collimator, suppressing scattering from the sample environment.

SANS: 10 m behind the sample, a SANS detector will be placed as a foreseen upgrade to cover reciprocal space from 10^{-3} to 0.1 Å^{-1}. A second SANS detector at 4 m together with the diffraction detectors will ensure a continuous Q coverage from 10^{-3} to 4 Å^{-1}.

NI: An imaging detector can be position behind the sample to collect absorption contrast images and Bragg-edge imaging. The simultaneously illuminated sample will be approx. 35 × 35 mm^2. Using the cold beam provides an intrinsic resolution of $\Delta\lambda/\lambda \sim 1.5\%$, while for the thermal beam the resolution can be adjusted by the pulse-shaping chopper. The NI detector will block the SANS detector. Consequently, NI and SANS cannot run simultaneously.

4.2.3. HEIMDAL expected performance

The pulse-shaping choppers allow resolution to be traded for flux, and beam slits are used to match the divergence to the time-of-flight resolution. Based on McStas calculations it is expected that when HEIMDAL runs in its relaxed-resolution mode with the pulse-shaping choppers at the source frequency of 14 Hz and a smooth divergence profile of ±0.5° at the sample, a neutron flux of ~10^9 n s^{-1} cm^{-2} will be reached. In the high-flux mode, the sample volume illuminated is up to 2.4 cm^3. A thorough simulation of the HEIMDAL detector taking the volume nature of the ^{10}B detector into account has been performed using GEANT4 [62].

In the high resolution mode, the choppers will run at 140 Hz, and the flux on the sample is reduced to 10^6 n s^{-1} cm^{-2}. In this setting, the resolution in the backscattering detector is $\Delta d/d \sim 0.04\%$. HEIMDAL will, in other words, be on par with the best high resolution instruments around the world, *e.g.*, HRPD@ISIS [63] and SuperHRPD@J-PARC [64], while in high flux mode it will exceed existing instruments by an order of magnitude. HEIMDAL can be adjusted between different flux/resolutions modes within minutes, taking full advantage of the long ESS pulse.

Four standard modes of operation are foreseen: High resolution, where the pulse-shaping choppers are running at n = 10× source frequency. Medium resolution n = 3× or 2× source frequency and high flux with n = 1× source frequency. Fig. 26 shows simulated data of the three different modes: High resolution (n = 10×), medium resolution (n = 2×), and high flux (n = 1×).

TNPD and SANS can run quasi-simultaneously with a 71 ms delay. Pulses from the thermal and cold moderators will be used for TNPD and SANS in an alternating fashion. A pulse suppression chopper on the thermal guide will allow a SANS pulse for every 1, 2, 3, 4 or 6 thermal pulses, to reach the sample. Generally, the small angle scattering patterns have two orders of magnitude more intensity than the Bragg diffraction peaks. The sequence of the pulses allows to adapt the speed of the TNPD and SANS measurements with respect to each other. In addition, it will be possible to collect cold neutron powder diffraction patterns in the diffraction detectors from the SANS pulses.

Table 11
MAGiC Quick Facts.

MAGiC Quick Facts	
Instrument Class	Diffraction
Moderator	Bispectral
Primary Flightpath	159 m
Secondary Flightpath	1 m
Wavelength Range	0.6–6 Å
Bandwidth	1.7 Å
Flux at Sample at 2 MW	1.5 × 10^9 n s^{-1} cm^{-2} (2.0–3.7 Å, full pulse)
Polarised Incident Beam	Permanent
Half-Polarised Detector Bank	
Q-Range	0.2–21 Å^{-1}
Q-Resolution Δd/d	Adjustable 1%–12%
Detector Coverage	60°[H] × 48°[V]
Polarisation Analysis Detector Bank	
Q-Range	0.2–6 Å^{-1}
d-spacing Resolution Δd/d	Adjustable 0.2%–4%
Detector Coverage	120°[H] × 6°[V]

HEIMDAL is built to focus on development and testing of new materials close to application in collaboration with industry. User-friendly software will aid the inexperienced and the changing user community.

4.3. MAGiC — Polarised single-crystal diffractometer for magnetism

4.3.1. MAGiC science case

MAGiC is a polarised single-crystal diffractometer with polarisation analysis dedicated to magnetism. The instrument has been designed to facilitate the study of magnetic systems, from magnetic structure refinement to magnetic diffuse scattering. As such, the instrument will offer a permanently polarised beam with a choice of the cold and thermal moderators, covering a Q-range of 0.1–20 Å^{-1}. The instrument will allow the study of sub-mm samples as well as thin films and interfaces with 2–50 Å lattice parameters (see Table 11).

Of high current interest in the scientific community is the role of spin–orbit interactions in solid materials and complex magnetic structures arising from competing interactions. Examples of current hot topics include the physical properties of iridium oxide materials [65], novel spin textures found in skyrmion-featuring materials [66], the complex interplay of magnetism and superconductivity in unconventional superconductors (pnictides, cuprates, heavy-fermion intermetallics and organic superconductors) [67], multifunctionality

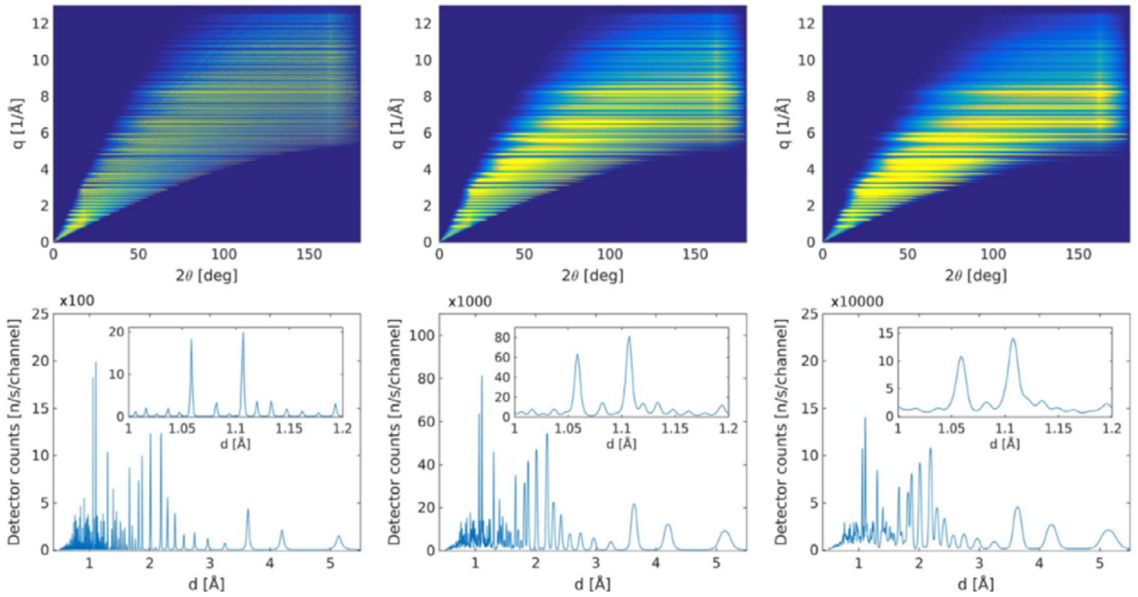

Fig. 26. Simulated powder diffraction patterns for the three modes of operation of HEIMDAL. From left to right: high resolution, medium resolution and high flux. The lower panels show the 2D data summed from 10° to 180°. The count rates shown correspond to a counting time of one second of data collection. The sample is $Na_2Ca_{12}Al_3F_{14}$ powder in a cylindrical cell. For the high-resolution-mode a sample size of 3 mm diameter and 10 mm height was used, while for the medium-resolution and high-flux modes the sample size was 5 mm in diameter and 20 mm in height. The instrument configuration of the simulation corresponds to an early version of the instrument design, but the performance for the final design will be similar. For more details on the simulation, see Ref. [61].
Source: Taken from [61].

in magnetically-induced ferroelectrics [68], and frustrated or low-dimensional magnetic materials featuring strong magnetic correlations [69] or spin-liquid-like quantum coherent ground states [70,71]. Some of these materials cannot be studied at present due to the unavailability of sufficiently large single crystals and/or the weakness of the magnetic contribution to the diffraction pattern.

4.3.2. MAGiC instrument layout

An overview of the MAGiC instrument can be seen in Fig. 27.

The instrument optics have been optimised to transport a neutron beam in the 0.6–6 Å range with a ±0.3° divergence both horizontally and vertically on a sample size of 5 × 5 mm^2. Efficient transport of the thermal neutrons is ensured by an elliptic guide system divided into three sections. The first one is a 74 m long half-ellipse starting at 6.9 m from the thermal moderator surface and oriented downwards by 0.5°. It extracts neutrons from the moderator and efficiently transports them to the second section, consisting of a polarising 3 m long straight guide part tilted by 0.25° compared to the first section. This section is vertically divided into 6 channels to ensure a polarising reflection for all thermal-neutron trajectories. The third section is a 74 m long half-ellipse focusing neutrons at the sample position (159.4 m), with a horizontal beam direction. When operating with cold neutrons, a solid-state bender located at 5.75 m from the moderator surface is translated into the beam to deflect and inject them into the guide axis, while rejecting the thermal neutrons. Finally, an optional 1 m long focusing guide can be inserted just before the sample to increase flux and divergence on sub-mm samples.

Cold neutron polarisation is ensured by the solid-state bender, coated with Fe-Si supermirrors and placed in a 3 kG saturation field. A 60 G magnetic guide field will maintain polarisation up to sample position. Thermal neutron polarisation is ensured by the polarising section at the half-way position of the guide. Each channel in the polarising section is coated with Fe-Si and placed in a 1 kG saturation field. The polarisation state can be switched with an RF spin flipper placed along the last guide section. At the sample position, an optional XYZ polarisation setup will allow users to freely rotate the incident polarisation. The cold neutron beam (λ > 1.8 Å) polarisation will be analysed by a 120° × 6° solid-state analyser.

The incident beam can be tailored to the user needs by a set of choppers and divergence slits. The pulse length can be tuned from the full 2.86 ms down to 200 μs improving the wavelength resolution while the incident divergence can be tuned down to ±0.1°.

The sample area is designed to host all required cryogenic equipment and superconducting magnets. A radial collimator will suppress most of the sample environment generated background and will be surrounded by two detectors based on the ^{10}B inclined geometry technology. With a radius of 1 m, the angular resolution is of ~0.1° × 0.3° (HxV). The first detector will cover 60° × 48° (HxV) and will be used for all experiments. The second one covers 120° × 6° (HxV) and will be dedicated to polarisation-analysis (PA) experiments.

4.3.3. MAGiC expected performance

The complete instrument has been simulated and optimised in McStas. An estimate of the flux and polarisation of the cold and thermal spectra has been extracted. At an initial power of 2 MW, the flux at sample position will be ~10^9 n s^{-1} cm^{-2} in the ±0.3° divergence range. The polarisation rate on the thermal spectrum is >98% for λ < 2 Å and strongly decreases for λ > 2 Å. On the cold spectrum, the solid-state bender achieves a polarisation rate >96% up to λ = 6 Å. To confirm these estimates, prototypes of the solid-state bender and analyser are under development.

Virtual experiments have been carried out to benchmark the instrument. On a typical 1 mm^3 sample, a complete half-polarised data collection with the thermal spectrum will be achieved in ~20 min. Polarisation analysis experiments with the XYZ setup allowing to separate the nuclear and magnetic contributions on a 10 mm^3 sample will be achieved in ~40 min. These benchmarks show promising performances with a gain factor compared to current instrumentation of one to two orders of magnitude.

5. Spectroscopy instruments

The properties and functionality of a specific material will depend on its atomic and magnetic symmetry in conjunction with the vibrational modes originating from the interactions between electrons and atoms. Vibrational modes can vary enormously from molecular

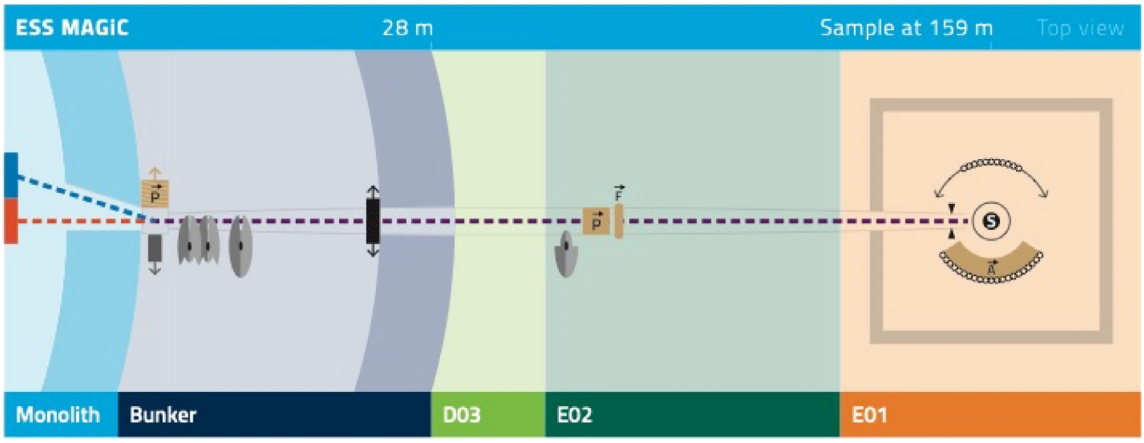

Fig. 27. MAGiC instrument layout.

vibrations in hydrogenous materials, as exemplified in the olfactory system of humans that detects change in the vibrational modes as an odour [72], to phonon modes, collective atomic modes the properties of which strongly determine thermal conductivity, quantum spin excitations that result in new states of matter, to diffusional motions of atoms, important in the study of hydrogen fuel cell technologies aimed at reducing air pollution. Inelastic neutron scattering measures the energy transfer of neutrons creating and annihilating these elementary excitations. The resultant scattering intensity depends on the wavevector transfer, representative of the crystalline and magnetic symmetry, and the incident and final neutron energies, representative of the vibrational mode of the material. A comparison of inelastic neutron scattering intensities with theoretical calculations provides the strictest test for any proposed physical model.

In the first suite of instruments, ESS will host 5 spectrometers, optimised for a range of dynamic modes with energies ranging from a few micro-eV to energies approaching the eV-range. Since inelastic scattering signals are inherently weak, the signal-to-noise ratio remains a strongly limiting factor for most state of the art experiments. ESS will be the worlds' brightest neutron scattering facility and as such the possibility to study, by spectroscopy, samples hitherto too small to yield results will become reality. In addition, the enhanced brightness of the ESS enables routine in-situ time-dependent studies with optimised sample environments — and thus widening the feasibility range of neutron spectroscopy even further.

The long pulse of the ESS serves to improve spectrometer performance in a variety of ways. First of all, it becomes preferable to build spectrometers with a rather long primary flight path, as compared to instruments at short-pulse sources. This results in unprecedented possibilities for background suppression, as the neutron detectors are situated very far from the spallation target. Line-of-sight can be eliminated even for some thermal instruments and far upstream in the guide system for the cold spectrometers. The fast-neutron environment at ESS will therefore be very quiet, greatly improving the signal-to-noise ratio, which is most crucial for the spectroscopy instruments.

The wavevector and energy coverage of the spectrometers is shown in Fig. 28, demonstrating the complementarity in dynamic range. The long pulse and primary flight path allow for both increased flexibility and new design features, especially for the indirect time-of-flight spectrometers. For instance, the intricate pulse-shaping chopper system of the VESPA vibrational spectrometer allows for a near-constant relative energy resolution down to 1% in a very wide energy range, greatly simplifying analysis of the recorded vibrational spectra. The extreme environment spectrometer, BIFROST, will be able to utilise the full ESS pulse while retaining a 150 μeV resolution, resulting in unprecedented neutron flux at the sample, while being able to trade neutron flux for energy resolution through pulse shaping, down to 20 μeV resolution. MIRACLES will provide an energy transfer range centred at the elastic line from −500 to +500 μeV, the largest of any backscattering spectrometer worldwide, with a tuneable energy resolution between 2 and 45 μeV. Thus, the indirect geometry time-of-flight spectrometers are all unique in the neutron community, each recording excitation energies of different orders of magnitude.

The two direct geometry spectrometers are both highly versatile and mutually complementary. CSPEC focuses on the cold regime and the corresponding broad scientific profile of low energy excitations, while T-REX has a broader dynamic range and a scientific emphasis on magnetism. Both instruments make extensive use of Repetition Rate Multiplication (RRM), illuminating the sample with a series of incident energies from a single ESS pulse within a wavelength band of 1.7 Å. At the cold-neutron energies employed by CSPEC, this bandwidth translates into a fairly limited range of incident energies which will often allow the multiple data sets obtained in this way to be combined, effectively increasing the counting rate. This is evident in the degree of overlap between the two lower shaded regions for CSPEC in Fig. 28. For the higher incident energies available on T-REX, RRM results in a much larger range of incident energies which cannot be straightforwardly combined, but instead provides a much larger dynamic range, allowing the exploration of the dynamics over several orders of magnitude, as is clear from the large degree of separation between the two upper shaded regions for T-REX in Fig. 28.

While the science cases of the ESS spectrometers overlap to some degree, the instrument capabilities do not, making the instruments highly complementary. The excitation energies covered at the ESS span five orders of magnitude, and each instrument has the beneficial combination of being both broadly applicable scientifically while specialising in specific types of measurement. This makes the suite perfectly suited for delivering world class science from the start of the user programme.

5.1. CSPEC — Cold chopper spectrometer

5.1.1. CSPEC science case

CSPEC has been developed to access picosecond dynamic behaviour in life sciences, energy and functional materials in addition to emergent magnetism. The weak interaction of neutrons with matter, in addition to the limited flux at present-day neutron sources, make it difficult to address certain pertinent scientific questions at this moment in time. The enhanced flux of the ESS, in addition to the unique possibilities gained via repetition rate multiplication (RRM) on a long cold chopper spectrometer, enables CSPEC to follow kinetic events in-situ or in-operando and probe materials for which the synthesis route results in samples that are too small to measure today (see Table 12).

CSPEC will probe the structures, dynamics, and functionality of large hierarchical systems as they change or operate. Hierarchical systems include liquids, colloids, polymers, foams, gels, and granular and

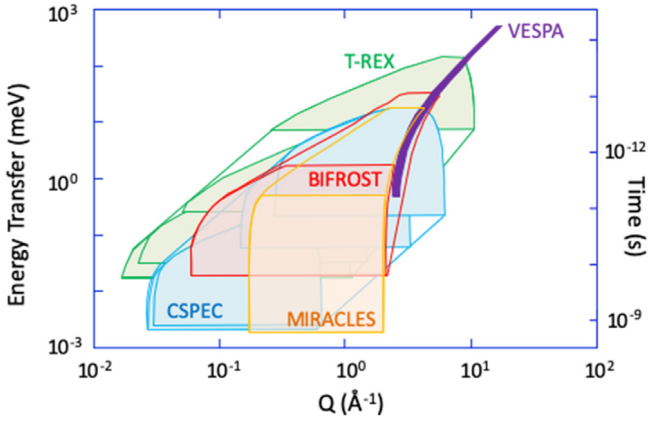

Fig. 28. The (Q, E) range accessible by the ESS spectrometer suite. Blue: CSPEC, Green: T-REX, Red: BIFROST, Purple: VESPA, Yellow: MIRACLES. The shaded regions indicate the Q-E coverage of a single measurement. In the case of BIFROST, two detector positions are required to cover the shaded kinematic range. The coloured outlines indicate the region which can be accessed by adjusting the range of incident energies. For CSPEC and T-REX, the four shaded regions indicate the range of incident energies accessible using RRM. From left to right: Minimum and maximum E_i for the lowest energy setting, minimum and maximum E_i for the highest energy setting. The upper bound shown for each region is the limit of greatest energy transfer in downscattering (neutron energy loss), while the lower bound is the limit of resolvable energy transfer (minimum resolution width).

Table 12
CSPEC Quick Facts. The quoted flux numbers do not take RRM gains into account.

CSPEC Quick Facts	
Instrument Class	Spectroscopy
Moderator	Cold
Primary Flightpath	160 m
Secondary Flightpath	3.5 m
Wavelength Range	2–20 Å
Bandwidth	1.72 Å
Flux at Sample at 2 MW	9×10^5 n s^{-1} cm^{-2} over 4 × 2 cm^2 (standard beam)
(λ = 5 Å, $\Delta E/E_i$=3%)	4×10^6 n s^{-1} cm^{-2} over 1 × 1 cm^2 (focused beam)
Detector Coverage	5°–140°[H] × ±8°[V]
	(5°–140°[H] × ±26°[V][a])
Energy Resolution	Adjustable 1%–5% of E_i

[a]Available as a foreseen upgrade.

biological materials as well as the ever-complex low-energy dynamics of energy and magnetic materials.

Particular examples include:

- Understanding the effect of spin–orbit coupling in the classification of quantum spin liquids [73,74].
- Magnetic excitations of emergent phenomena in magnetically frustrated materials [74,75].
- Time dependence of the rotational or translational diffusive processes in enzyme catalysis [76,77].
- Time dependent phenomena of hydrogen storage in clathrates [78].
- Proton diffusion in metal organic frameworks [79].
- Diffusion dynamics and the relation to the ordering mechanism of solidification [80,81].
- Understanding light induced dynamics of antenna pigment/protein complexes [82].

5.1.2. CSPEC instrument layout

CSPEC is a 160 m instrument, from the moderator to the sample position, with a 3.5 m sample-to-detector distance in the equatorial plane (see Fig. 29). The guide views the para-hydrogen cold moderator before vertically curving twice out of line of sight in an S-shape, and once out of line-of-sight in the horizontal direction in a C-shape.

Bandwidth choppers extract a 1.72 Å bandwidth before a counter rotating double-disc pulse-shaping (PS) and a double-disc monochromating (M) chopper, at 105.7 and 158.5 m respectively from the moderator, providing a series of up to 10 monochromatic pulses for each ESS source pulse, with an adjustable energy resolution. The length of each individual time frame can be chosen to optimise for quasielastic or inelastic scattering, via a frame overlap chopper positioned before the monochromating chopper. The long length of CSPEC ensures that adjacent pulses are close in incident energy E_i (Fig. 30), and comparable in energy resolution (Fig. 30 inset). The figure shows the time-distance diagram for the extraction of 3–4.6 Å neutrons with an M chopper frequency of 336 Hz, resulting in an energy resolution (full width at half maximum) ranging from 1.6% to 1.35% for the RRM set of wavelengths starting at λ = 3 Å — see Fig. 30 (inset). Large flux gains can be made by combining pulses within each repetition period if the experiment can tolerate the variation in energy and wavevector transfer resolution across the bandwidth.

An exchangeable focusing guide can reduce the beam size from 4 × 2 cm^2 to 1 × 1 cm^2 at the sample position, increasing the flux by a factor of 5 at a wavelength of 5 Å. Translation of the slit system towards the sample ensures a good signal-to-noise ratio. The sample environment pot is integrated into the detector tank with an aluminium gate valve between the two, that can be closed to enable experiments under ambient pressure, and opened to minimise excess scattering from aluminium, e.g. for single crystal experiments. The sample environment pot has been designed to offer both access from the top and from the side, facilitating in-situ and in-operando experiments.

First day sample environment includes:

- Cryofurnace
- ^{3}He insert
- Access to a 12 T magnet via the sample environment pool
- Sample rotation stage & goniometer
- In-situ capabilities (pump–probe).

Scattering from the sample will pass through an oscillating radial collimator into the detector tank with a lateral angular range −30°< 2θ < +140° and a vertical angular range from −8° to +8° on day one, extendable as a foreseen upgrade to −26.5° to +26.5°, resulting in 2.65 sr of detector coverage. The detector tank is evacuated and conforms to the amagnetic requirements to house a 12 T magnet at the sample position. Neutron detection is based on ^{10}B multigrid layer technology [83] using 25 × 25 × 10 mm^3 (height × width × depth) voxels to cover the detector area.

5.1.3. CSPEC expected performance

CSPEC will provide world-leading performance for a chopper spectrometer. According to neutronics calculations an improvement in flux, for each pulse on sample, of a factor of 2–6 (at 5 MW) can be expected with respect to current leading cold chopper spectrometers. Further substantial flux gains, at minimal expense of energy resolution, can be made by accumulating RRM pulses. CSPEC will therefore make it possible to study the dynamic nature of materials under real time kinetic events. This will be particularly feasible with the versatile sample environment that is optimised to perform in-operando experiments.

5.2. T-REX — Bispectral chopper spectrometer

5.2.1. Science case

The T-REX spectrometer is devoted to measuring a wide range of energy transfers, between 20 μeV and 140 meV, with good wave vector resolution in combination with Polarisation Analysis (PA). The correspondingly large choice of instrument configurations and operational modes will deliver the flexibility and versatility requested by the wide user community.

In particular, the PA option will enable the separation of the magnetic spectra from nuclear scattering, the analysis of polarisation and

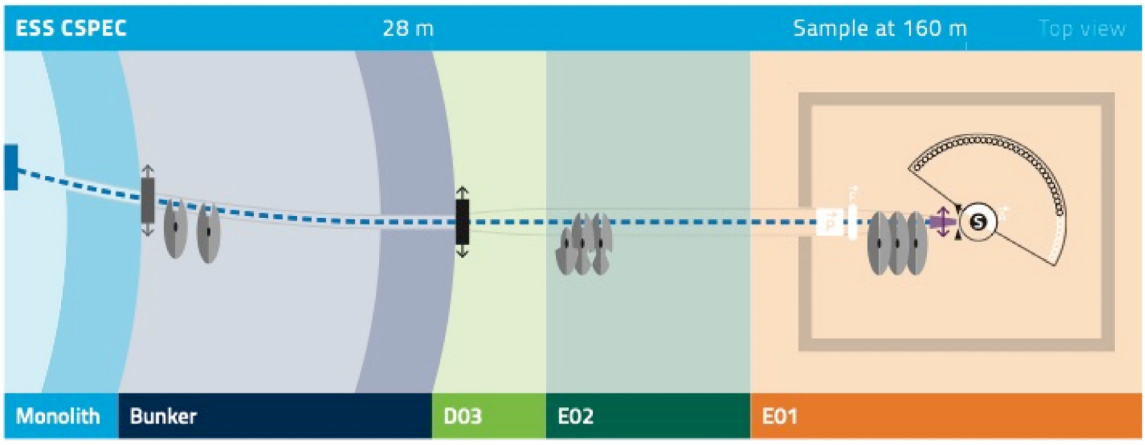

Fig. 29. CSPEC instrument layout. Components shown in white are foreseen upgrades.

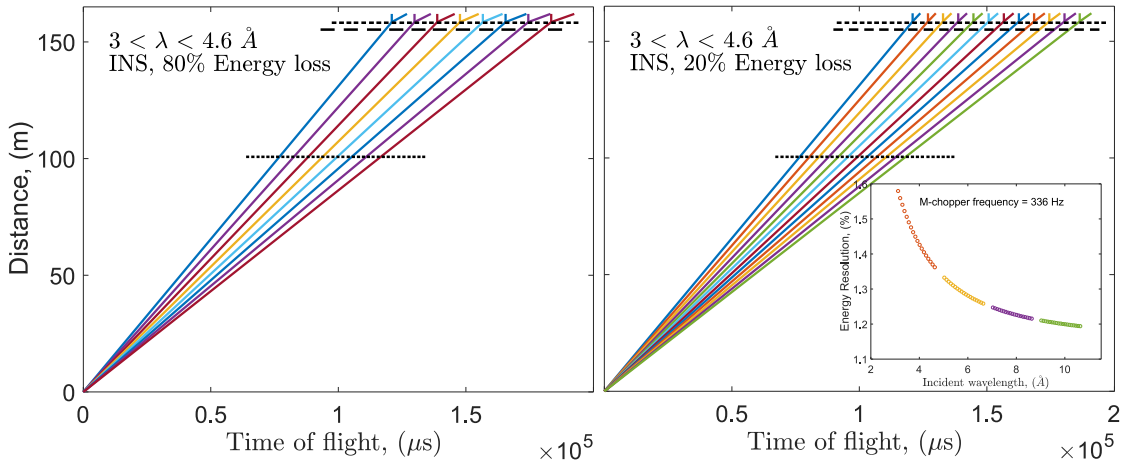

Fig. 30. Time of flight diagram for 3–4.6 Å neutrons across the 1.72 Å bandwidth of CSPEC. Dashed horizontal lines represent chopper positions and respective opening times. The coloured lines between the sample and detector indicate an energy loss of (left) 80% of E_i and (right) 20% of E_i, and an infinite energy gain. Inset: Range of elastic energy resolutions across the bandwidth for a range of incident wavelength settings with minimum wavelengths of: 3, 5, 7, and 9 Å.

Table 13
T-REX Quick Facts. The quoted flux numbers do not take RRM gains into account.

T-REX Quick Facts	
Instrument Class	Spectroscopy
Moderator	Bispectral
Primary Flightpath	164 m
Secondary Flightpath	3 m
Wavelength Range	0.7–6.5 Å
Bandwidth	1.7 Å
Incident Beam Polarisation	Optional
Polarisation Analysis	Optional
Flux at Sample at 2 MW (E_i = 8 meV)	0.8–5 × 10^6 n s^{-1} cm^{-2}
Flux at Sample at 2 MW (E_i = 50 meV)	0.3–2 × 10^6 n s^{-1} cm^{-2}
Detector Coverage	1°–72°[H] × −25°–15°[V] (−36°–144°[H] × −25°–15°[V][a])
Energy Resolution (E_i = 2 meV)	Adjustable 1%–2.5% of E_i
Energy Resolution (E_i = 100 meV)	Adjustable 4%–7% of E_i

[a]Available as a foreseen upgrade.

eigenvectors of magnetic excitations and permit the separation of coherent and nuclear spin incoherent scattering, which is of particular importance for hydrogen-containing samples in energy research, soft matter and life sciences. Spectroscopy using non-polarised neutrons in the wide dynamical range offered by T-REX will enable the investigation of coherent excitations, spin correlations and fluctuations, relaxation and diffusion processes in a broad range of samples and applications.

The instrument can be configured in a versatile fashion. The long and bright pulse from the ESS moderators in combination with fast-spinning counter-rotating choppers enables energy resolution settings from high resolution to high flux simply by changing the chopper frequency. T-REX is designed to perform repetition-rate multiplication (RRM), in which the choppers select a range of incident energies from a single source pulse. Each individual spectrum is measured with a well-adapted energy resolution. This characteristic is crucial for the study of large energy transfer to the sample and particularly useful for experiments on single crystals. With tuneable beam collimations, the balance between Q-resolution and flux can be tailored to the needs of each experiment, and good background conditions at the lowest detection angles can be achieved in cases where weak signals are under investigation with thermal incident energies at small Q values, such as for the study of collective excitations in disordered systems.

In view of the variety of expected user communities, the sample area shall be spacious and capable of hosting various pieces of sample environment equipment, enabling the application of high and low temperatures, pressure, and magnetic or electric fields. More complex studies, such as *in-operando* measurements or levitation experiments require convenient side access to the sample area to allow also auxiliary characterisation tools in parallel to the neutron scattering experiment.

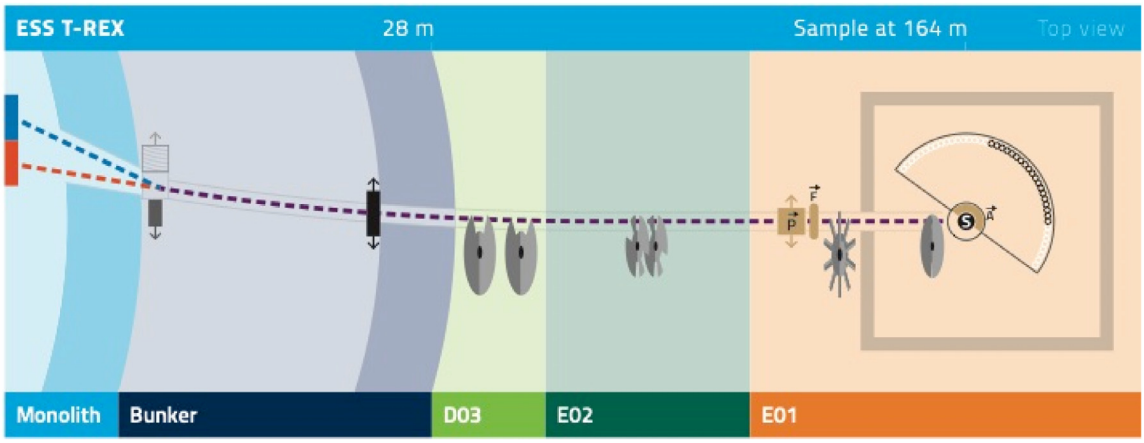

Fig. 31. T-REX instrument layout. Components shown in white are foreseen upgrades.

5.2.2. Instrument layout

In order to achieve its scientific mission T-REX is equipped with a bispectral extraction system. The neutron guide axis is oriented towards the thermal part of the moderator, so that neutrons from the cold moderator arrive with an angular offset towards the guide entrance and need to be reflected into the axis direction. This function is performed with a bender that reflects only neutrons from the cold moderator, with high efficiency for wavelengths above 2 Å. A motorised stage moves the bender element into place when cold neutrons are needed for the experiment and exchanges it with a standard guide element to reach unperturbed guide illumination from the thermal moderator (see Fig. 31). The main instrument parameters are listed in Table 13.

The shape and properties of the neutron optics have been optimised with the help of ray-tracing simulations for a beam collimation increasing from ±0.25° in the thermal band to ±1° in the cold band, and a beam cross section at the sample position of 10 × 30 mm^2. The vertical profile consists of two half-elliptic extremities connected with a straight section in the middle. As a measure to reduce background, the horizontal shape consists of a curved section of 60 mm width (R=12 km), 90 m long, to ensure that the direct line-of-sight is broken, while the end section has an elliptic profile.

When specific measurements require a clean access to the small-angle region of the detector (down to 1°), such as collective dynamics of disordered systems or spin dynamics of powder samples, the last elements of the neutron guide can be replaced with a collimator by means of a motorised exchanger.

The chopper cascade of T-REX implements five different functions. Two discs spinning at 14 Hz are used to select the experimental band and avoid overlap from previous pulses. A pair of counter-rotating choppers placed at 108 m from the moderator, spinning at frequencies below 252 Hz, defines the source pulse width and hence the wavelength resolution of the incoming beam. A pair of counter-rotating choppers placed at 162 m from the moderator, spinning at frequency below 336 Hz, defines the pulse width of the incoming beam at the sample and hence the time-of-flight resolution of the scattered beam. A specially developed *fan* chopper is used to avoid frame-overlap in the scattering pattern, by suppression of specific wavelengths from the polychromatic beam. All choppers are placed outside the bunker. In addition, the project includes the provision for adding a T0 chopper inside the bunker at distance < 19 m, in case the hot commissioning indicates that it is necessary to further reduce background.

Realising PA for the entire neutron wavelength band of T-REX is a challenging task and, due to the bispectral character, it requires different components for cold and thermal neutrons, so that the best performance will be achieved in both the energy ranges. To realise polarisation of cold neutrons, the polarisation system includes a polarising multichannel V-cavity, whereas for thermal neutrons it includes a polarised ^{3}He cell and a guide field for adiabatic spin rotation. The analysis of the neutron spin direction after scattering from the sample will be obtained with a "Magic PASTIS" setup [84], which will include a wide angle ^{3}He cell (see Fig. 33).

The secondary flight path on T-REX will be kept under cryogenic vacuum conditions (10^{-6} mbar). The detectors for T-REX will be based on the new MultiGrid design. The active area will cover the polar angular range from −25° to +15° and the azimuthal angular range from −36° to +144°, with a minimum scattering angle of 1°. In the day-one configuration of the instrument, the detectors will be installed at angles from 1° to 72°. Given the sample to detector distance of 3 m, the detection area specified in the foreseen upgrade is 21 m^2, with a full height of 2.2 m. In order to achieve the expected scientific performance in terms of energy and Q resolution, the detector voxels will be 20 × 20 × 10 mm^3 (width × height × length).

5.2.3. Expected performance

Two anticipated chopper configurations have been tested using ray-tracing simulations: the instrument configuration with the highest achievable energy resolution (HR) and the one with the highest flux (HF). We performed virtual experiments using as a sample an ideal isotropic scatterer, in order to mimic Vanadium calibration. The results of virtual experiments have been analysed with respect to elastic energy resolution and flux at sample. We have compared the flux values obtained, for an ESS power of 2 MW, to comparable values for existing world-class instruments also obtained by simulation. Simulated flux and elastic energy resolution versus incident energy for T-REX are plotted in Fig. 32. T-REX shows a gain factor of 3 when compared to IN5 at an incident energy of 3 meV and an elastic energy resolution of 100 μeV (FWHM). When compared to 4-SEASONS at an incident energy of 100 meV and an elastic energy resolution of 4 meV (FWHM), the calculated gain factor is 6, for a J-PARC accelerator power of 1 MW. Since T-REX is optimised for RRM, an additional gain is expected ranging from 1 to 20, which is difficult to quantify, as it depends mainly on the experiment.

We stress that with the design of T-REX we aim at performing inelastic neutron scattering differently and not simply faster because of the increased flux, by combining the use of polychromatic experiments with Polarisation Analysis over a wide dynamic range. This characteristic is not available nowadays at any instrument and will make the instrument unique to the needs of the user community.

5.3. BIFROST — High-flux extreme environment spectrometer for small samples

5.3.1. BIFROST introduction

BIFROST will be a high flux cold neutron indirect geometry spectrometer, optimised for taking full advantage of the entire ESS pulse.

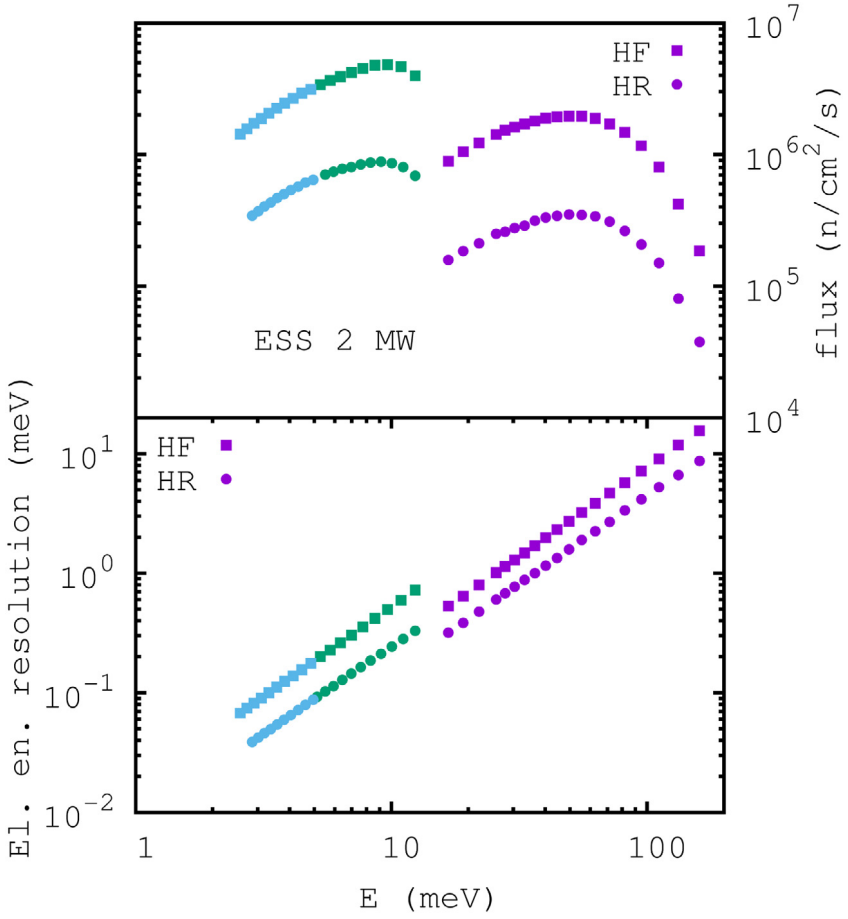

Fig. 32. Results of Vitess simulations of T-REX for flux and elastic energy resolution are shown as a function of incident energy at 2 MW ESS source power, for two anticipated chopper configurations termed HF (highest flux) and HR (highest resolution).

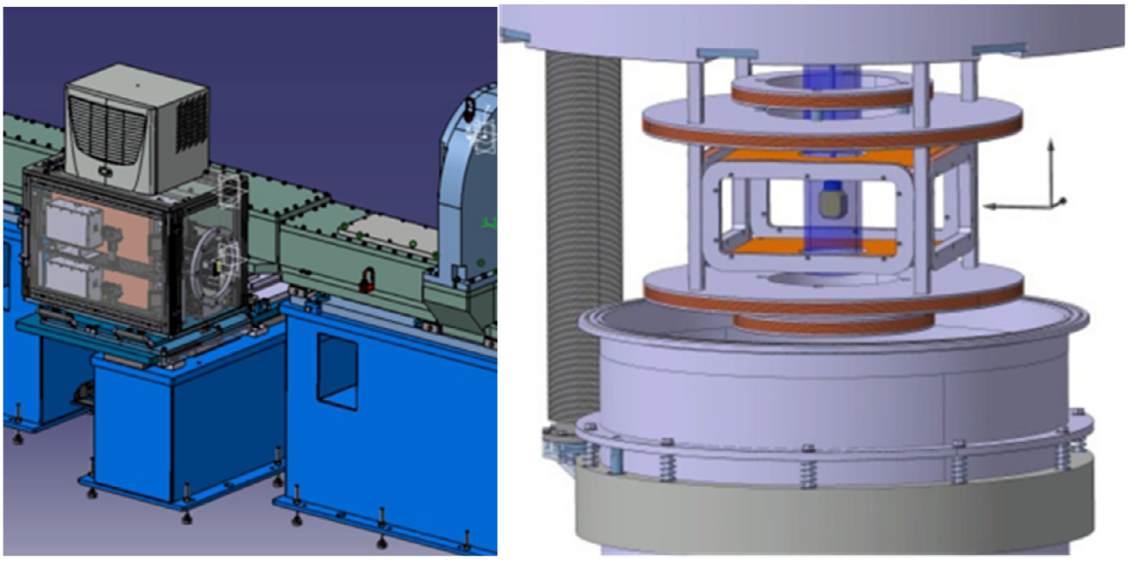

Fig. 33. T-REX polarisation components. Left: Thermal Beam Polariser Unit. Right: "Magic PASTIS" set-up for polarisation analysis.

Allowing a polychromatic beam to reach the sample position, BIFROST will attain a flux up to 10^{10} n s^{-1} cm^{-2} while retaining the typical resolution of cold neutron spectrometers. The 0.7 m^2 large analyser array is confined to the horizontal scattering plane. These unique features make BIFROST the instrument of choice for investigating low-energy dynamics in small samples and in extreme sample environments.

5.3.2. BIFROST science case

BIFROST is expected to massively impact the field of magnetism. Although abundant in applications, this field persists as a subject of immense fundamental interest.

Low-dimensional magnets in particular give rise to puzzling phenomena, usually studied using cold neutron spectroscopy. Fractional

Table 14
BIFROST Quick Facts.

BIFROST Quick Facts	
Instrument Class	Spectroscopy
Moderator	Cold
Primary Flightpath	162 m
Sample-Analyser Flightpath	1.1–1.7 m
Wavelength Range	1.5–6 Å
Bandwidth	1.7 Å
2θ Range	7°–135°
2θ Coverage	90° in 2 settings
2θ Resolution	0.7°–1.2°
Analyser Energies	2.7, 3.2, 3.8, 4.4, 5.0 meV
Energy Transfer Range	−3 to +55 meV
High Flux Mode [2.3–4.0 Å]	
Flux at Sample at 2 MW	6×10^9 n s^{-1} cm^{-2}
Resolution ($E_f = 5$ meV, $\hbar\omega = 0$)	190 μeV
Resolution ($E_f = 5$ meV, $\hbar\omega = 5$ meV)	450 μeV
High Resolution Mode [2.3–4.0 Å]	
Flux at Sample at 2 MW	9×10^8 n s^{-1} cm^{-2}
Resolution ($E_f = 5$ meV, $\hbar\omega = 0$)	50 μeV (prismatic)
Resolution ($E_f = 5$ meV, $\hbar\omega = 5$ meV)	50 μeV (prismatic)

excitations in square-lattice quantum antiferromagnets [85] and confinement bound states in 1D quantum magnets [86], are good examples. Applying magnetic fields to such model magnets can induce baffling phenomena like Higgs amplitude modes [87] and Bose–Einstein condensation [88], while applied pressure can give rise to quantum phase transitions in quantum spin liquids [89]. Cryomagnets are a standard tool in neutron spectroscopy, but pressure cells much less so, due to severe limitations on the sample space. As BIFROST allows cold neutron spectroscopy on much smaller samples than previously feasible, the instrument is expected to unchain the field of high pressure quantum magnetism.

High-temperature superconductivity arises in the antiferromagnetic square CuO_2 layers of the well-studied cuprates. A resonance mode at the antiferromagnetic wavevector appears in the superconducting state [90–92] and has also been observed in multiple Fe-based superconductors [93]. In general, our knowledge of the spin-excitations in these unconventional superconductors is limited by neutron flux, and in the case of the cuprates, only crude details of these complex dynamics are currently experimentally accessible. A more detailed experimental picture might prove crucial for our understanding of the spin dynamics of the cuprates, both at low [94] and high [95] energies. BIFROST will be able to provide such a picture, especially by studying the interplay of superconductivity with competing order parameters that come into prominence as superconductivity is suppressed by high magnetic fields [96].

Many potentially functional magnetic materials work via mechanisms which are poorly understood. Recently, Skyrmion lattices [97] offer the possibility of ultra-dense data storage, and the dynamics of these chiral magnets are studied using neutron spectroscopy [98]. The multiferroic materials are intensely studied as well. Besides playing a crucial role in the emergent field of spintronics [99], they give rise to curious magnetic states such as electromagnons [100] and solitonic lattices [101]. They also harbour exceedingly complex (H,T) phase diagrams [102,103]. Parametric studies of the dynamics related to this plethora of magnetic phases will be offered by BIFROST for the first time.

The order of magnitude flux gain delivered by BIFROST also has the potential of making cold neutron spectroscopy much more accessible outside the magnetism community. For example neutron flux has to date been a limiting parameter for studies of quasielastic scattering under very high pressures, which has the potential to yield unique information about the diffusion of water in the Earth's crust [104], important in the field of geoscience. Another example is collective dynamics in biological samples, e.g. the investigation of lipid membranes on a triple axis spectrometer [105].

5.3.3. BIFROST instrument layout

An overview of the BIFROST instrument is shown in Fig. 34. The in-monolith feeder efficiently accepts the appropriate neutron beam phase space from the cold source, and focuses the neutrons horizontally onto a virtual source 6.32 m from the moderator. Here, a 210 Hz double-disc Pulse-Shaping Chopper (PSC) will be able to reduce the pulse duration down to 0.1 ms in the high-resolution mode. A parked PSC allows the full ESS pulse to reach the sample in the high-flux mode. Further downstream, two Frame-Overlap-Choppers (FOCs) remove unwanted frames from the PSC. At 78 m from the moderator, the bandwidth chopper (BW) tunes the neutron band to avoid frame overlap at the sample position. After the sample, the analysers are arranged in a single scattering plane, accommodating the geometries of high field magnets. There are 9 Q-channels, each covering a scattering angle interval of 5.2°, and spanning a 90° 2θ-interval in two tank settings. A beryllium filter between the sample and the analysers eliminates scattered neutrons with energies above 5 meV from the tank, preventing higher-order contamination from the analysers. Each Q-channel will contain 5 analysers reflecting neutrons with energies of 2.7–5.0 meV (see Table 14), following the CAMEA concept [106], with analysers placed behind one another. Prototypes of this backend concept were tested both on time-of-flight [107] and triple-axis [108] front-ends, and currently a triple-axis implementation of this back-end is in user operation [109]. For each analyser channel, the prismatic analyser concept is implemented [110], offering the option for greatly improving backend resolution. The detector for each channel consists of 3 position-sensitive 1D tubes, offering continuous coverage in 2θ (along the tube axis) and the option of splitting the scattering from the analysers into 3 distinct energy channels, each accepting a much narrower energy band than that of a simple similar analyser/detector arrangement. This gives BIFROST a unique combination of very high flux, mapping capabilities and a flexible energy resolution.

5.3.4. BIFROST expected performance

The BIFROST guide is optimised for a sample area of 1×1 cm^2, with both a vertical and horizontal divergence of ±0.75°. The polychromatic incoming beam has a bandwidth of 1.7 Å, due to the repetition rate of the accelerator and the length of the instrument. The useful dynamic range of BIFROST lies in the wavelength interval 1.5–6.0 Å. Looking primarily at the cold source, the optimal flux setting is between 2.3 and 4.0 Å, the expected workhorse mode of the instrument. In this wavelength interval, the coarsest resolution mode offers a neutron flux approaching 10^{10} n/s/cm^2. At the shortest wavelengths the flux is reduced by factor of 5–10, and implementing the highest resolution (PSC opening time of 0.1 ms) reduces the flux by a factor of 30. However, even in the highest resolution mode in the near-thermal range, BIFROST delivers a flux well in excess of 10^7 n/s/cm^2. The energy resolution is a convolution of the front- and back-end resolutions, respectively. Therefore, the prismatic use of the back-end channels is not needed in the coarse resolution mode of BIFROST, where the front-end resolution dominates. Here, the back-end channels would be more similar to that of a standard triple-axis spectrometer, with similar resolution in the entire dynamic range. However, in the high resolution mode, the prismatic use of the detector arrays offers a greatly improved resolution, not only at the elastic line, but retainable inelastically. Thus, a resolution of down to 20 μeV [111] is achievable in the interval $\hbar\omega$ = 0–6 meV, using the prismatic analyser concept, for a final energy of E_f = 2.7 meV. The high flux, together with the prismatic concept, allows for an unprecedented real-time resolution of 20 μs, allowing for pump–probe studies [111]. The instantaneous Q-E coverage and resolution in the standard wavelength and high flux mode is shown in Fig. 35. The Q-resolution is wavelength-dependent, and it is therefore more useful to present the angular resolution of the spectrometer. The angular resolution of the backend is fixed, both horizontally (1.2° at E_f = 2.7 meV and 0.7° at E_f = 5.0 meV) and vertically (2°). The divergence of the incoming beam is fixed vertically (0.5°–1.2° depending on wavelength), and can be adjusted horizontally by divergence jaws within the interval 0.4°–1.5°.

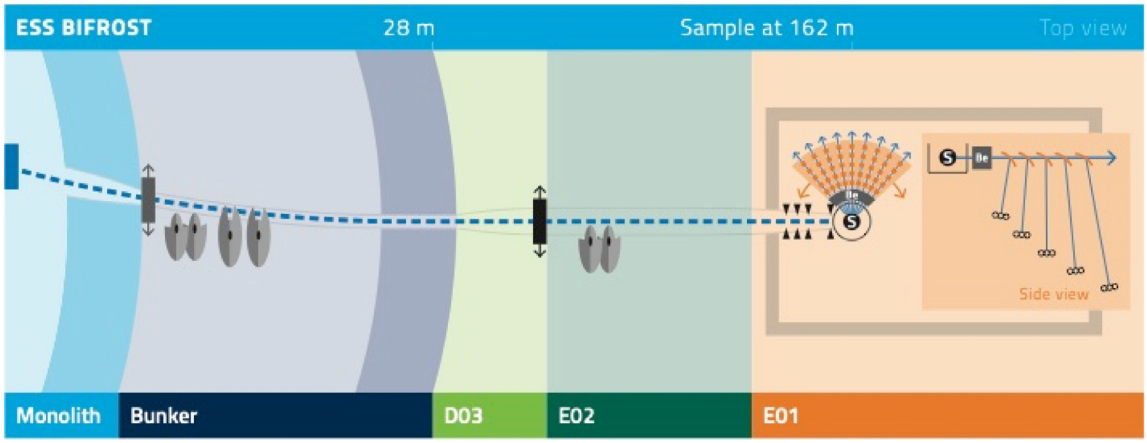

Fig. 34. BIFROST instrument layout.

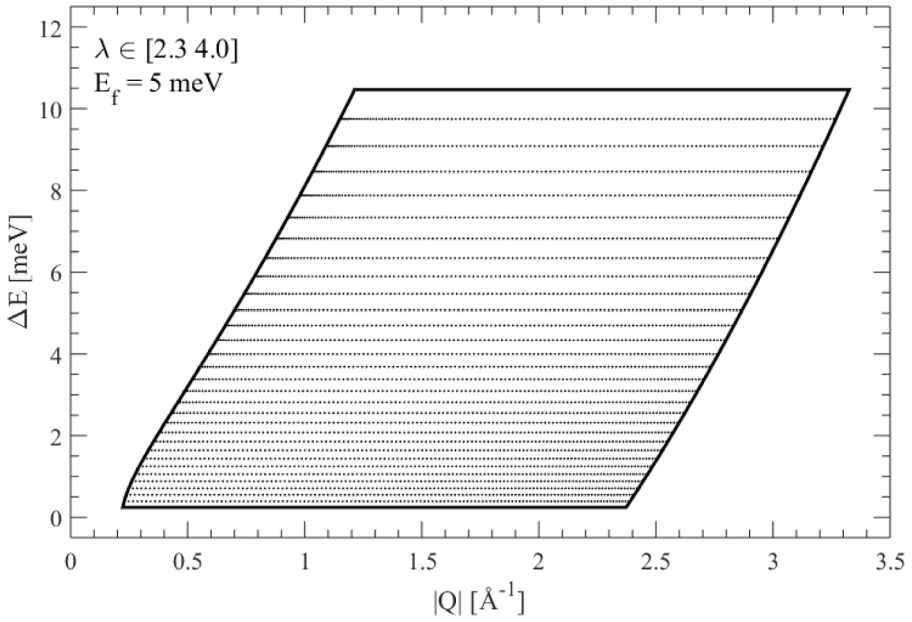

Fig. 35. Low angle continuous (|Q|, E) coverage of BIFROST for E_f = 5 meV in the wavelength interval 2.3–4 Å, in high flux mode. The spacing between the horizontal dotted lines indicates the FWHM of the energy resolution of the primary spectrometer, at that energy transfer.

5.3.5. *BIFROST conclusion*

In conclusion, BIFROST is a cold spectrometer optimised for the unique ESS source, with a great deal of flexibility in terms of dynamic range, sample environment, energy resolution and Q-resolution. The instrument offers massive gains in performance at high applied fields and using pressure cells, as compared to the current state-of-the-art.

5.4. *VESPA — Vibrational spectrometer*

5.4.1. *VESPA science case*

The fundamental idea behind the neutron vibrational spectroscopy (NVS) [112] technique is analogous to that exploited in optical vibrational spectroscopy (i.e., infrared and Raman): a sampling probe, carrying energy larger than that of the internal excitations, is directed at the sample. The resulting energy loss upon excitation of a vibration mode gives direct information on the vibrational energy level structure of the sample. In general, vibrational spectroscopy is an important technique frequently used in both fundamental and applied research laboratories all over the world. Its applications to the investigation of solids and liquids, soft matter, complex fluids, and bio-materials are well-known. Alone or in combination with other techniques, vibrational spectroscopy permits the identification of bonds and functional groups, as well as the transformations that occur when bonds are broken and made in chemical reactions (e.g., in catalysis or thermal decomposition). In addition, the vibrational density of states is of great interest in itself, being related to various thermodynamic properties such as specific heat and entropy. NVS exploits the large incoherent scattering cross section of the hydrogen nucleus. Proton dynamics or vibrations connected to the movement of H atoms can be easily detected spectroscopically, even if hydrogen is dissolved at very low concentrations in materials composed mostly of heavier atoms. For this reason, the technique attracts a considerable level of interest in the scientific community operating in the fields of chemistry, materials science, physics, and biology, and will be complemented on VESPA by standard neutron diffraction capabilities.

5.4.2. *VESPA instrument layout*

The VESPA spectrometer (see Fig. 36) can be conceptually divided into the following functional blocks [113]: (1) neutron optics system; (2) shielding; (3) chopper system; (4) shutters; (5) end-station; (6)

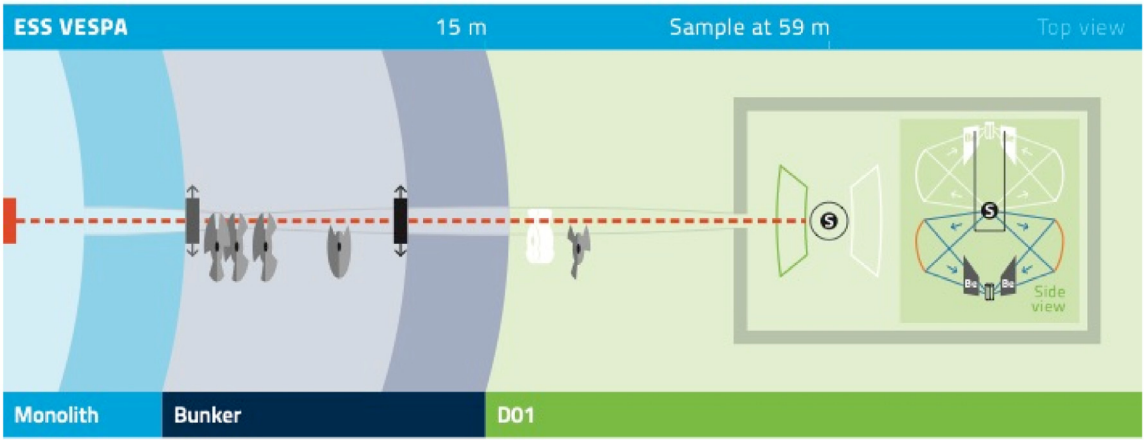

Fig. 36. VESPA instrument layout.

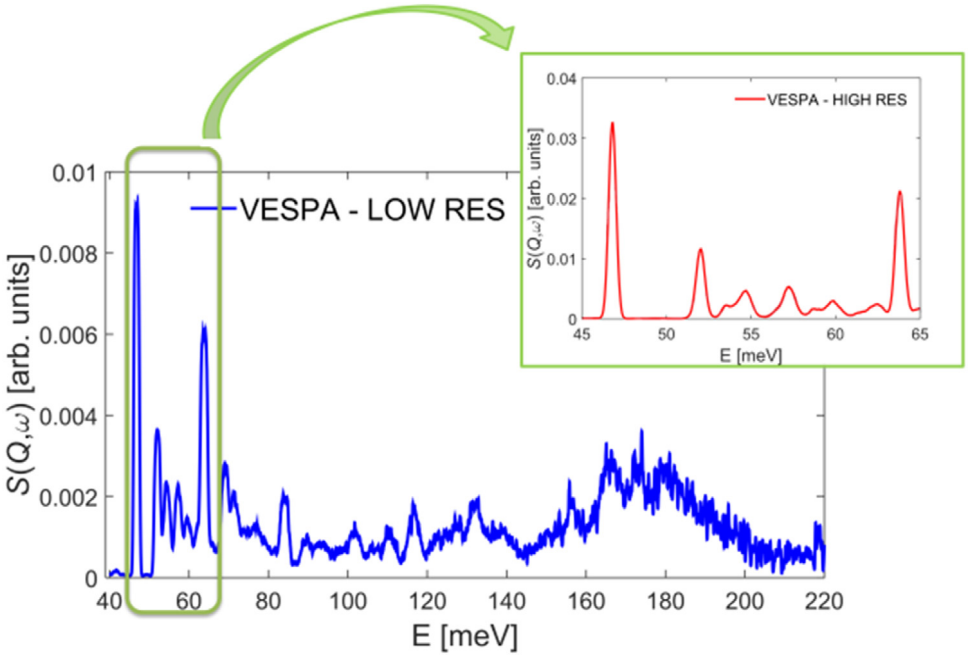

Fig. 37. Simulated spectrum of a hexamethylenetetramine sample at low temperature with the two different resolution levels available on VESPA.

Table 15
VESPA Quick Facts.

VESPA Quick Facts	
Instrument Class	Spectroscopy
Moderator	Thermal
Primary Flightpath	59 m
Sample-Analyser Flightpath	0.61–0.69 m
Wavelength Range	0.4–4.7 Å
Bandwidth	4.3 Å
Analyser Coverage	0.75 (5.25[a]) sr
Analyser Energies	3.7–4.8 meV
Energy Transfer Range	−1 to +500 meV
High Flux Mode	
Flux at Sample at 2 MW	2.3×10^8 n s^{-1} cm^{-2}
Energy Resolution	$\Delta E/\hbar\omega \approx 2.6\%$
High Resolution Mode	
Flux at Sample at 2 MW	6.5×10^7 n s^{-1} cm^{-2}
Energy Resolution	$\Delta E/\hbar\omega \approx 1.0\%$

[a]Available as a foreseen upgrade.

analysers, filters, and detectors; (7) beam stop. The neutron optics system will be able to perform an efficient transport of a large spectral bandwidth (0.4 Å $< \lambda <$ 4.7 Å) in order to give rise to a homogeneously illuminated sample area (25 × 40 mm^2, angular divergence up to ±1.4°) at 59 m. The neutron guide will stretch from 2.0 m to 58.5 m, slightly tilted with respect to the target-to-sample line in order to maximise the thermal component of the incoming neutron spectrum. The main instruments parameters can be found in Table 15.

Approximately the first 3.5 m of the guide (the "feeder") will be inserted in the monolith, followed downstream by about 1.0 m of straight guide crossing the chopper area (see below). After that, an elliptic guide (with $3 < m < 5$) of about 51.0 m will transport neutrons up to the end of the optical system. The chopper system is the central part of the instrument. The chopper discs we have used can be classified according to their function into: three pulse-shaping choppers (PSC, 3 pairs of counter-rotating discs), one frame overlap chopper (FOC, 1 disc) and one sub-frame overlap chopper (s-FOC, 1 pair of counter-rotating discs). Together (using two PSC's out of three at the same time) they will form the wavelength frame multiplication (WFM) chopper system enabling the required variation of the instrumental

energy resolution. The rotation speeds will be fairly low (154, 28, and 42 Hz, respectively) compared to the state-of-the-art capability.

VESPA will use highly oriented pyrolytic graphite (HOPG) crystals to determine the final neutron energy, as fixed by the selected Bragg reflection (002). Such a configuration requires a high-pass filter coupled to the HOPG analysers to remove higher order harmonics before detection. A low-temperature beryllium filter will be used to fulfil this task (the Be Bragg cut-off being $\lambda_{co} = 3.97$ Å). The "day-one" configuration of the VESPA spectrometer includes 2 backscattering crystal analyser arrays, placed at an average scattering angle 2θ of about 135°. These analysers will select neutrons whose first harmonics correspond to the following final neutron energy range: 3.7 meV < E_f < 4.8 meV. Each HOPG crystal array will illuminate 8 detector tubes (see below for details) through a beryllium filter (14 cm thick) forming a module (known as an "analyser-filter-detector" module). With 2 modules, a total solid angle of 0.75 sr will be provided. Neutron vibrational spectrometers are normally equipped with standard commercial detectors such as ^{3}He PSD tubes. In our case thin cylindrical tubes (e.g. with an 8.0 mm diameter) will be particularly suitable since the neutron travel time in the tube is a significant contribution to the time-of-flight (i.e. energy transfer) instrumental resolution. As for the diffraction capabilities, since the requested performances are simply standard, similar cylindrical ^{3}He tubes will be adequate.

5.4.3. VESPA expected performance

VESPA will cover a wide range of energy transfers, −1 < E < 500 meV, in one shot: the full neutron spectrum is collected in a single ESS time frame, making kinetic or parametric experiments feasible. Simulation results show that VESPA will be able to provide an excellent neutron flux up to 125 meV (in the high-flux setting), covering about half of the so-called "fingerprint region" (60–220 meV), which is the crucial interval in neutron vibrational spectroscopy. The instrument resolution was accurately calculated achieving (over most of its energy transfer range) two constant relative energy resolution values, either $\Delta E/E_i \approx 1.0\%$ ("high resolution" mode) or $\Delta E/E_i \approx 2.6\%$ ("high flux" mode), see Fig. 37 for an example. Moreover, the possibility of improving the resolution at the expense of the count rate or, on the contrary, sacrificing the resolving power to increase the instrument flux at the sample position, is a feature that makes VESPA unique among all indirect-geometry inelastic instruments worldwide. For example, in the aforementioned fingerprint region, when moving from the "high resolution" mode to the "high flux" mode, one obtains an increase in the incoming neutron flux of a factor of 5, at the expense of the average relative resolution, which increases from 0.7% to 2.6% (see Fig. 38). As for the "high resolution" mode diffraction capabilities, the day-one d-range will be 0.25–3.86 Å (at medium resolution, $\Delta d/d \approx 10^{-2}$), upgradeable in the future with an additional interval of 0.20–2.41 Å (at high resolution, $\Delta d/d \approx 5 \times 10^{-3}$).

5.5. MIRACLES — High-resolution backscattering spectrometer

5.5.1. MIRACLES introduction

MIRACLES is the time-of-flight backscattering spectrometer at the ESS. Its incident energy and pulse of the moderator can be tailored by means of a chopper cascade extended along its 162.5 m guide. MIRACLES will have a broad bandwidth in energy transfer, $\hbar\omega$, of ±500 μeV, when centred at the elastic line, thus allowing measurement of quasi-elastic and low-energy inelastic excitations. Variations in energy of the incoming neutrons interacting with the samples will be analysed using Si(111) crystals in near-backscattering geometry reflecting neutrons with energy $E_f = 2.08$ meV to the detector area near the sample. Contributions from the primary (beamline) and secondary (backscattering system) spectrometer to the energy resolution are balanced to reach an optimised elastic resolution, $\Delta(\hbar\omega)$, of 2 μeV — the high-resolution mode. This energy resolution can be tuned and relaxed to achieve record values of flux, taking advantage of the unique pulse structure and excellent brilliance provided by the ESS source (see Table 16).

Table 16
MIRACLES Quick Facts.

MIRACLES Quick Facts	
Instrument Class	Spectroscopy
Moderator	Cold
Primary Flightpath	162.5 m
Sample-Analyser Flightpath	2.5 m
Wavelength Range	2–20 Å
Bandwidth	1.5 Å, ±0.5 meV[a]
Energy Transfer Range	−2 to +20 meV
Q Range	0.2–2 Å^{-1}[a]
High Flux Mode	
Flux at Sample at 2 MW	1.5×10^9 n s^{-1} cm^{-2}[a]
Elastic Energy Resolution	45 μeV
High Resolution Mode	
Flux at Sample at 2 MW	4×10^7 n s^{-1} cm^{-2}[a]
Elastic Energy Resolution	2 μeV

[a]When centred on $\lambda = 6.27$ Å.

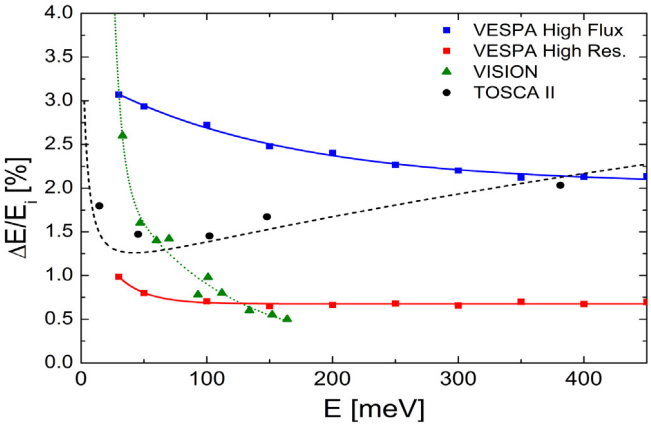

Fig. 38. VESPA relative resolution as a function of the energy transfer: blue squares represent the 'high flux' mode, while red squares the 'high resolution' mode. VISION and TOSCA-II estimated performances [112,114] are reported as green triangles and black circles, respectively. Lines are only a guide for the eye.

The energy range of the instrument comprises the cold region (wavelengths from ~2 to 20 Å). The backscattering spectrometer (Si-analysers + collimator + detectors) covers a range of scattering angles of 150°, and thus a Q range for the elastic line using Si(111) reflections of between 0.2 and 2 Å^{-1}. Increasing capabilities are envisioned as a future upgrade with the use of the Si(333) reflection ($\lambda = 2.08$ Å) and/or the Si(311) ($\lambda = 3.28$ Å), which will allow for an extended Q-range [115].

5.5.2. MIRACLES science case

The choice of spectrometer is generally defined by the energy transfer range covered ($\hbar\omega$), wave-vector range (Q) over which one can measure different excitations, with an associated energy and wave-vector resolution ($\Delta(\hbar\omega)$ and ΔQ, respectively). Thus, to select the most suited spectrometer for a certain measurement, both the type of excitation(s) of interest (for example molecular vibrations, phonons, magnons, local diffusion and rotation, crystal field excitations) as well as the overall scale of the motion needs to be considered. On today's instruments, it is often necessary to collect data on more than one spectrometer in order to cover the complete energy range of these excitations [116]. This is clearly the case for polymer science [117], where the large observation time, large energy bandwidth, energy range and tuneable resolution offered by MIRACLES, will, for the first time, provide complete information using a single spectrometer. Here we also recall that neutron backscattering spectroscopy provides unique access to the ns time-scale and allows unambiguous measurement of

the single-particle self-correlation function. Moreover, the analysis of quasi-elastic neutron scattering (QENS) data associated with molecular dynamics simulations (MD) is one of the most suitable approaches to support the use of MD generated structures [118,119]. Finally, as the energy resolution, of the order of μeV and selected with the optimised chopper cascade, is kept throughout the extensive incident energy range, MIRACLES will allow unique high-resolution inelastic scattering capabilities [120].

All these features highlight the suitability of MIRACLES to carry out studies of dynamics at the ns–ps range, applied to an extended list of topics. Some examples linked to the science case and extracted from state of the art research include:

- Life sciences: degenerative diseases, protein dynamics and enzyme catalysis
- Pharmaceutical studies, including drug implementation/delivery.
- Energy sciences: catalysis, fuel cells and H_2 storage, CO_2 capture, proton diffusion and enzymes encapsulation in MOFs.
- Polymer sciences: organic electronic devices, viscoelasticity.
- Climate change: waste containment, ice formation, Portland-alternative cements.
- Next-generation magnetic materials: molecular nanomagnets, spin dynamics in novel magnetic materials.

5.5.3. MIRACLES instrument layout

The layout of the MIRACLES spectrometer is illustrated in Fig. 39. The beamline is centred at the cold moderator. The guide design (including beam extraction and loss of direct line-of-sight) can be split into vertical and horizontal layouts, according to needs and technical (system) requirements for backscattering QENS and INS experiments [121]. For the neutron beam extraction, the horizontal layout is constrained by the guide section at the pulse-shaping chopper position, that along with the slit width for the pulse-shaping chopper must be small enough, to deliver short opening times of about ~70 μs, and thus a final elastic energy resolution $\Delta(\hbar\omega) \approx 2$ μeV. The vertical layout for the neutron beam extraction system, in turn, is designed to maximise collection and transport of neutrons, by using an elliptic profile with the focal point slightly shifted with respect to the centre of the cold source.

After the pulse-shaping/selection choppers region, the guide has a curved shape (R ~ 2 km) in the horizontal layout to cut off neutrons with $\lambda < 2$ Å and to efficiently lose direct line-of-sight not only from the primary source (radiation that comes out of the monolith insert) but also any other secondary neutron source originating from the beamline components, like choppers, etc. A long straight segment starts with a tapered guide (divergent trumpet) aimed to reduce the horizontal angular divergence distribution. Following this strategy, a neutron transport >90% along the ~80 m straight guide coated with m = 1.5 is achieved. Finally, the focusing guide is designed to illuminate samples of $\leq 3 \times 3$ cm^2 located at 30 cm from the guide exit.

The MIRACLES chopper cascade is designed to adjust the balance between resolution and flux through the pulse shape and length [122]. A pulse-shaping/pulse-selection chopper assembly, located after the exit of the monolith, is designed to ensure a wide, flexible range of configuration modes that range from the aforementioned high-resolution elastic mode ($\Delta(\hbar\omega) \approx 2$ μeV) to the high-flux mode, capturing almost the whole pulse delivered by the ESS source, with a bandwidth of $\Delta\lambda = 1.7$ Å and an elastic resolution of $\Delta(\hbar\omega) = 45$ μeV. An additional chopper is added at the long straight section of the beamline with a threefold purpose: defining the final wavelength bandwidth, minimising frame overlap between pulses in the high flux modes, and removing contaminating long wavelength harmonics that escape through the pulse-shaping system. Rephasing the chopper system allows the selection of shorter or longer wavelengths, so that inelastic processes far from the elastic line can be accessed.

Once the selected neutrons hit the sample, the variations in energy of the neutrons interacting with the sample are scrutinised using a Si(111) analyser, with a radius of R = 2.5 m [123], that scatters neutrons with a wavelength λ of 6.27 Å in a near-backscattering configuration ($2\theta \approx 88.5°$). Backscattered neutrons are then collected using a ^{3}He detector array, in a cylindrical configuration surrounding the sample chamber, slightly above and below the sample position. A radial collimator located between the analyser and the detectors improves the signal-to-background ratio. All these components together with the backscattering analyser Si-system are hosted within a 90 m^3 vacuum tank. The vessel is located within the cave, designed to shield/isolate the scattering vessel from the outside and to host the scientific activities that involve a scientific experiment which will be developed at its roof.

5.5.4. MIRACLES expected performance

Neutron optics calculations, using Monte Carlo simulations, have been performed to calculate the performance, shown in Fig. 40. The energy bandwidth can be tuned and tailored using the chopper cascade. The figure shows the simulation results obtained when tuning the beam prepared for a QENS Si(111) operation (i.e. clean pulses with neutron wavelength centred at $\lambda = 6.27$ Å with a bandwidth of 1.5 Å). Estimates of the neutron flux at sample position for different configuration modes yield values ranging from 4×10^7 n s^{-1} cm^{-2} in the high-resolution mode (with the pulse-shaping chopper running at the maximum speed, $\Delta(\hbar\omega) = 2$ μeV at the elastic line) to 1.5×10^9 n s^{-1} cm^{-2} in the high-flux mode $\Delta(\hbar\omega) = 45$ μeV at the elastic line, while keeping the full dynamic range of ±500 μeV).

6. Summary

The ESS will provide a suite of world-leading instruments for use by the neutron user community. Each of them is designed to provide breakthrough new scientific capability, not currently available at existing facilities, building on the inherent strengths of the ESS long-pulse neutron source of high flux, flexible resolution and large bandwidth, resulting in an order-of-magnitude gain in performance averaged over the 15 instruments, compared to the best-in-class instruments currently operating. This technical capability translates into a very broad range of scientific capabilities. The 15 user instruments currently in construction are chosen to maximise the breadth and depth of the scientific impact.

The instruments for large-scale structures cover SANS, reflectometry and macromolecular crystallography. LoKI and SKADI are complementary SANS instruments, specialising in large bandwidth and low Q, respectively. Estia and FREIA are reflectometers with very different capabilities, optimised for small samples and magnetism, and kinetics of free liquid surfaces, respectively. NMX is dedicated to neutron macromolecular crystallography, complementing the vast array of X-ray protein crystallography instruments, with the ability of neutrons to locate the hydrogen atoms relevant for the biological function of the macromolecules.

BEER is a diffractometer optimised for fast and flexible measurement of lattice strains and residual strain in engineering components, while ODIN, a multipurpose imaging station will provide an unparallelled combination of wavelength and spatial resolution, flux and flexibility.

Powder diffraction is served by two instruments. DREAM is a wide-bandwidth diffractometer, allowing a very flexible trade-off between flux and resolution, while HEIMDAL is optimised for functional materials and in-situ chemistry with a multi-length-scale design allowing for later installation of SANS and imaging options. MAGiC is a single-crystal diffractometer for magnetism, covering both thermal and cold neutron applications.

The general-purpose chopper spectrometers CSPEC and T-REX offer complementary cold and thermal neutron capabilities, with one favouring soft matter studies and the other providing polarisation analysis for problems such as single-crystal magnetism. BIFROST is a spectrometer optimised for the study of single-crystal excitations at high magnetic fields and pressures. VESPA is dedicated to neutron vibrational spectroscopy with an emphasis on the energy range of primary importance

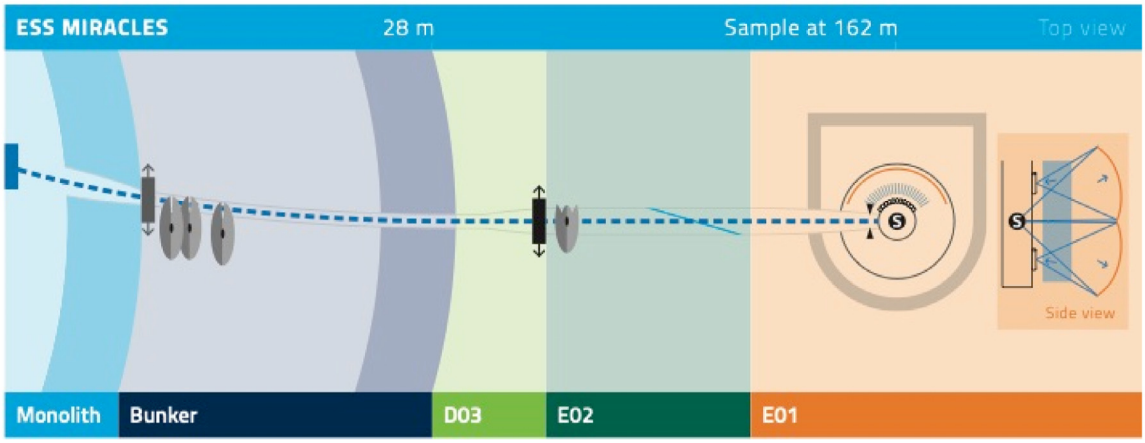

Fig. 39. MIRACLES instrument layout.

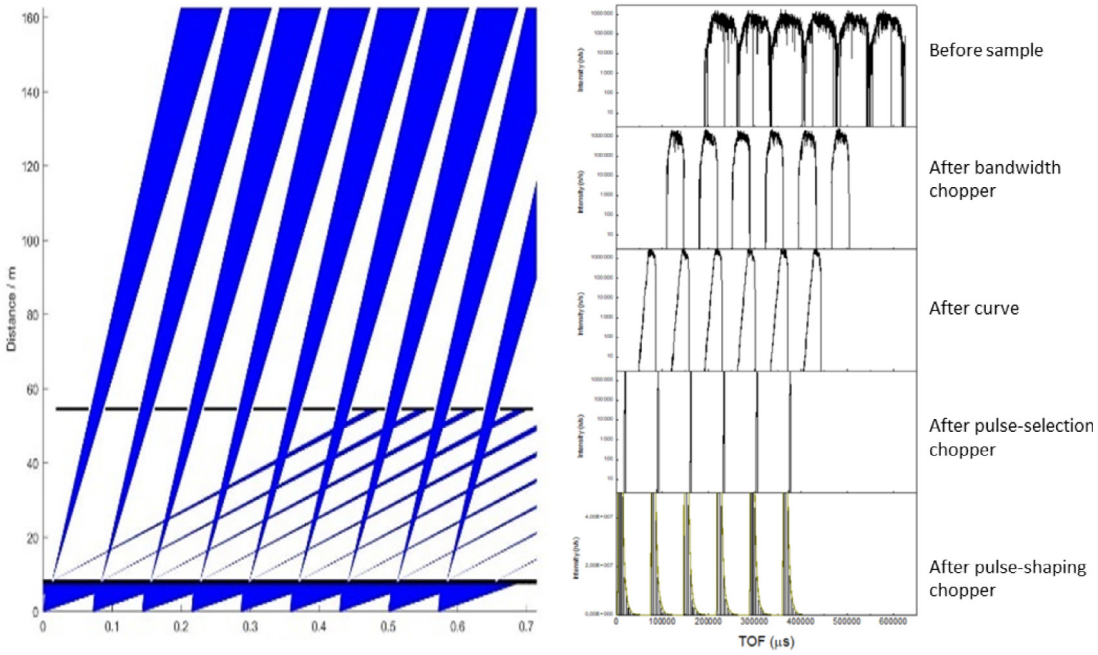

Fig. 40. Time-Distance Diagram and Monte Carlo time of flight calculations for $\lambda = 6.27$ Å on MIRACLES.

to the study of functional groups in energy materials, while the highest energy resolution available at ESS will be provided by MIRACLES, a backscattering spectrometer with a flexible resolution down to about 2 μeV.

Further extension of the instrument suite to reach the full suite of 22 instruments will start in the coming years, which will take the form of open calls for instrument proposals, to be evaluated based on performance and scientific merit, similarly to the process employed for selecting the current 15 instruments. A capability gap analysis [18] has identified particle physics and high-resolution neutron spin-echo as the highest-priority instruments to add to the suite.

The ESS has been carefully designed to allow for extension and renewal of its instrument suite. Each beamport allows views of both cold and thermal moderators, and the relatively narrow beamport separation of 6°, combined with the large size of the experimental halls permits future installation of many more instruments than 22. In addition, upgrade areas outside the current experimental halls will allow for extension or construction of new experimental halls, and the currently unoccupied lower-moderator position [2,3] is foreseen for future moderator developments providing new, as yet unforeseen, capabilities. The primary upgrade path to ESS beyond its 22-instrument suite, is the addition of more instruments on its main target station.

ESS will not only provide world-class neutron science capabilities from the start of its user programme, but its instrument suite and overall design will ensure it remains at the forefront of the field for the lifetime of the facility.

Declaration of competing interest

The authors declare that they have no known competing financial interests or personal relationships that could have appeared to influence the work reported in this paper.

Acknowledgements

Some of the work described here is part of projects that have received funding from the European Union's Horizon 2020 research programme: SINE 2020 under grant agreement number 654000, BrightnESS under grant agreement number 676548, and SoNDe under grant agreement number 654124.

Financial support for the fast-shutter upgrade for FREIA from Swedish Research Council VR, grant no 2018-05013, is acknowledged.

The VESPA team gratefully acknowledges the Science & Technology Facilities Council (STFC) and the CNR, within the CNR-STFC Agreement (2014–2020) No. 3420.

The MIRACLES team wishes to thank the IN16B team (Bernhard Frick and Tilo Seydel), the BASIS team (Kenneth W. Herwig, Eugene Mamontov and Niina Jalarvo), the DNA team (Kaoru Shibata and Yukinobu Kawakita), and the IRIS/OSIRIS team (M.T.F. Telling, V. Garcia-Sakai, F. Demmel) for fruitful discussions.

References

[1] S. Peggs (Ed.), ESS Technical Design Report, 2013.
[2] K.H. Andersen, M. Bertelsen, L. Zanini, E.B. Klinkby, T. Schönfeldt, P.M. Bentley, J. Saroun, Optimisation of moderators and beam extraction at the ESS, J. Appl. Cryst. 51 (2018) 264–281.
[3] L. Zanini, K.H. Andersen, K. Batkov, E.B. Klinkby, F. Mezei, T. Schönfeldt, A. Takibayev, Design of the cold and thermal neutron moderators for the European Spallation Source, Nucl. Instrum. Methods Phys. Res. A 925 (2019) 33–52.
[4] F. Mezei, The Raison d'Etre of long pulse spallation sources, J. Neutron Res. 6 (1997) 3–32.
[5] H. Schober, E. Farhi, F. Mezei, P. Allenspach, K. Andersen, P.M. Bentley, P. Christiansen, B. Cubitt, R.K. Heenan, J. Kulda, P. Langan, K. Lefmann, K. Lieutenant, M. Monkenbusch, P. Willendrup, J. Šaroun, P. Tindemans, G. Zsigmond, Tailored instrumentation for long-pulse neutron spallation sources, Nucl. Instrum. Methods A 589 (2008) 34–46.
[6] K. Lefmann, K.H. Klenø, J. Okkels Birk, B.R. Hansen, S.L. Holm, E. Knudsen, K. Lieutenant, L. von Moos, M. Sales, P.K. Willendrup, K.H. Andersen, Simulation of a suite of generic long-pulse neutron instruments to optimise the time structure of the European Spallation Source, Rev. Sci. Instrum. 84 (2013) 055106.
[7] F. Mezei, M. Russina, S. Schorr, Physica B 276 (2000) 128.
[8] Nakajima Kenji, Ohira-Kawamura Seiko, et al., AMATERAS: A cold-neutron disk chopper spectrometer, J. Phys. Soc. Japan 80 (2011) SB028.
[9] K. Lieutenant, F. Mezei, J. Neutron Res. 14 (2006) 177;
M. Russina, F. Mezei, Proc. SPIE 4785 (2002) 24.
[10] K.H. Klenø, K. Lieutenant, K.H. Andersen, K. Lefmann, Systematic performance study of common neutron guide geometries, Nucl. Instrum. Methods A 696 (2012) 75–84.
[11] L.D. Cussen, D. Nekrassov, C. Zendler, K. Lieutenant, Multiple reflections in elliptic neutron guide tubes, Nucl. Instrum. Methods Phys. Res. A 705 (2013) 121–131, http://dx.doi.org/10.1016/j.nima.2012.11.183.
[12] M. Bertelsen, H. Jacobsen, U.B. Hansen, H.H. Carlsen, K. Lefmann, Exploring performance of neutron guide systems using pinhole beam extraction, Nucl. Instrum. Methods Phys. Res. A 729 (2013) 387–398, http://dx.doi.org/10.1016/j.nima.2013.07.062.
[13] H. Jacobsen, K. Lieutenant, Zendler, K. Lefmann, Bi-spectral extraction through elliptic neutron guides, Nucl. Instrum. Methods Phys. Res. A 717 (2013) 69–76, http://dx.doi.org/10.1016/j.nima.2013.03.048.
[14] S. Holm-Dahlin, M.A. Olsen, M. Bertelsen, J.O. Birk, K. Lefmann, Optimisation of performance, price, and background of long neutron guides for ESS, Quantum Beam Sci. 3 (3) (2019) 16, http://dx.doi.org/10.3390/qubs3030016.
[15] F. Mezei, M. Russina, United States of America Patent No. US20050157831 A1, 2003.
[16] F. Mezei, Advances by innovation and building on experience, The ESS project Vol II, New Science and Technology for the 21st Century, 2002;
H. Jacobsen, K. Lieutenant, C. Zendler, K. Lefmann, Bi-spectral extraction through elliptic neutron guides, Nucl. Instrum. Methods Phys. Res. A 717 (2013) 69–76.
[17] T. Kai, M. Harada, M. Teshigawara, N. Watanabe, Y. Ikeda, Nucl. Instrum. Methods Phys. Res. A 523 (2004) 398.
[18] K.H. Andersen, et al., The ESS Instrument Suite – a Capability Gap Analysis, ESS-1959173, ESS internal report, 2019.
[19] Kim Lefmann, K. Nielsen, McStas, a general software package for neutron ray-tracing simulations, Neutron News 10 (3) (1999) 20;
P. Willendrup, K. Lefmann, McStas(i): introduction, use, and basic principles for ray-tracing simulations, J. Neutron Res. (2019) 1–16.
[20] K. Lieutenant, G. Zsigmond, S. Manoshin, M. Fromme, H.N. Bordallo, D. Champion, J. Peters, F. Mezei, Neutron instrument simulation and optimisation using the software package VITESS, Proc. SPIE 5536 (2004) 134–145.
[21] Z. Xie, J. Zhou, Y. Song, J.L. Lacy, L. Sun, Z. Sun, B. Hu, Y. Chen, Nucl. Instrum. Methods Phys. Res. A 888 (2018) 235–239.
[22] S. Jaksch, D. Martin-Rodriguez, A. Ostermann, J. Jestin, S.D. Pinto, W.G. Bouwman, et al., Concept for a time-of-flight small angle neutron scattering instrument at the European Spallation Source, Nucl. Instrum. Methods Phys. Res. A 762 (2014) 22–30.
[23] S. Jaksch, R. Engels, G. Kemmerling, U. Clemens, S. Désert, H. Perrey, et al., Recent developments SoNDe high-flux detector project, in: Proceedings of the International Conference on Neutron Optics, NOP2017, 2018, p. 011019.
[24] S. Jaksch, R. Engels, G. Kemmerling, C. Gheorghe, P. Pahlsson, S. Désert, F. Ott, Cumulative reports of the sonde project, July 2017, 2017, arXiv preprint arXiv:1707.08679.
[25] J. Stahn, A. Glavic, Nucl. Instrum. Methods Phys. Res. A 821 (2016) 44–54.
[26] F. Piscitelli, et al., J. Instrum. 13 (2018) P05009.
[27] G. Mauri, et al., Proc. R. Soc. Lond. Ser. A Math. Phys. Eng. Sci. 474 (2018) 20180266.
[28] F. Piscitelli, et al., J. Instrum. 12 (2017) P03013.
[29] F. Piscitelli, et al., J. Instrum. 9 (2014) P03007.
[30] D. Pfeiffer, et al., J. Instrum. 11 (2016) P05011.
[31] M. Blakeley, private communication.
[32] M.T. Hutchings, P.J. Withers, T.M. Holden, T. Lorentzen, Introduction To the Characterisation of Residual Stress By Neutron Diffraction, CRC Press, 2005.
[33] N. Kardjilov, I. Manke, A. Hilger, R. Woracek, J. Banhart, Advances in neutron imaging, Mater. Today (2018) available online 3 May 2018.
[34] M. Strobl, I. Manke, N. Kardjilov, A. Hilger, M. Dawson, J. Banhart, Advances in neutron radiography and tomography, J. Phys. D: Appl. Phys. 42 (2009) 243001.
[35] R. Woracek, J. Santisteban, A. Fedrigo, M. Strobl, Diffraction in neutron imaging—A review, Nuclear Instrum. Methods Phys. Res. A 878 (2018) 141–158.
[36] M. Rouijaa, R. Kampmann, J. Saroun, J. Fenske, P. Beran, M. Müller, P. Lukas, A. Schreyer, Nucl. Instrum. Methods Phys. Res. A. 889 (2018) 7–15.
[37] J. Šaroun, J. Fenske, M. Rouijaa, P. Beran, J. Navrátil, P. Lukáš, A. Schreyer, M. Strobl, J. Phys.: Conf. Ser. 746 (2016) 012011.
[38] G. Nowak, M. Störmer, H.-W. Becker, C. Horstmann, R. Kampmann, D. Höche, M. Haese-Seiller, J.-F. Moulin, M. Pomm, C. Randau, U. Lorenz, R. Hall-Wilton, M. Müller, A. Schreyer, J. Appl. Phys. 117 (2015) 034901.
[39] I. Stefanescu, M. Christensen, J. Fenske, R. Hall-Wilton, P. Henry, O. Kirstein, M. Müller, G. Nowak, D. Pooley, D. Raspino, N. Rhodes, J. Šaroun, J. Schefer, E. Schooneveld, J. Sykora, W. Schweika, J. Instrum. 12 (2017) P01019.
[40] http://j-parc.jp/researcher/MatLife/en/instrumentation/ns_spec.html#bl19.
[41] K. An, H.D. Skorpenske, A.D. Stoica, D. Ma, X.L. Wang, E. Cakmak, Metall. Mater. Trans. A 42 (2011) 95.
[42] X.L. Wang, T.M. Holden, A.D. Stoica, K. An, H.D. Skorpenske, A.B. Jones, Mater. Sci. Forum 652 (2010) 105.
[43] M. Strobl, Future prospects of imaging at spallation neutron sources, Nucl. Instrum. Methods A 604 (2009) 646–652.
[44] N. Kardjilov, et al., Neutron imaging in materials science, Mater. Today 14 (6) (2012) 248–256.
[45] M. Strobl, R.P. Harti, C. Grünzweig, R. Woracek, J. Plomp, Small angle scattering in neutron imaging—A review, J. Imaging 3 (2018) 64.
[46] M. Strobl, The scope of the imaging instrument project ODIN at ESS, Physics Procedia 69 (2015) 18–26.
[47] M. Strobl, M. Bulat, K. Habicht, The wavelength frame multiplication chopper system for an ESS test-beamline and corresponding implications for ESS instruments, Nucl. Instrum. Methods A 705 (2013) 74–84.
[48] R. Woracek, T. Hofmann, M. Bulat, M. Sales, K. Habicht, K. Andersen, M. Strobl, The testbeamline of the European Spallation Source – instrumentation development and wavelength frame multiplication, Nucl. Instrum. Methods A 839 (2016) 102–116.
[49] M. Seifert, Simulation of a Chopper System for a Time-of-Flight Imaging Beam Line at the European Spallation Source (Bachelor thesis), Physics Dep. E 21 Technical University Munich.
[50] P. Schmakat, Phase Transitions & Wavelength-Frame Multiplication Chopper System for the Imaging Instrument ODIN at the ESS (Ph.D. thesis), Physics Dep. E 21 Technical University Munich.
[51] ess-public-legacy.esss.se/sites/default/files/odin_imaging_instrument_construction_proposal.pdf.
[52] M. Morgano, E. Lehmann, M. Strobl, Detector requirements for the ODIN beamline at ESS, Physics Procedia 69 (2015) 152–160.
[53] Triestino Minniti, Kenichi Watanabe, Genoveva Burca, Daniel E. Pooley, Winfried Kockelmann, Characterisation of the new neutron imaging and materials science facility IMAT, Nucl. Instrum. Methods Phys. Res. A 888 (2018) 184–195.
[54] Takenao Shinohara, Tetsuya Kai, Commissioning start of energy-resolved neutron imaging system, RADEN in J-PARC, Neutron News (2015) 11–14.
[55] https://www.mlz-garching.de/antares.
[56] https://www.psi.ch/en/sinq/icon.
[57] A. Houben, et al., Nucl. Instrum. Methods A 680 (2012) 124.
[58] G. Modzel, et al., Nucl. Instrum. Methods A 743 (2014) 90.
[59] W. Schweika, et al., J. Phys. Conf. Ser. 746 (2016) 012013.
[60] P. Jacobs, A. Houben, W. Schweika, A.L. Tchougréeff, R. Dronskowski, J. Appl. Cryst. 48 (2015) 1627.
[61] S.L. Holm, et al., Nucl. Instrum. Methods A 828 (2016) 229–241.
[62] I. Stefanescu, M. Christensen, R. Hall-Wilton, S. Holm-Dahlin, K. Iversen, M. Klein, D. Mannix, J. Schefer, C.J. Schmidt, W. Schweika, U. Stuhr, Performance study of the jalousie detector baseline design for the ESS thermal powder diffractometer HEIMDAL through GEANT4 simulation, J. Instrum. (2019) http://dx.doi.org/10.1088/1748-0221/14/10/p10020.

[63] R.M. Ibberson, Nucl. Instrum. Methods Phys. Res. A 600 (2009) 47–49.
[64] S. Torii, et al., J. Phys. Soc. Japan 80 (2011) SB020.
[65] B.J. Kim, et al., Phys. Rev. Lett. 101 (2008) 076402.
[66] S. Mühlbauer, et al., Science 323 (2009) 915.
[67] V. Balédent, et al., Phys. Rev. Lett. 105 (2010) 027004.
[68] T. Kimura, et al., Nature 426 (2003) 55.
[69] W. Witczaek-Krempa, G. Chen, Y.B. Kim, L. Balents, Annu. Rev. Cond. Matter Phys. 5 (2014) 57.
[70] Kitaev, Ann. Phys. 321 (2006).
[71] G. Jackeli, et al., Phys. Rev. Lett. 102 (2009) 017205.
[72] S. Gane, et al., PLoS One 8 (1) (2013) e55780.
[73] Axel Hoffmann, Sam D. Bader, Opportunities at the frontiers of spintronics, Phys. Rev. Appl. 4 (2015) 047001.
[74] Yi Zhou, Kazushi Kanoda, Tai-Kai Ng, Quantum spin liquid states.
[75] M.R. Norman, Herbertsmithite and the search for the quantum spin liquid, Rev. Modern Phys. 88 (2016) 041002.
[76] C. Riedel, et al., The heat released during catalytic turnover enhances the diffusion of an enzyme, Nature 517 (2015) 227.
[77] R. Golestanian, Enhanced diffusion of enzymes that catalyze exothermic reactions, Phys. Rev. Lett. 115 (2015) 108102.
[78] Toshiro Takabatake, et al., Phonon-glass electron-crystal thermoelectric clathrates: Experiments and theory, Rev. Modern Phys. 86 (2014) 669.
[79] S. Pili, et al., Proton conduction in a phosphonate-based metal–organic framework mediated by intrinsic “Free Diffusion inside a Sphere”, J. Am. Chem. Soc. 138 (2016) 6352.
[80] H.Y. Zhang, The molecular dynamics study of vacancy formation during solidification of pure metals, Sci. Rep. 7 (2017) 10241.
[81] S. Komura, H. Furukawa (Eds.), Dynamics of Ordering Processes in Condensed Matter, Plenum Press, New York & London, 1988.
[82] Nicoletta. Liguori, et al., From light-harvesting to photoprotection: structural basis of the dynamic switch of the major antenna complex of plants (LHCII), Sci. Rep. 5 (2015) 15661.
[83] A. Khaplanov, et al., J. Instrum. 12 (2017) P04030.
[84] E. Babcock, Z. Salhi, P. Pistel, A. Ioffe, G. Simeoni, J. Phys. Conf. Ser. 528 (2014) 012018.
[85] B. Dalla Piazza, et al., Nat. Phys. 11 (2015) 62–68.
[86] R. Coldea, et al., Science 327 (2010).
[87] T. Hong, Nat. Phys. 13 (7) (2017) 638.
[88] Ch. Ruegg, Nature 423 (2003) 62–65.
[89] Ch. Ruegg, Phys. Rev. Lett. 93 (2004) 257201.
[90] Rossat-Mignot, et al., Physica C 185 (1991) 86–92.
[91] N.B. Christensen, et al., Phys. Rev. Lett. 93 (2004) 147002.
[92] M.K. Chan, et al., Nature Commum. 7 (2016) 10819.
[93] Pengcheng Dai, Rev. Modern Phys. 87 (2015) 855.
[94] H. Jacobsen, et al., Phys. Rev. Lett. 120 (3) (2018) 037003.
[95] P. Hinkov, Nat. Phys. 3 (2007) 780–785.
[96] B. Lake others, Nature 415 (2002) 299–302.
[97] S. Mühlbauer, et al., Science 323 (2009) 5916.
[98] P.Y. Portnichenko, Nature Commun. 7 (2016) 10725.
[99] S. Fusil, et al., Annu. Rev. Mater. Res. 44 (2014) 91–116.
[100] S.P.P. Jones, Nature Commun. 5 (2014) 3787.
[101] S. Artyukhin, Nature Mater. 11 (2012) 694.
[102] H. Nojiri, et al., Phys. Rev. Lett. 106 (2011) 237202.
[103] E. Fogh, et al., Phys. Rev. B 96 (2017) 104420.
[104] L.E. Bove, et al., Phys. Rev. Lett. 111 (2013) 185901.
[105] M.C. Rheinstädter, Phys. Rev. Lett. 93 (2004) 108107.
[106] Felix Groitl, et al., Rev. Sci. Instrum. 87 (2016) 035109.
[107] Marko Marton, et al., Rev. Sci. Instrum. 89 (2018) 015105.
[108] Rasmus Toft-Petersen, et al., Nucl. Instrum. Methods A 830 (2016) 338–344.
[109] F. Groitl, et al., Sci. Rep. 7 (1) (2017) 12637.
[110] J. Okkels Birk, et al., Rev. Sci. Instrum. 85 (2014) 113908.
[111] J. Okkels Birk, (Ph.D. thesis), University of Copenhagen, 2014.
[112] A. Fedrigo, et al., Rev. Sci. Instrum. 87 (2016) 065101.
[113] M. Zanetti, et al., Physica B 562 (2019) 107.
[114] D. Colognesi, et al., Appl. Phys. A 74 (2002) S64.
[115] N. Tsapatsaris, R.E. Lechner, M. Markó, H.N. Bordallo, Conceptual design of the time-of-flight backscattering spectrometer, MIRACLES, at the European Spallation Source, Rev. Sci. Instrum. 87 (2016) 085118.
[116] M.C. Berg, A.R. Benetti, M.T.F. Telling, T. Seydel, D. Yu, L. Daemen, H.N. Bordallo, Nanoscale mobility of aqueous polyacrylic acid in dental restorative cements, ACS Appl. Mater. Interfaces 10 (2018) 9904–9915.
[117] D. Bhowmik, J.A. Pomposo, F. Juranyi, V. García-Sakai, M. Zamponi, Y. Su, A. Arbe, J. Colmenero, Microscopic dynamics in nanocomposites of poly(ethylene oxide) and poly(methyl methacrylate) soft nanoparticles: A quasi-elastic neutron scattering study, Macromolecules 47 (2014) 304–315.
[118] A. Desmedt, J.C. Soetens, M. Prager, M. Russina, J. Ollivier, Dynamics of methyl iodide clathrate hydrate, investigated by MD simulations and QENS experiments, J. Phys. Chem. C 115 (26) (2011) 12689–12701.
[119] Jeremy C. Smith, Pan Tan, Loukas Petridis, Liang Hong, Dynamic neutron scattering by biological systems, Annu. Rev. Biophys. 47 (1) (2018) 335–354.
[120] Tony Pham, Katherine A. Forrest, Rahul Banerjee, Gisela Orcajo, Juergen Eckert, Brian Space, Understanding the H2 sorption trends in the M-MOF-74 series (M = Mg, Ni, Co, Zn), J. Phys. Chem. C 119 (2) (2015) 1078–1090.
[121] P. Luna, et al., in preparation.
[122] P. Luna, H.N. Bordallo, N. Tsapatsaris, K. Andersen, I. Herranz, F. Sordo, F. Jimenez-Villacorta, Tailoring the energy resolution of MIRACLES, the time-of-flight - backscattering spectrometer at the ESS: an updated proposal for the chopper cascade, Physica B 564 (2019) 64–69.
[123] N. Tsapatsaris, P.K. Willendrup, R.E. Lechner, H.N. Bordallo, From BASIS to MIRACLES: Benchmarking and perspectives for high- resolution neutron spectroscopy at the ESS, EPJ Web Conf. 83 (2015) 03015 (6 pages).